THESIS

SYNTHESIS AND CHARACTERIZATION OF COMPLEX METAL HYDRIDES FOR HYDROGEN TECHNOLOGY

Submitted by

David Martin Nitsche

Department of Mechanical Engineering

In partial fulfillment of the requirements

For the Degree Master of Science

Colorado State University

Fort Collins, Colorado

Summer 2010

COLORADO STATE UNIVERSITY

May 13, 2010

WE HEREBY RECOMMEND THAT THE THESIS PREPARED UNDER OUR SUPERVISION BY DAVID MARTIN NITSCHE ENTITLED SYNTHESIS AND CHARACTERIZATION OF COMPLEX METAL HYDRIDES FOR HYDROGEN TECHNOLOGY BE ACCEPTED AS FULFILLING IN PART REQUIREMENTS FOR THE DEGREE OF MASTER OF SCIENCE.

Committee on Graduate work

_____

Mingzhong Wu

_____

Advisor: Venkatesan Manivannan

_____

Department Head: Allan T. Kirkpatrick

ABSTRACT OF THESIS

SYNTHESIS AND CHARACTERIZATION OF COMPLEX METAL HYDRIDES

FOR HYDROGEN TECHNOLOGY

The limitation as well as the environmental impact of fossil fuels has encouraged the development of alternative energies. As an alternative, hydrogen and its applications have been established due to its favorable physical and chemical properties. Production as well as storage of hydrogen is seen to be key challenges to for a transition to a hydrogen based infrastructure. A possible storage method is seen to be chemical hydrides, where hydrogen is chemically bonded to matrix materials and can be controllable released. The chemical synthesis of these hydrides can become complex with increasing hydride structures. Therefore, mechanochemical synthesis methods have been developed, which simplify the synthesis process. The material characteristics are being determined with an XRD apparatus as well as TGA and DSC analysis. In the present study, hydrides with the general composition MH, MH_2, $MAlH_4$, and $MAlH_6$ have been synthesized and tested for desorption characteristics, where M stands for Li, Na, K, Ca, Mg, and Ti. Doping of the materials is being applied to improve desorption characteristics of the material, where catalyst materials are implemented into the hydride structure and cause a change in the structural composition linked with a decrease of the hydrogen desorption temperature.

Finding a material that fulfills the governmental guidelines for storage materials will give the possibility to a hydrogen based infrastructure.

David Nitsche
Mechanical Engineering Department
Colorado State University
Fort Collins, CO 80523
Summer 2010

ACKNOWLEDGEMENTS

God gives the nuts, but he does not crack them.

(Franz Kafka, 1883-1924)

Within the past 10 months, I was in the fortunate situation to gain cultural, educational, and personal experiences, which improved my professional knowledge as well as my personal character. Reviewing the past months, I found many nuts on my way through the jungle of bureaucracy, cultural differences, and educational challenges, which were under my responsibility whether to crack them or not.

On my personal path, many people crossed my way and influenced me in their individual way. For that, I want to thank Dr. Mani, who gave me the opportunity to work under his responsibility and finish my Master's degree within my stay. During my time in Fort Collins, he found time to take the responsibility over my educational process to spite his extremely busy schedule. I sincerely thank both additional committee members, Dr. Mingzhong Wu and Dr. Allan Kirkpatrick, who both had the confidence in me, being able to manage the course work as well as the research work.

Working in the facilities of the US Air Force Academy, Colorado Springs, was an extremely impressive experience as a growing engineer. For my great experiences gained during my long days in Colorado Springs, I sincerely thank Dr. John Wilkes and his team including Peg Williams, Cynthia Corley, and Michael Krein, who impressed me as scientists as well as with their individual strong personality, always willing to answer my questions in a patience, that gave me the impression being welcome at this place.

Despite my educational progress, many individuals appeared and influenced my stay in Colorado. All lab members and friends are mentioned, who went through good but also exhausting times with me. Thank you Nikola, Steffie, Dominik, Rishi, Sid,Madhu, Bhavin, Anish, Josh, Brandon, and many more. Furthermore, I want to thank Katie, who has spent an incredible amount of time at Wild Boar with me, correcting each line of my thesis. Without her, my thesis would have never reached the quality that it has achieved. Besides that, she always had an open ear for my concerns and complains, mainly improved my English abilities, and showed me the most wonderful places in Colorado. All I can give back is a sincere “Thank You” from the bottom of my heart.

All my experiences and cracked nuts in the USA would never have become reality, if one person in Germany would not have such a deep trust in me. Prof. Dr. Birgit Scheppat gave me the possibility to work in her lab from the beginning of my study, where I gained first experiences with metal hydrides. She developed the idea for a “Fulbright” Scholarship in the United States, mainly supported me during the long and intense application process in 2008, and stand on my side even when being in another country.

Many other people made this stay to a wonderful time for me, who I will keep in good memories. Many thanks to: Family Kuhlman, Jenn Christ, Christy Eylar, Karen Mueller, the circle of friends around Katie, the officers from both, IIE and the Fulbright Commission, and allow fellows from the “*International Presidential Fellowship*” program.

To my family written in German:

Mama, Papa und Doro,

Ich bedanke mich fuer die vergangenen Jahre, in denen Ihr immer an der Seite meiner studentischen Aktivitaeten wart. Die Entscheidung, Euch in Deutschland zurueck zu lassen ist mir wahrlich nicht leicht gefallen und ich bin dankbar ueber den finanziellen

und seelischen Beistand, den Ihr mir in dieser Zeit gegeben habt. Die Zeit hier hat mich in vieler Hinsicht gepraegt und gezeigt, welchen Stellenwert die Familie fuer mich hat.

Kerstin, Du hast eine unglaubliche Leistung gezeigt, indem du mich 10 Monate hast gehen lassen, und trotzdem die Kraft aufbringen konntest, mich immer wieder aufzubauen wenn es mir schwer gefallen ist, Motivation und Kraft aus meinen Taten zu schoepfen. Euch Allen danke ich fuer den Beistand in dieser und jeder vergangenen Zeit.

Content

List of Figures

List of Tables

1. Introduction

1.1. Purpose and Aim of research

Since the beginning of industrialization in the 18th century, energy consumption has been steadily increasing and has still not reached its peak. As a result, fossil fuels, such as raw oil, natural gas and coal emerged as a primary energy sources. The limitations of these fossil fuels require the development of alternative sources that will be, in combination with each other, able to replace the current technologies and meet the energy demand of emerging markets. The major alternative sources emerging as potential candidates to meet these requirements are photovoltaics, wind, water, biomass, and hydrogen, where each technology has its specific advantages in its field of application.

Hydrogen, as an energy carrier, is favorable for several different reasons, such as its high energy density and its appearance in nature in its gaseous form. Fuel cells, as a hydrogen based application, convert the electrochemical stored energy directly into electric energy by producing water as a byproduct. Due to their high efficiency (≥75%) when compared to combustion engines (≥20%), fuel cells are being seriously considered as an alternative to existing technologies for mobile and stationary applications. In order to integrate hydrogen into the infrastructure, two main challenges have to be addressed; the production of hydrogen based or renewable sources and the effective storage of hydrogen.

Commonly used storage methods are high pressure vessels and low temperature vessels, which, due to their safety risks, are not preferable for mobile application. Therefore, the development of alternative methods, such as metal hydrides, have emerged over time. Metal hydrides share the ability to adsorb and to desorb hydrogen

under discrete conditions (pressure and temperature) and can act as a storage medium for hydrogen based applications. The Department of Energy (DoE) has set guidelines for the use of these storage materials such as

- Reversible storage density: ≥6.5 wt %
- Working temperature: -30℃ ≤ T ≤ 100℃
- Cycle lifetime: ≥1000 for mobile applications
- Safety codes and standards
- Fuel cost: ≤ \$133/kg H_2

Materials that are able to fulfill these guidelines may be able to replace current storage methods and allow for the transition to a renewable based infrastructure possible.

1.2. History of Hydrogen Technology

Even though hydrogen has been recognized as an alternative to fossil fuels in the recent past, its history is much older. It can be linked with famous scientists, popular engineers, and great discoveries, but also with tragedies and drawbacks. Its history began in the years around 1766 when it was first discovered by Henry Cavendish. Even though he did not establish the name hydrogen, he proved the coexistence of two different types of air. Later experiments allowed him to predict detailed values for specific weight and density. In the course of time, he also performed experiments with hydrogen-oxygen mixtures producing water.

In 1788, the name ‘hydrogen’ was first introduced by Antoine Lavoisier, a French scientist who set up his experiments based on results made by Cavendish earlier. Based on the Greek word ‘hydor’, which can be translated as ‘water- former’, the element became what it is known as today [1].

In the period from 1800 till 1839 important steps for hydrogen production technology were made by different scientists. The first began in 1800, when William Nicolson and Anthony Carlisle split water into its two elements hydrogen and oxygen by passing a current through it. From then on, hydrogen was introduced into small industrial applications. In 1839, William Grove developed the first ‘gas voltaic battery’, which can be seen as a forerunner of modern fuel cells. Based on the advances made by Nicolson and Carlisle, he was able to produce the reverse reaction. The combination of hydrogen and oxygen under controlled conditions produces water and an electrical current. The name ‘fuel cell’ was introduced when the first practical device using air and industrial coal gas was developed.

With the growing fuel cell market in 1898, hydrogen storage became of increasing interest. During that time, James Dewar developed a technique to liquefy hydrogen. Using liquid nitrogen to precool gaseous hydrogen and subsequent expansion of an insulated vessel, he created liquid hydrogen. This ‘Joule-Thompson Cycle’ made it possible to liquefy hydrogen and store it effectively over a long period of time.

After many years of industrial growth, OPEC (Organization of Petroleum Exporting Countries) suggested that the era of cheap oil had ended. As a result, the DoE (Department of Energy) was founded in 1977 which controls and manages different alternative fuel based projects. Beginning in 1990, efforts in basic research became visible and found their way into industrial applications. The first solar powered hydrogen production plant was established in 1990, followed by the first fuel cell engine car in 1994. [2, 6].

1.3. Hydrogen Technology in Modern Society

The world energy crisis in the early 70's of the last century, foreshadowed the consequences of the limitations of fossil fuels. During that time, hydrogen technology was established as one of the most important alternative technologies for two main reasons; global warming and security of energy supply.

The transportation industry turned to be the most propelling factor for hydrogen related development. Reasons for that are clear; fossil fuels are limited and will become more expensive within the following decades. Therefore, the development of alternative fuels became a major interest. Global warming is the second important reason to focus research on alternative fuels. The transportation industry realized the strong influence of pollution in politics and science. The steadily increasing amount of vehicles on the streets causes toxic greenhouse gases such as CO_2, CO and C_m,$H_{n,}$ which seem to be responsible for the global warming.

Regarding environmental aspects, the term "sustainability" grew to a major component of modern technology. By definition, sustainability is a process where the same amount of resources is taken from nature as it can produce. Looking at today's growing industry, it is of high interest to upgrade existing technologies and develop novel devices.

Today, 80% of the total energy consumption is provided by fossil fuels. The remaining 20% are provided by nuclear and renewable fuels, respectively (6.5% nuclear, 13.5% renewable). These numbers show the weight of fossil fuels in current society and the need for a transition to renewable energies.

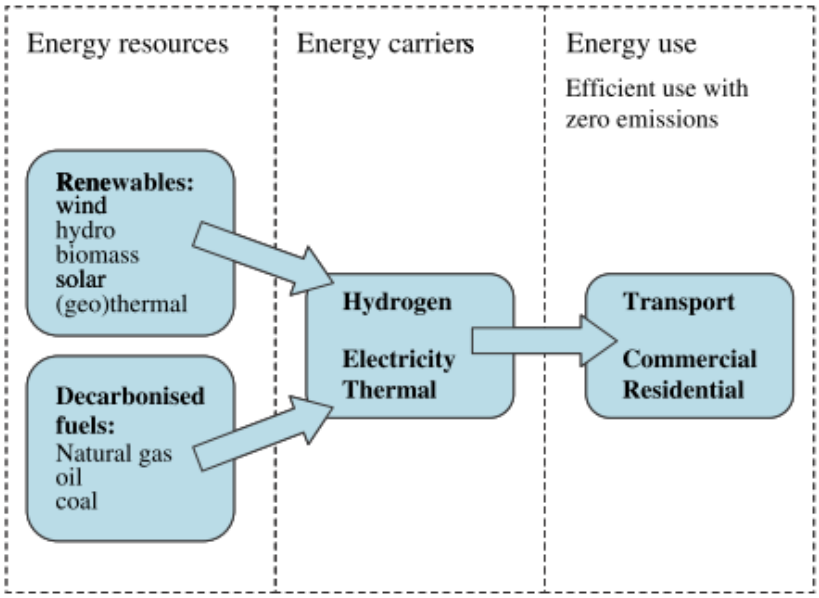

Figure 1 Vision for a Hydrogen based Technology[2]

Figure 1 visualizes the overall vision for a hydrogen based technology. Hydrogen itself is just an energy carrier. Therefore, devices which transform internal energy into electric energy play a crucial role in the whole infrastructure.

The whole hydrogen infrastructure can be broken down into different aspects; hydrogen delivery, hydrogen production, hydrogen storage and the end use of hydrogen. All different fields include their specific safety issues, codes, standards and international partnership. Each of these aspects has to be regarded separately and solutions for each problem have to be found individually. In present, four crucial points which might determine the success or failure of the hydrogen technology are known.

- How can hydrogen be produced by sufficient amounts from renewable energies?
- In which form will hydrogen be transported, either gaseous or liquid?
- How can hydrogen be stored effectively in terms of storage density, cost and safety?
- How can the efficiency be enhanced?

Out of all open points, hydrogen production and hydrogen storage are the most critical points and will be discussed in detail in Chapters 1.4.1 and 1.4.2.

However, hydrogen technology and its applications take a special place in the current market, even though an annual amount of 10.54 billion tons of oil equivalent (2005) are consumed with steady rising tendency.

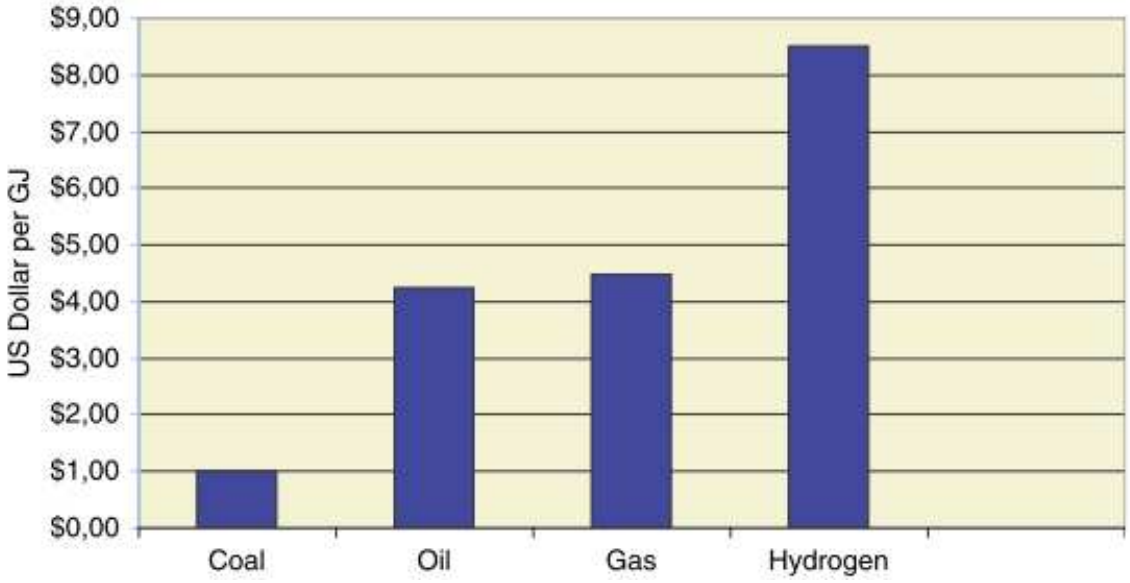

Figure 2 Overview of Fuel Costs [2]

In order to establish hydrogen technology in modern society, one has to focus on innovative and new technologies. Depending on the working conditions, different types of fuel cells are the bridging factor. Hydrocarbons are not a long term solution, whereas hydrogen as a fuel, provided by renewable energies (wind, water and biomass), is the key to a clean environment. Cost plays an important role in the economics. As shown in Figure 2, the gap between costs of fossil resources and hydrogen is big, as predicted. The main reason for that is the inexpensive hydrogen reformation from natural gas. Natural gas as an energy source will be the only possible method to provide for the rising demand of energy for the next decade.

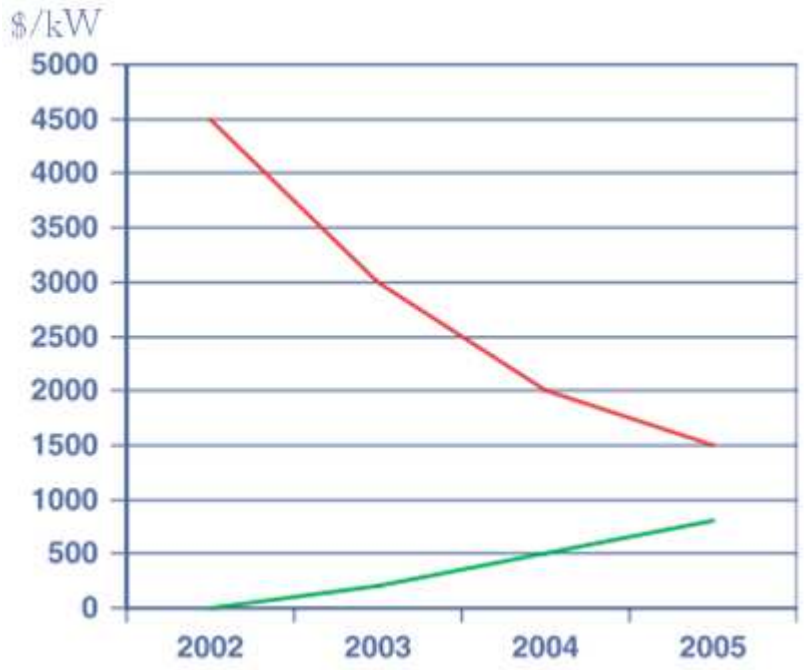

Figure 3 Prize development in $/kW vs. time[2]

Figure 3, above, visualizes the price development of energy provided by hydrogen within the last years. As a result of high scale production processes, the price for energy per unit decreases. Therefore, the goals for industry are clear: Encouragement of high scale production lines in order to adapt prizes of energy made from hydrogen to those on energy made by fossil fuels.

As a short conclusion, hydrogen itself is a promising material as an alternative to fossil fuels due to its physical properties and characteristics. Yet, for a successful transmission into a hydrogen based technology, key problems such as storage and production have to be solved immediately. The success or failure of that technology will depend on the key questions mentioned above [1-3, 6].

1.4. Key areas of Hydrogen Technology

The transition to a hydrogen based infrastructure depends on several factors. Besides cost, which is a major factor in industrial application, technical challenges have to be solved, too. Main factors therefore are hydrogen production and hydrogen storage. Both aspects are supposed to have great influence over the success or failure of the technology.

1.4.1. Hydrogen Storage

As previously mentioned, hydrogen storage is one major aspect of this technology and a great challenge to reach the process of commercialization. Aspects of safety, storage density and reversibility are of main interest in the field of hydrogen storage.

Depending on country and continent, governmental organizations control national and international research. In the United States, the Department of Energy (DoE) oversees that task. It also sponsors different research groups and organizations. In order to integrate alternative fuels successfully into the existing infrastructure, it sets individual requirements and guidelines to each technology. Therefore, the overall aim is to introduce fuel cell powered cars with driving performances comparable to modern gasoline powered cars as soon as possible. Regarding commonly used hydrogen storage systems, it is from major importance to invent methods which allow an equivalent gravimetric and volumetric storage density to existing gasoline tanks.

Due to its physical and chemical properties, hydrogen can be found in various forms, depending on the ambient conditions such as pressure and temperature. The solid state phase appears at low temperatures (11.15℃) with a density of 70.8$\frac{kg}{m^3}$. The liquid phase exists at a small temperature range between the triple point and the critical temperature,

with a density of 70.6$\frac{kg}{m^3}$. The gas phase can be found at higher temperatures with a density of 0.0898$\frac{kg}{m^3}$. Depending on its phases, different methods to store hydrogen are possible [1].

High pressure storage

High pressure storage tanks are the most commonly used storage systems right now and are working in a pressure range of 20- 80MPa. Their volumetric density is 36$\frac{kg}{m^3}$, which is approximately half of that of a liquid hydrogen storage system. Because of their safety issues, these kinds of tanks are inadequate for mobile and portable application.

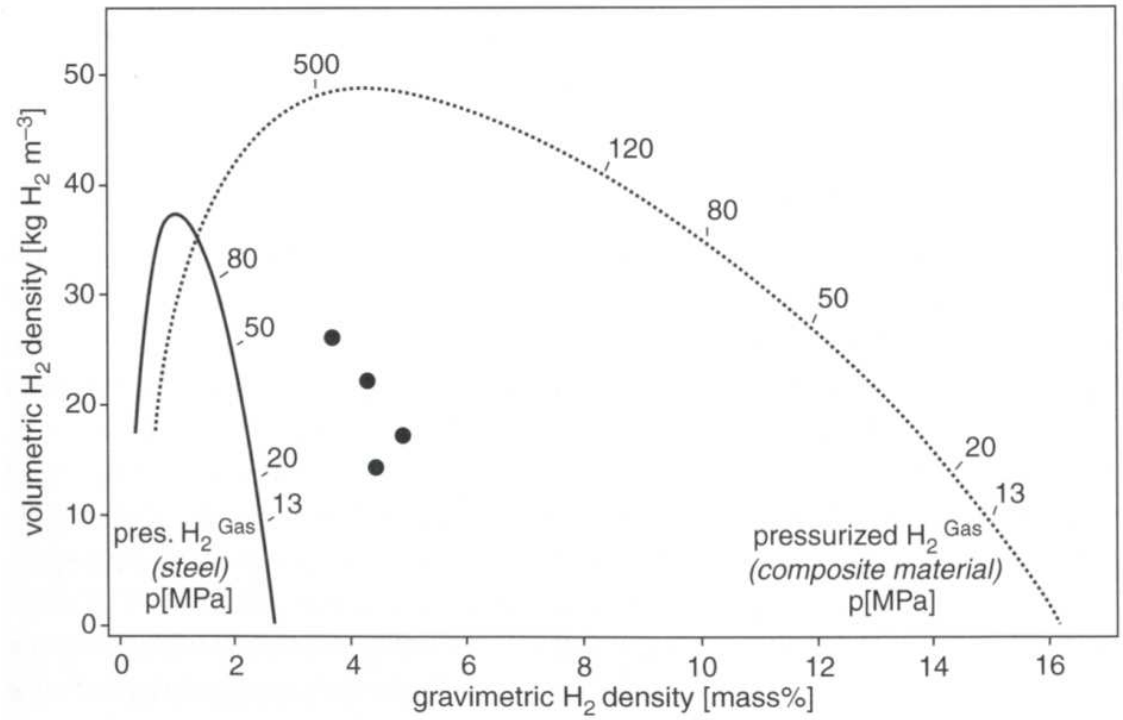

Figure 4 Gravimetric storage density dependent on pressure[1]

Typical for high pressure vessels is the decrease in gravimetric storage density with increasing pressure. An obvious reason for that are thicker walls and the improvement of the factor of safety of the systems.

For stationary application, high pressure tanks are still of major interest. A lot of research work is spent in order to improve existing storage tanks, especially on the use of novel materials. Industry has set itself a goal of reaching a gravimetric storage density of 6wt %, which is about double of the storage density that is reached with common steel vessels.

Another important aspect regarding high pressure storage tanks is the amount of energy used to compress the gas to its final state. The theoretical value for that is given by the following equation

$$\Delta G = R * T * \ln \frac{p}{p_0} \qquad 1.1$$

where G, the free Gibbs energy, R, the gas constant (R= 8.314$\frac{J}{mol*K}$), T, the absolute temperature and p and $p_{0,}$ the end pressure and starting pressure. The theoretical value for a compression from 1MPa to 100MPa is 2.21$\frac{kWh}{kg}$ and is seven times higher in a real process [1, 7, 8].

Cryogenic Storage

Liquid storage methods work at temperatures of 21.2ºK and are an alternative in high scale application to high pressure tanks. Due to their boiling rate and the resulting hydrogen vapor, cryogenic must be open systems, which imply a valve to release gaseous hydrogen. That fact makes them similar to high pressure tanks, unsuitable for mobile and portable application.

Main challenges in this field of research are lowering the boil off rate and the improvement of the liquefaction process. Due to the coexistence of two states, para and ortho, hydrogen needs a special liquefaction treatment: hydrogen needs to be precooled

with liquid nitrogen. During that process, the spin of the electrons change from parallel to antiparallel. As a result, its state changes from ortho to para. Even though the transformation is an exothermic process, it needs to be catalyzed. The catalytic process is realized by precooling with nitrogen down to 35°K. The most common liquefaction process is the Joule Thompson process, developed by Linde, Germany, where the gas first will be compressed and then cooled. After an isenthalpic expansion, some amount of hydrogen liquefies. This liquid hydrogen will be separated from the residual gas [1, 2, 7, 8].

Metal Hydrides

Another hydrogen storage method is the adsorption of hydrogen in solid state materials. Thereby it can be distinguished between physisorption and chemisorptions. Physisorption describes the binding between hydrogen in the gas phase and the solid state phase caused by weak physical van der Waals forces. The interactions have their origins in the fluctuations of the electron distribution of the molecule and the surface.

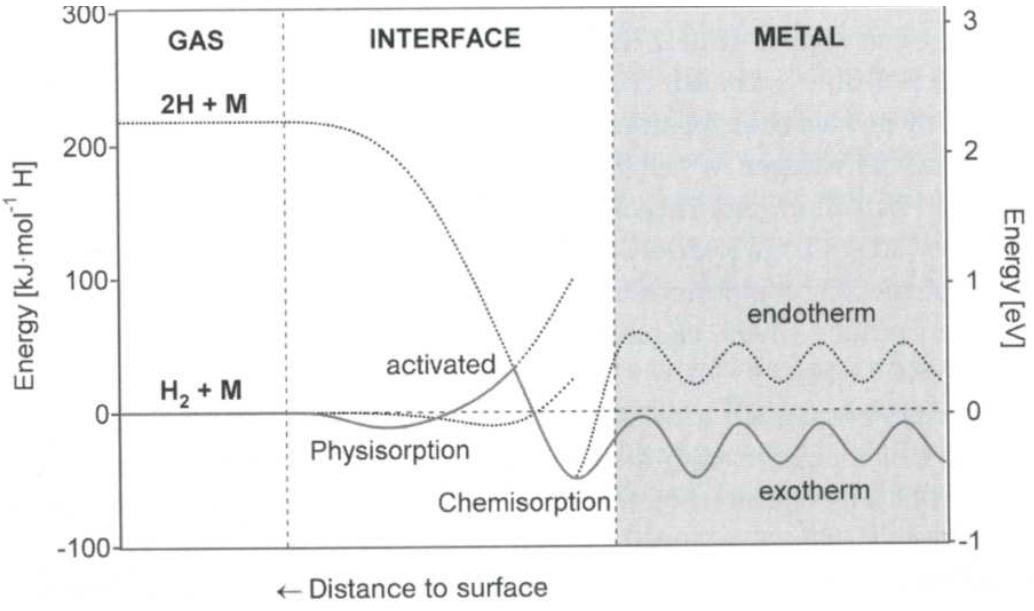

Figure 5 Interaction between Hydrogen and surface [1]

As shown in Figure 5, the interactions between the gas and the solid phase depend strongly on the distance between each other. At a discrete distance between the hydrogen molecule and the surface, the potential energy reaches its minimum. At this point, the bond between hydrogen and the surface is stable. In general, the distance between molecule and surface is approximately 1 atom radius and the energy minimum corresponds to 1-10$\frac{kJ}{mol}$ [1]. Gas adsorption processes caused by physisorption are always of molecular form and take place at low temperatures. Therefore, the maximum storage density is limited by 1 monolayer, the so called Langmuir monolayer, of gas on the surface at temperatures near the liquefaction point.

The second adsorption process is called chemisorption, where hydrogen atoms and surface atoms bond covalently. This process is characterized by stronger bonds than the bonds caused by physisorption.

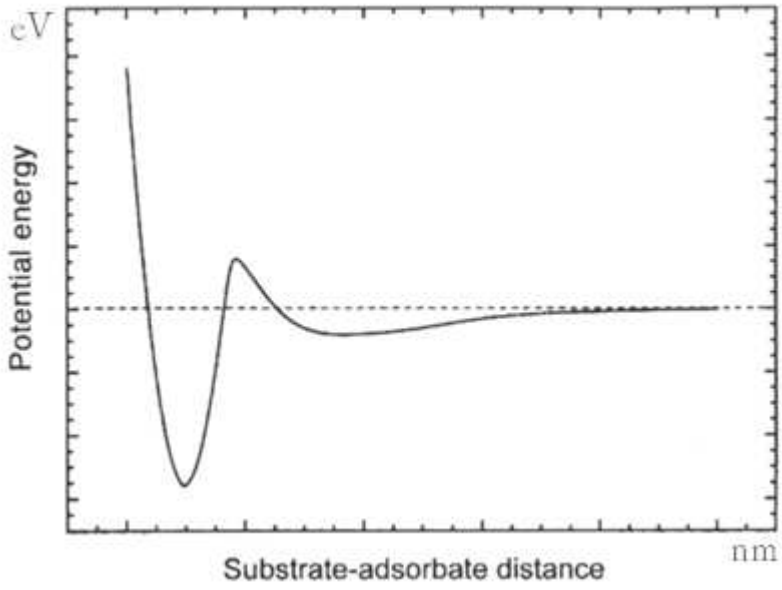

Figure 6 Potential Energy in relation to distance to surface [1]

Figure 6 describes the potential energy between the hydrogen atom and the surface as a function of the distance. The first peak characterizes physisorption processes, which mostly act as a pre- reaction to chemisorption processes, whereas the peak next to the

surface characterizes the bonds of the chemisorption process. It is recognizable, that the distance to the surface is much smaller compared to the physisorbed bond. Comparing the height of the two peaks, which is an indicator of the strength of the bond, it becomes clear that the bond itself is stronger than that of a bond caused by physisorption. In general, physisorption is a precursory process to the chemisorption. Due to their covalent character, bonds caused by chemisorption are much stronger than bonds caused by physisorption and need either an external activation process or high temperatures to take place.

Metal hydrides are a serious candidate as storage materials. In general, a metal hydride is defined by the mode of adsorption of the hydrogen atom into a metal lattice. Depending on the surface atoms, hydrogen can form ionic, covalent or metallic bonds with its partners. As a result, one classifies metal hydrides into different groups, depending on their composition.

- AB_5 ($LaNi_5$)
- AB_2 (ZrV_2,$ZrMn_2$)
- AB_3 ($CeNi_3$,YFe_3)
- A_2B_7 (Y_2Ni_7,Th_2Fe_7)
- A_6B_{23} (Y_6Fe_{23})
- AB (TiFe,ZrNi)
- A_2B (Mg_2Ni,Ti_2Ni)

A and B stand for the metal with strong and weak affinity, respectively, to form a hydride. The reaction kinetics of the hydride formation can be described by a one dimensional potential energy curve shown in Figure 5, which is also called Lennard Jones potential. After overcoming an activation barrier, hydrogen atoms are able to dissolve into the

surface lattice of the material. In that chemisorbed state, the hydrogen atoms can diffuse into the interstitial sites in the bulk without the need of external energy.

Depending on the hydrogen concentration in the lattice, two possible phases coexist. At low concentrations, the α- phase dominates, where H-H interactions can be neglected, whereas at higher concentrations, the β- phase emerges with remarkable H-H interactions dominating.

Regarding to the thermodynamic aspects of a hydride formation, one can state that the solubility of hydrogen into the metal lattice is a function of pressure and temperature in the following relationship:

$$x = \sqrt{\frac{p}{p_0}} * e^{\frac{\Delta S}{k}} * e^{-\frac{\Delta H}{kT}} \qquad 1.2$$

where ΔS the entropy, T the temperature, ΔH the enthalpy, p and p_0 the start and end pressure.

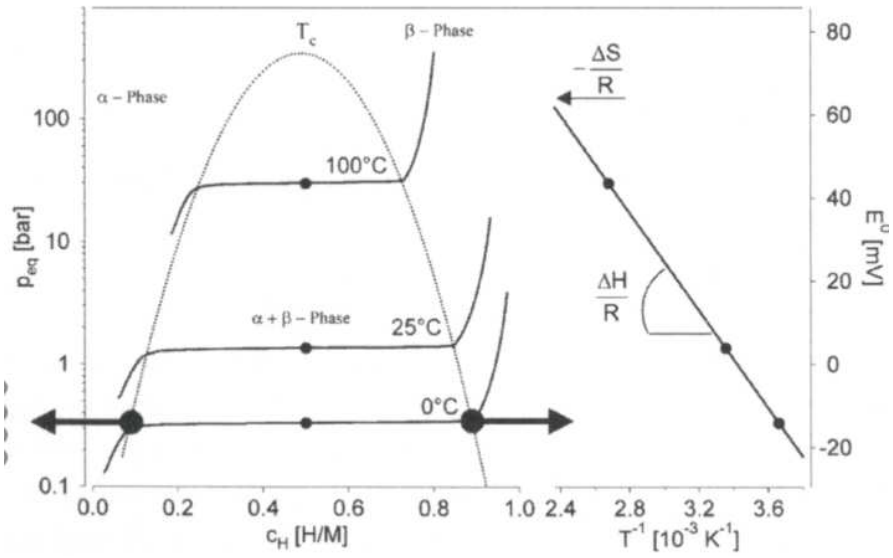

Figure 7 Hydride Formation [1]

The hydride formation can be described in its general form by a pressure composition isotherm. Basically, the curve can be divided into 3 parts. At low hydrogen concentrations, internal pressure increases with only minor hydride formation. With increasing pressure a flat plateau appears, which indicates the formation of the hydride and is characterized by the coexistence of α- and β- phase. At high pressures, the third part describes the hydride behavior at high hydrogen concentrations.

The isotherm also proves the temperature dependency of the hydride formation. Furthermore, the plateau describes the hydride formation,

$$M + 0.5 * x * H \rightleftharpoons MH_X + \Delta Q \qquad 1.3$$

where M stands for the metal, H for hydrogen and ΔQ for heat. This reaction is characterized by the equality of the chemical potential of hydrogen in the two phases, the atomic state and the bond [9].

$$0.5\,\mu^g = \mu^{\alpha,\beta} \qquad 1.4$$

Under consideration of statistical thermodynamics, Equation 1.4 leads to the following expression,

$$\ln\frac{p_{eq}}{p_{eq}^0} = \frac{\Delta H^0}{R} * \frac{1}{T} - \frac{\Delta S^0}{R} \qquad 1.5$$

where ΔH and ΔS stand for the enthalpy and entropy, respectively, p and p^0 for the start and end pressure, respectively and R for the gas constant [9].

Plotting this curve in terms of p over 1/T leads to a curve presented in Figure 8 called van't Hoff plot.

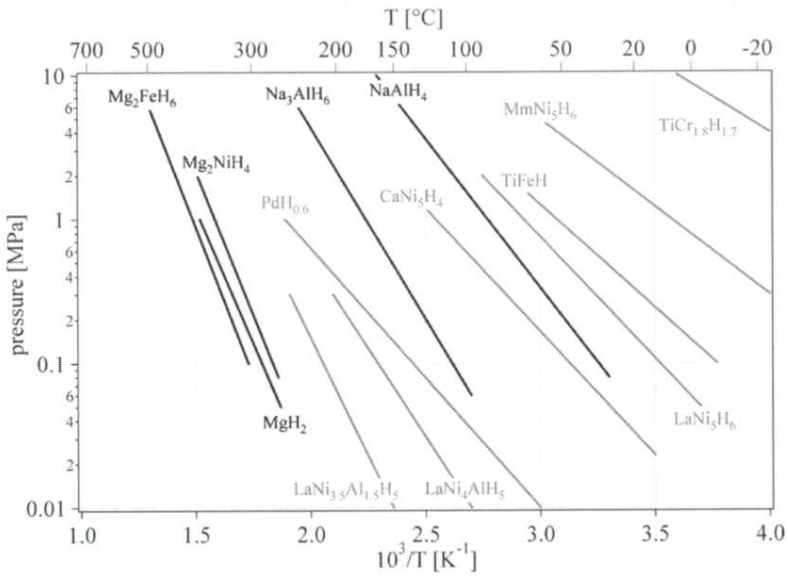

Figure 8 Van't Hoff Plat of different Hydrides [1]

The slope of the curves is equal to the change of enthalpy divided by the gas constant, R, as shown in Figure 8. Furthermore, the intercept of the curve is equal to the change of entropy divided by the gas constant. Interpreting both terms entropy and enthalpy, one comes to the conclusion that the entropy characterizes the stability of the M-H bonds, whereas the enthalpy describes the heat evolution.

It is known that general hydrides are not able to fulfill all the guidelines given by the DoE, such as

- Reversible storage density ≥ 6wt %
- Cost: ≤133$/kg H_2
- Cycle lifetime ≥1000 for mobile applications
- Working temperature -30≤ T ≤ 100℃
- Safety codes and standards

Therefore, research leads to more complex structures and mixtures of metal hydrides. As a result, doping of hydrides with alloys has been established as a common used method to improve the properties of the hydrides.

In principal, three different doping methods are possible:

- Doping of presynthesized material with an doping agent
- Direct synthesis of the hydride under dopant presence
- Hydrogenation of Al-Ti with hydride precursors

Aspects such as the amount of dopant, preparation process and reaction time are of major relevance for the improvement of the physical properties of hydrides. A prime criteria for the applicability of metal hydrides as a storage medium is the dissociation and reversibility in the required temperature range. Since many structures already fail that requirement, sodium alanate has been established as a potential storage candidate. A potential material seems to be Ti doped sodium alanate.

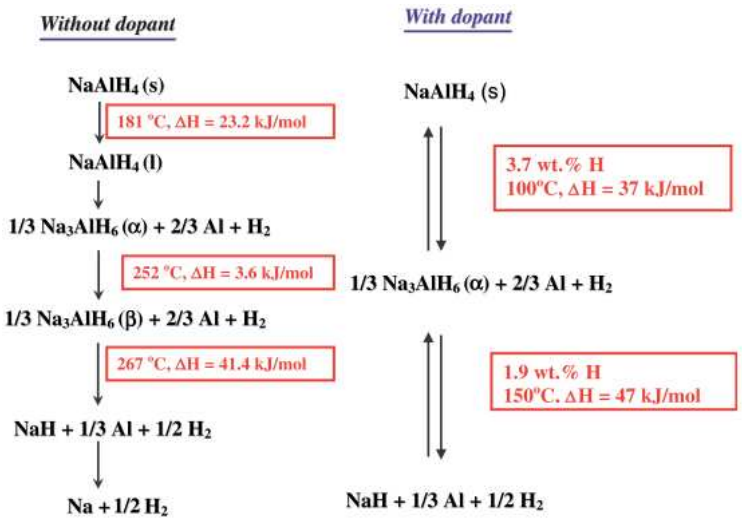

Figure 9 Desorption Kinetics of $NaAlH_4$ [2]

Figure 9 demonstrates the transition from $NaAlH_4$ to Na and NaH, respectively. The decomposition of the tetrahydride to the pure element without a dopant starts with melting of the material at 186℃. Then, the melt de composes to release hydrogen at a

temperature of 240℃ by forming the hexahydride. At a temperature of 270℃, the hexahydride decomposes under H_2 to release sodium hydride. In a last step, at 450°C, the hydride decomposes into its elements, sodium and hydrogen. The reaction of the doped tetrahydride shows significant differences in its kinetics. Unlike undoped material, this decomposition takes place in two steps and under more moderate temperatures. The tetrahydride starts decomposing at a temperature of 100℃ and releases 3.7wt % of hydrogen. In that point, two phases coexist, Na_3AlH_6 and the Al phase. In a second step, the hexahydride decomposes at a temperature of 110°C to its final state NaH and release 1.9wt % of hydrogen.

Even though the amount of desorbed hydrogen cannot be improved by adding a dopant agent, doping still has a great influence. As shown in the presented example, titanium doping leads to a significant decrease of desorption temperature, which is an important aspect for industrial application. Furthermore the reaction kinetics can also be improved by adding a dopant to the material [1, 2, 7-9].

1.4.2. Hydrogen Production

Hydrogen as a raw material is of high importance in many different industries (e.g. chemical-, pharmaceutical-, electrical industry). Moving away from a fossil fuel based infrastructure to a hydrogen based infrastructure will cause a dramatic increase of hydrogen demand. Therefore factors like feedstock, availability, costs and product purity control the selection of hydrogen and its production process.

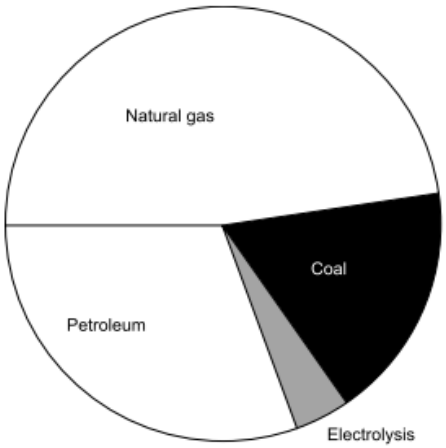

Figure 10 Distribution of Hydrogen Production Sources [3]

Figure 10 depicts the current world's distribution of resources for hydrogen production. One can clearly see that 78% of the world's hydrogen production is provided by hydrocarbons such as natural gas, coal or raw oil. In present, only a small amount of hydrogen is synthesized by sustainable processes such as water electrolysis or other "clean" methods. From an economical point of view, hydrogen from hydrocarbons is the cheapest opportunity due to the small energy amount used during the production process. Natural gas, a light hydrocarbon, is the most used raw material for the hydrogen production. In principle, three methods have been established for industrial hydrogen production and will be discussed in detail in the following [4, 10, 11].

1.1.1.1. Steam Methane Reforming (SMR)

Steam Methane Reforming is one of the major manufacturing methods for the hydrogen production. More than 40% of the world's hydrogen production is manufactured by SMR.

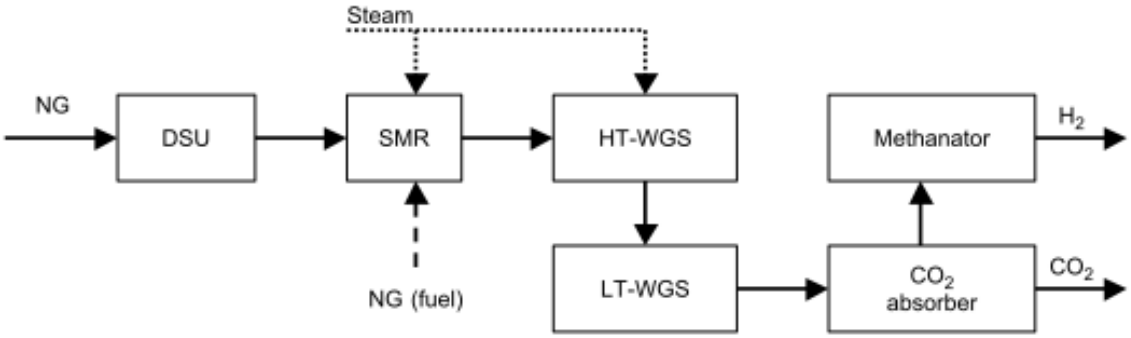

Figure 11 Steam Methane Reforming Cycle [2]

Figure 11 shows a general build up of a SMR plant. Main stages of a SMR are desulfurization, catalytic reforming, CO conversion and gas separation.

The catalysts in the reforming chamber and in the shift chamber are from high sensitivity against sulfur. Therefore, sulfur organic compounds in the natural gas need to be converted into H_2S by a hydrogenation reaction. This process takes place prior to the reforming process itself in order to avoid toxication of the catalyst. After that, the desulfurized natural gas is fed into a second chamber, where it is mixed and reformed to hydrogen. According to the following reaction,

$$CH_4 + H_2O \rightarrow 3H_2 + CO \qquad \Delta H = 206\frac{kJ}{mol} \tag{1.6}$$

hydrogen will be reformed in an endothermic reaction. In a second reaction, called water shift reaction, toxic CO is converted into CO2 represented by the following equation.

$$CO + H_2O \longrightarrow CO_2 + H_2 \qquad \Delta H = -41.2\frac{kJ}{mol} \tag{1.7}$$

In a last step, hydrogen is purified and separated from other byproducts. CO and CO_2 as waste products were fed into a methanation reactor where they were converted to CH_4 [1, 4, 9-11].

1.1.1.2. Partial Oxidation (POx)

Partial Oxidation is the second major hydrogen production process on a high commercial scale using hydrocarbons as feedstock. In that process, fuel and oxygen are combined in proportions that the fuel is converted into hydrogen. Basically, one can distinguish between catalytic and non- catalytic partial oxidation. Catalytic POx usually works at a temperature range of 600- 900℃, whereas the non ca talytic POx works at temperatures of 1100- 1500℃. In both cases, both heavy and ligh t hydrocarbons can be used to produce hydrogen due to the high working temperatures. The overall equation of the POx reforming process can be written as

$$C_m H_n S_p + \frac{m}{2} O_2 \rightarrow \left(\frac{n}{2} - p\right) H_2 + mCO + pH_2S \qquad 1.8$$

The equation indicates that the feedstock contains sulfur groups. Unlike SMR, these groups do not need to be removed from the feedstock. During the reforming process, these sulfur groups combine to H_2S and will be removed from the product in a later separation process.

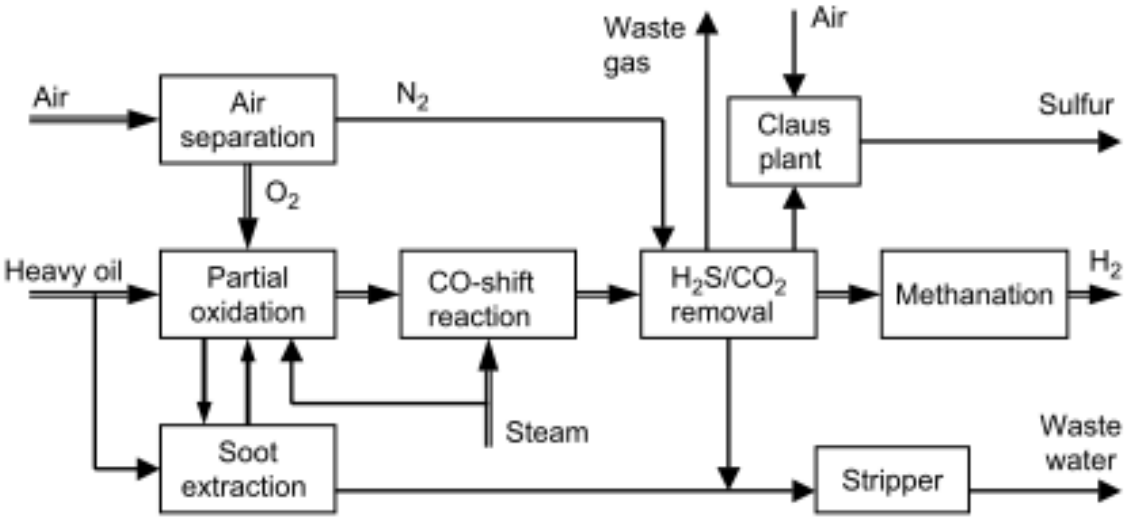

Figure 12 Partial Oxidation Cycle [2]

Figure 12 shows a general composition of a reforming facility. After the partial oxidation, which is the first step of the reforming process, the CO shift reaction takes place. This reaction converts the toxic CO to CO_2. In a later process, the residual CO_2 can be converted into CH_4, which acts as the fuel for the SMR. Afterwards, the toxic sulfur groups and the CO_2 are separated from the hydrogen [2, 4, 10-12].

1.1.1.3. Water electrolysis

The electrolysis of water is a promising alternative to both Steam Methane Reforming and Partial Oxidation. The advantage of this method is clear: Unlike POx and SMR, the electrolysis of water is a zero- CO_x emission process, and therefore an important step towards a hydrogen based infrastructure.

Even though, electrolysis is less cost effective than both other production processes, it is obvious why the following aspects outline the importance the importance of this technology

- Water is more abundant than hydrocarbons are.
- Costs must be seen in the overall system
- Electrolyzer may be embedded into existing systems
- Electrolysis is a long term solution

Taking these aspects into the overall system, electrolysis becomes interesting not only for niche applications, but also for high scale commercial applications. The basic principle of electrolysis is the dissociation of water into its elements hydrogen and oxygen. Basically, one distinguishes between two possible electrolyze methods, the solid polymer electrolyte method and the liquid electrolyte method. Both methods share the same principle but differ in the electrolyte. The following will discuss the working principle method in detail.

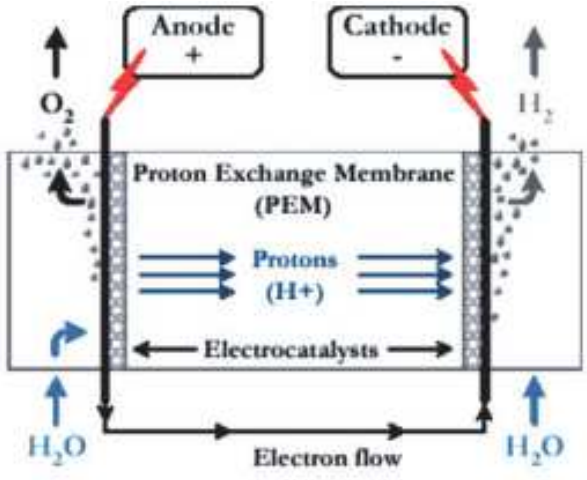

Figure 13 Working Principle of the Electrolysis [2]

Figure 13 depicts the general buildup of a liquid electrolyzer. At first glance, the general build up seems to be simple, with the main parts being a membrane, two electrodes and the electrolyte. Basically, the electrolyzer is a fuel cell, working in reverse mode. Between cathode and anode lies a potential, which initiates the ion movement in the electrolyte, depending on their charge. The O^{2-} ions are forced to the anode, whereas the H^{+} ions are forced to the cathode. As a result, oxygen ions and hydrogen ions are separated in the membrane and accumulate at their electrode. At the electrode, the ions neutralize and form H_2 and O_2 molecules, respectively. In a following step, both gases are purified and channeled to a storage tank.

The principle of water electrolyze is a long known process, and as a result, modern processes are highly optimized. In present, modern electrolyzers reach efficiencies of 75% and are able to convert more than 100kg hydrogen per hour with a high purity (99.999%). Based on that, electrolyzers seem to be a promising alternative hydrogen production method to SMR and POx [1, 4, 9-12].

1.5. State of Art and Future Challenges

The transition to a hydrogen technology based infrastructure requires a general concept beginning with the production of hydrogen to the point of energy conversion and energy storage. As previously mentioned, hydrogen production and hydrogen storage will be the two key aspects determining the success of this technology.

Modern hydrogen production methods can be distinguished between fossil fuel based production processes and renewable energy based production processes. In present, mainly fossil fuel based methods are used for high commercial production. These techniques are on the latest standard and work with high grades of efficiency. As

a result, existing technologies can hardly be upgraded, so a significant CO_2 reduction should not be expected by developing new techniques. The only alternative to reduce CO_2 emission in the production process is a transition to a renewable energy based production concept. In present, many concepts are auspicious and might be a serious alternative to current production methods. Particularly, the combination of water electrolysis with wind, solar or nuclear energy seems to be a promising alternative. These techniques are, because of the current state of art, the only possibilities to produce “green” hydrogen. Compared to fossil fuel based production methods, all other methods are relatively undeveloped and cannot accommodate the hydrogen demand. High scale applications are either too expensive or their grade of efficiency is too low to ensure a constant hydrogen supply.

Hydrogen storage is the second major challenge to a hydrogen based infrastructure. Especially for mobile applications, storage is still a critical aspect because both, high pressure and cryogenic storage systems, due to their safety risks, are not preferable.

High Pressure Storage Systems

High pressure vessels are commonly used storage systems for stationary application.

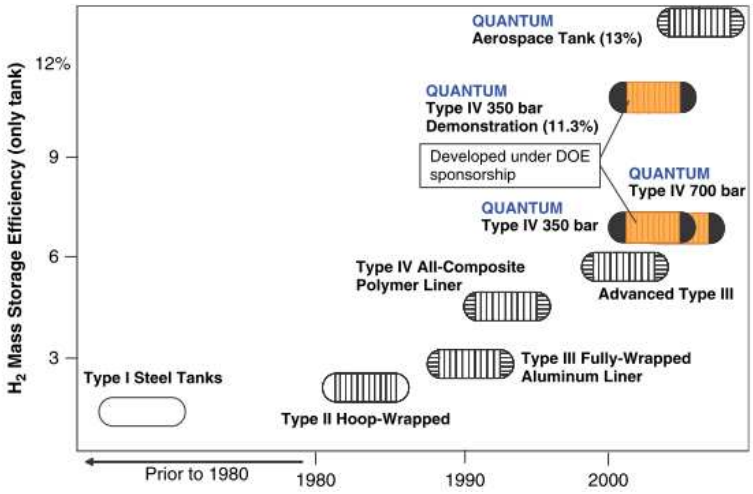

Figure 14 Development of High Pressure vessels [1]

Figure 14 depicts the development of modern high pressure vessels within the last 50 years. The transition from Type 1 steel vessels to lightweight polymer and fiber vessels enabled permanent new areas of application. Modern fiber vessels can hold a pressure up to 1000MPa, which is a factor of 10 more than commonly, used steel vessels. In the course of time, the requirements of storage tanks have changed. Modern hydrogen tanks need to fulfill regulations given by industry and governmental institutions.

- Compatibility to hydrogen
- Compatibility to extreme temperature changes (-50°C to +85℃)
- Compatibility to variety of pressurization modes
- Resistance to external corrosion
- Safety

In order to fulfill these requirements, polymers and fibers were developed which allow higher pressures and higher storage densities compared to steel vessels. It is still unclear if these systems will replace current vessels because mass production, which would lead to a cost reduction, is not yet guaranteed. Furthermore, standards and clear guidelines to suppliers and systems do not exist, which results in unreliability of current systems [1, 2].

Cryogenic Storage Systems

Besides high pressure vessels, cryogenic storage tanks found their way into commercial applications. Due to their high storage density and their cost efficiency, cryogenic tanks are a serious alternative to high pressure tanks in stationary applications. Due to their safety risks, no high scale mobile application based on this storage method is planned.

One main challenge connected with these systems is the minimization of heat leaks, which cause evaporation of hydrogen gas. In applications with long stand by periods, this can result in dramatic fuel loss. For cryogenic systems, weight is an even more

challenging aspect since many peripheral devices are required to guarantee a working system. Since the gravimetric storage density is related to the weight of the whole system, development of lightweight materials such as aluminum alloys are of high importance. The safety issue is a major aspect for cryogenic storage systems as well as in high pressure tanks. Basic requirement of low temperature tanks are the following:

- Double walled cladding
- Withstand extreme temperatures (-250℃)
- Withstand high vacuums
- Compatibility against outer influences (mechanical, chemical)

Existing commercial vessels share a storage capacity of 5kg- 12kg and consist of two walls which are perfectly adapted to the conditions. Modern refueling stations prevent the boil off by sucking evaporated hydrogen to the station during the refilling process. There, the hydrogen gas is stored, liquefied and transported back to the customer.

For a successful implementation of a hydrogen based infrastructure, improvements in areas of thermal management, pressure behavior and materials have to be made [2].

Metal Hydride Storage Systems

Another possibility to store hydrogen effectively is the solid state metal hydride system. In present, over 200 different materials are found, analyzed, and characterized in terms of hydrogen adsorption, reaction kinetics and material costs.

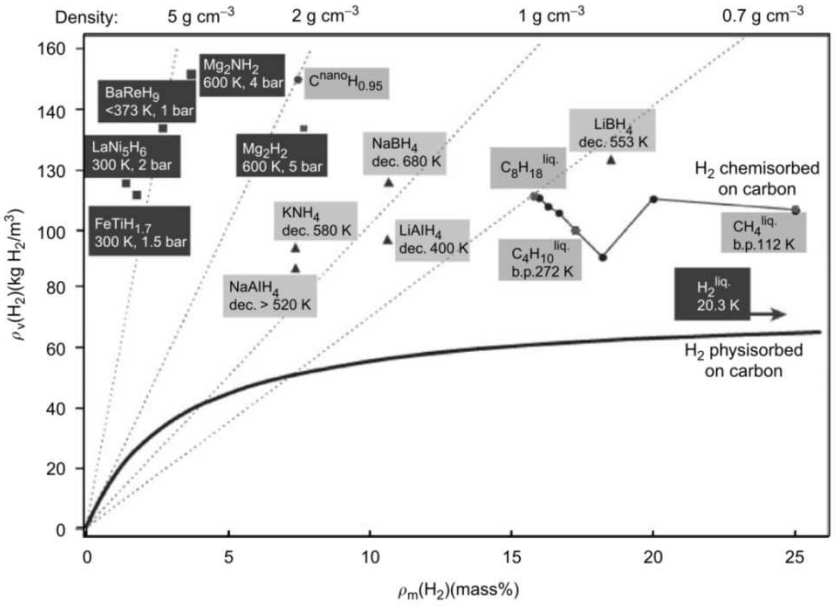

Figure 15 Overview of existing Materials [12]

Figure 15 shows a brief overview of existing materials and their storage capacity. Requirements given by industry and governmental institutions already exclude many of these materials as a potential candidate for mobile application. Besides finding a fitting material which fulfills all requirements, technical challenges such as thermo management, volume change and hydrogenation rates need to be solved as well. Currently, no material has been found, so the search for alternatives has begun [1].

Borates

Borates, metal organic frameworks and zeolites might be an alternative to metal hydrides. Borates are chemical compounds which are based on a reaction of a metal with boron in a hydrogen ambience. A general equation can be written as follows

$$M + B + 2H_2 \rightarrow M[BH_4] \qquad 1.9$$

where M is the metal and B is the chemical symbol for boron. The general structure of these compounds is not yet clearly described due to controversial results between X-ray and neutron diffraction, but promising results in terms of storage density and desorption kinetics could be achieved [1]. The bond between the metal atom and the boron atom is of main interest because it characterizes the stability of the borates. Since this bond is of covalent character, all existing borates have a high stability, as shown in Figure 16.

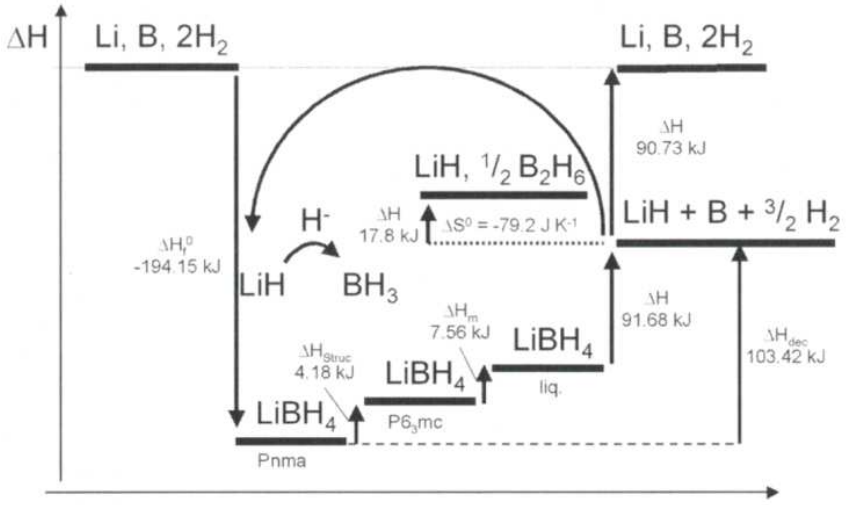

Figure 16 Decomposition Kinetics for Lithiumborate [1]

Figure 16 also describes how borates decompose. Lithiumborate decomposes reversibly under hydrogen adsorption to the stable LiH. In present, Borates are not usable for commercial application due to their unfavorable thermodynamics and their inadequate storage density [1].

Zeolites

Zeolites, which are 3 dimensional silicate structures with isomorphous replacement of Si^{4+} ions with Al^{3+} and SiO_2, ought to be another alternative to metal hydrides.

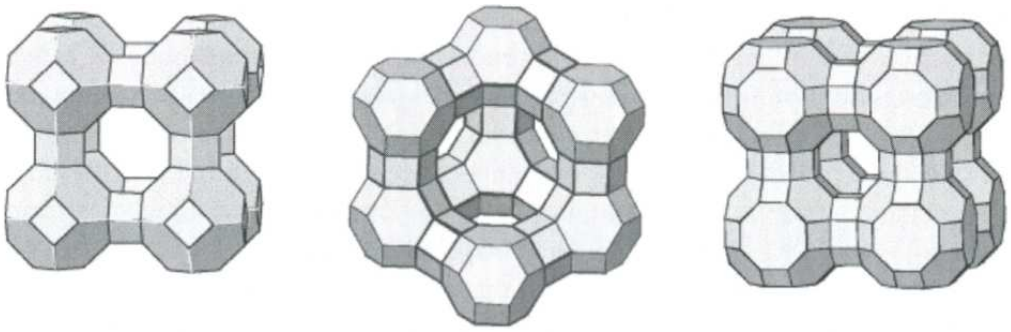

Figure 17 Structure of Zeolites [1]

Figure 17 shows the general structure of possible zeolites, where the corners represent aluminum or silicon atoms and in between oxygen atoms, which bridge neighboring Si/Al atoms. These high porous structures are able to adsorb and desorb molecules such as hydrogen in their structure. Zeolites will probably not find their way into commercial scale application. The storage density of these materials lies between 0.3% - 1% depending on the temperature, where 0.3% is reached at room temperature. These materials might find their utilization in low temperature niche applications [1].

Metal Organic Framework

Metal organic frameworks (MOF) are porous polymeric structures which consist of metal ions linked together through organic ligands.

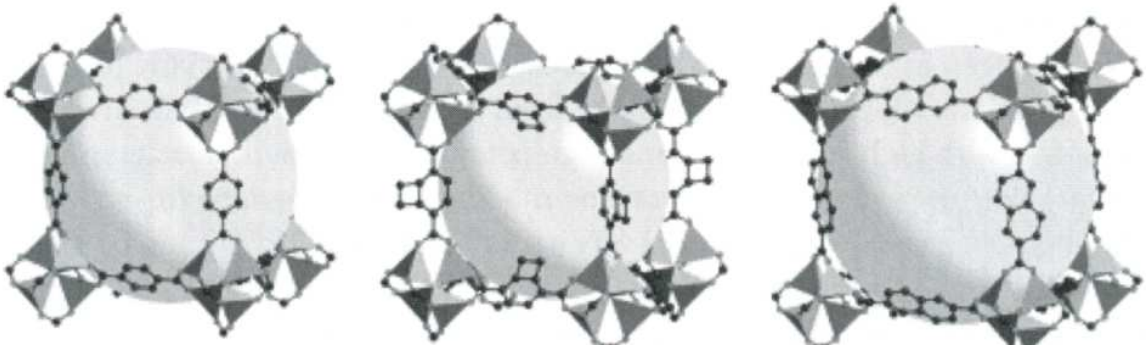

Figure 18 Structure of Metal Organic Frameworks (MOF) [1]

Figure 18 depicts 3 different MOF structures where molecules such as hydrogen can be absorbed into their structure. Each of these suprahedron structures is hold together over organic chains to form complex cubic structures. Similar to zeolites, MOF might not find their way to high scale mobile application due to their reaction kinetics. Unlike zeolites, MOF reach storage densities of 4.5%, but under a temperature of 78℀K, which is too low for mobile application. At room temperature, the storage density decreases to 1% at ambient pressure of 20bar.

Due to the lack of knowledge, especially in the field of zeolites and MOF, it is hard to predict their future place in a hydrogen based infrastructure. Their complex structures give the possibility to investigate an infinite number of new structures, where some might be applicable for mobile application. Therefore additional research work has to be done in the near future [1, 4, 6-8, 10, 11].

1.6. Hydride production methods

In principle, metal hydrides can be synthesized based on chemical reactions or in a mechanochemical way. Both methods are described in detail in the course of the chapter. In general, metal hydrides are highly reactive with water and moisture. Therefore, it is of high importance to prepare all hydrides in an inert gas atmosphere. Preferred are all noble gases, particularly nitrogen or argon for two main reasons: their low affinity to react with the material and their low thermal conductivity.

1.6.1. Chemical Synthesis

1.6.1.1. Description

Standard glassware used for handling under inert gas is called Schlenk Glassware, named after its innovator, Wilhelm Schlenk. The basic buildup of a Schlenk line is depicted in Figure 19.

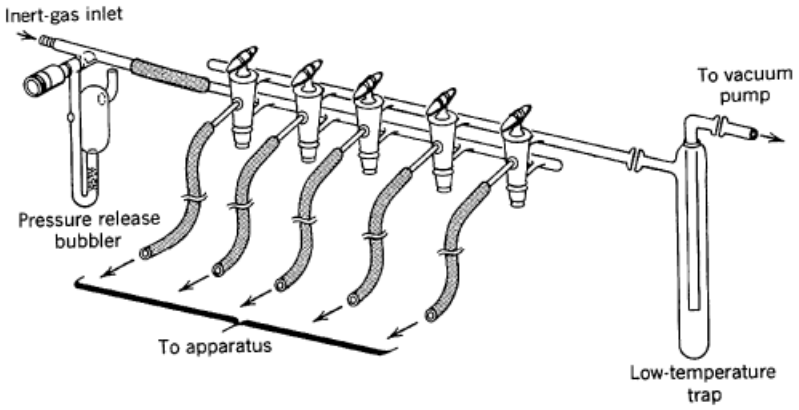

Figure 19 Schlenk Glasware apparatus[2]

The Schlenk line consists of several glass tubes and plugs, depending on the size of the line. On the one side, the line is connected over a valve with the purge gas vessel. On the other side, a vacuum pump is connected to the line in order to ensure the evacuation

of the apparatus. Many commonly used Schlenk lines also have a low temperature trap which additionally cleans the inner atmosphere from residual gases and moisture.

The synthesis of hydrides requires an extreme clean inert atmosphere because already traces of moisture will cause effects on the purity of the sample. Several standard methods have been developed in order to dry the inner system of the apparatus. One possibility is the evacuation and then the refilling of the apparatus with purge gas. This procedure will be repeated until the desired quality of inert atmosphere is reached. Another standard method is the evaporation of residual moisture by heating all parts to 130˚C. In most cases, a combination of both methods is used to prepare the Schlenk line for a metal hydride synthesis. Therefore, all tubes and connections were heated and then plugged. This process is followed by an evacuation and refilling cycle until the desired inert atmosphere can be provided [1, 2, 7].

1.6.1.2. Synthesis of Hydrides

The chemical synthesis of metal hydrides is based on the equilibrium between the hydride phase and the precursor phase and will be discussed in the following by the example of sodium aluminum hexahydride.

The synthesis of the metal hydrides can be done either in a double step reaction given by following reaction equation

$$Na + Al + 2H_2 \rightarrow NaAlH_4 \qquad 1.10$$

$$NaAlH_4 + 2NaH \rightarrow Na_3AlH_6 \qquad 1.11$$

or in a single step reaction as described below.

$$3Na + Al + 3H_2 \rightarrow Na_3AlH_6 \quad 1.12$$

Both procedures result in the same product but differ in the reaction conditions. Observing the 2 step reaction, the first reaction step takes place at temperatures of 270°-280℃ and a pressure of approximately 175bar, where as the second step takes place at a temperature of 165℃ and a pressure of 140bar occ urs. In contrast, the direct synthesis of Na_3AlH_6 takes place at a temperature of 165℃ but a pressu re of 350bar. In the beginning of the 2 step reaction, precursors sodium, aluminum and hydrogen react in a tetrahydrofuran solution to $NaAlH_4$ as described in Eq. 2.1 to $NaAlH_4$. The resulting material, $NaAlH_4$, is purified and separated from the precursor material. Afterwards, ether will be added to the solution, which causes sedimentation of $NaAlH_4$. In a last step, $NaAlH_4$ is going to be vacuum dried and a white crystalline powder from high purity remains as product. In the second step, the final product, Na_3AlH_6 will be synthesized from the two precursors $NaAlH_4$ and NaH in a heptane solution based on Equation 2.2 under discrete outer conditions.

The final product is again separated from the solution in order to receive the end product. Filtration and vacuum drying are the last steps for the chemical synthesis of the metal hydride. The chemical synthesis results in a white metal hydride powder from high purity which can be analyzed depending on its claims. Metal hydrides as a commercial storage product need to be doped with alloys in order to adjust the physical properties to the working conditions.

For chemical doping, the metal hydride will be mixed with the dopant in an ether solution. In most cases $TiCl_3$ acts as the dopant precursor and forms in a chemical reaction the titanium doped Na_3AlH_6. As a reaction product between the two precursors, hydrogen is formed and fumigates from the solution. As soon as the hydrogen evaporation stops, the reaction equilibrium is reached and the overall reaction comes to an end as well. In a last

step of the synthesis, ether is removed and the residual end product powder vacuum dried. The resulting product is a Ti- doped Na_3AlH_6 powder [1, 7-9].

1.6.2. Mechanochemical Synthesis

Besides the chemical synthesis, mechanochemical synthesis emerged as a second synthesis method due to its high grade of simplicity. High energy ball milling is an easy and effective method to produce many nanoscale metal hydride powders. The milling process has significant impact on the later product and has to be chosen carefully. One distinguishes between different variances of ball milling.

Mechanical alloying describes the generic term of mixing and milling different powder in order to improve their physical and chemical characteristics, respectively. During that process, the material can either change its state from solid to any other state or it can stay in its original state. The change of state can be influenced by several parameters such as energy, material, or ball milling time.

Another form of ball milling is mechanical milling. Unlike mechanical alloying, where material transfer is obtained, mechanical milling only leads to a change in grain size and surface area. A main advantage of this method compared to mechanical alloying is the reduction of milling time. Gaining the same effects as mechanical alloying processes, the process time is reduced by 50%, which results in increased quality and purity of the sample.

Reactive ball milling is a process connected with a chemical solid state reaction. This method is attractive for the metal hydride synthesis. Precursors of the metal hydride are charged together in their molar ratio and milled under a hydrogen atmosphere. During the chemical synthesis, high effort has to be spent on a clean system because existing traces of impurities can have dramatic effect on the final product. The reactive ball milling

method enables a riskless way to synthesize complex hydride structures. Additionally, doping of the material with catalyst can be realized with this method as well [2].

1.6.2.1. Description

Chemical synthesis is generally time consuming and could become complex, whereas ball milling is an easy and effective way to produce nearly every possible metal hydride composition. The precursors are mixed in the desired ratio and loaded with the graining balls in a vial. Special attention has to be paid to the material of both, balls and vial. During an unclean synthesis, samples could be cross contaminated by vial and milling medium. Therefore, the material of vial and balls has to be chosen carefully in order to minimize impurities. Vial and balls should be made of a material which is nonreactive with the sample material but also harder than the material itself.

During the milling process, the powder is trapped between the balls or between vial and balls. As a result, plastic deformation occurs which is linked to an increase of the particle temperature. Another outcome of the collisions during the milling process is fracturing of particles which results in an increase of the reaction rate of the material [2, 7, 8].

At this point a phase transition and the process of alloying takes place. Depending on factors such as rotation frequency, ball to powder weight ratio, milling time or number of balls, median grain sizes of 1-100nm can be controlled synthesized. Different types of ball mills have been established for laboratory applications. Nanoscale metal hydrides were mostly produced with planetary ball mills. In these mills, the balls and the vial rotate around their own axis on a counter rotating disc, as displayed in Figure 20.

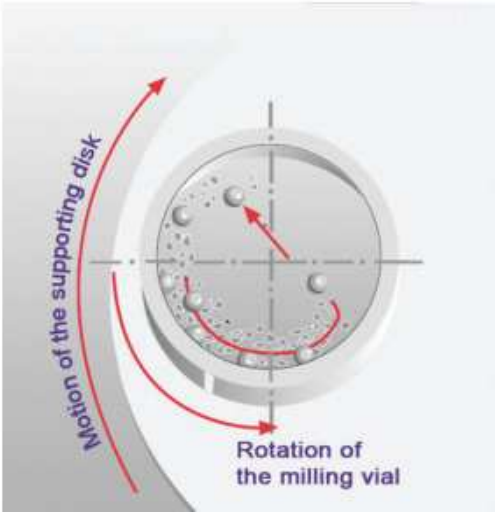

Figure 20 Planetary Ball Milling Method [2]

Shaking ball mills are another commonly used form, where balls and vial swing in a complex motion combined with a forward and backward motion, as illustrated in

Figure 21 Shaking Ball Milling Method [2]

Figure 21. Since the hydride formation is a temperature and pressure dependent process, conditions in the vial are of major interest. Telemetric sensors in the vial have been developed in order to provide information about inner conditions, even if the vial is in motion. Pressure and temperature signals were transmitted via radio signals to outer parts of the mill and can be analyzed in real time. These data give information about the impact of pressure and temperature on phase transition [2, 7, 8].

1.6.2.2. Important Parameters

Parameters such as ball milling time or the addition of catalysts have significant influence on the hydrogen desorption behavior. In the following, the impact of these parameters on the behavior of discrete examples is presented.

1.6.2.2.1. Particle Size

Particle size is a parameter, which can be controlled by varying the ball milling time. In general, size decreases exponentially with the milling time. After few minutes of ball milling, particle sizes of a few microns can be reached. However, in the early years of hydride research, MgH_2 was expected as one of the promising storage materials due to its high storage density of 7.7wt %.

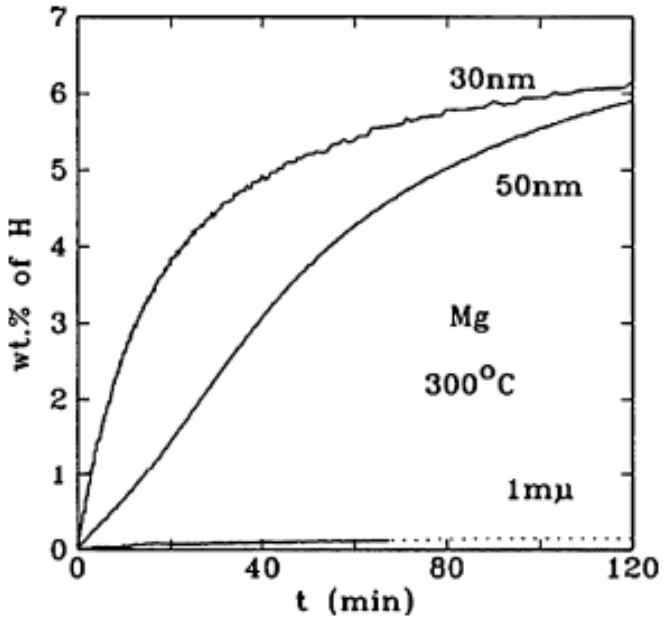

Figure 22 Influence of Particle Size on Desorption Kinetics[2]

Figure 22 depicts the hydrogen adsorption as a function of time. In this experiment three samples have been analyzed, which differed from each other in their grain size (1µm, 50nm and 30nm). The diagram shows the enhanced adsorption dynamics of the sample

with the smallest grain size. Regarding the hydrogen adsorption at 120 minutes, samples with a grain size of 30nm and 50nm absorbed ~6wt. %, whereas the third material showed no significant hydrogen adsorption. Comparing the first two samples with each other, the optimized reaction kinetics can be recognized. At the first sample, 90% of the whole hydrogen is adsorbed after 60 minutes, whereas at the second sample 85 minutes passed until it reached an equivalent value for hydrogen adsorption [2].

1.6.2.2.2. Catalytic Dopants

Dopants such as titanium or vanadium are commonly used methods to improve the reaction kinetics and thermodynamics of a metal hydride. Sodium alanate is a complex metal hydride, with sodium and aluminum as its host material. Its ability to store reversible 5.6wt % hydrogen under moderate condition made it a promising material, especially for mobile applications in the beginning of hydride research. It decomposes in two steps, as shown in the following reaction,

$$3NaAlH_4 \rightleftharpoons Na_3AlH_6 + 2Al + 3H_2 \rightleftharpoons 3NaH + Al + 1.5H_2 \quad (1.13)$$

where the first reaction takes place at 33℃ and th e second reaction at 110℃. By adding a dopant, in this case $TiCl_3$, into the reaction, it is supposed to change the thermodynamics of the reaction. Therefore, the dopant is added and mixed with the material and reacts with the hydride

$$3NaAlH_4 + TiCl_3 \rightarrow 3NaCl + Ti + 3Al + 6H_2 \quad (1.14)$$

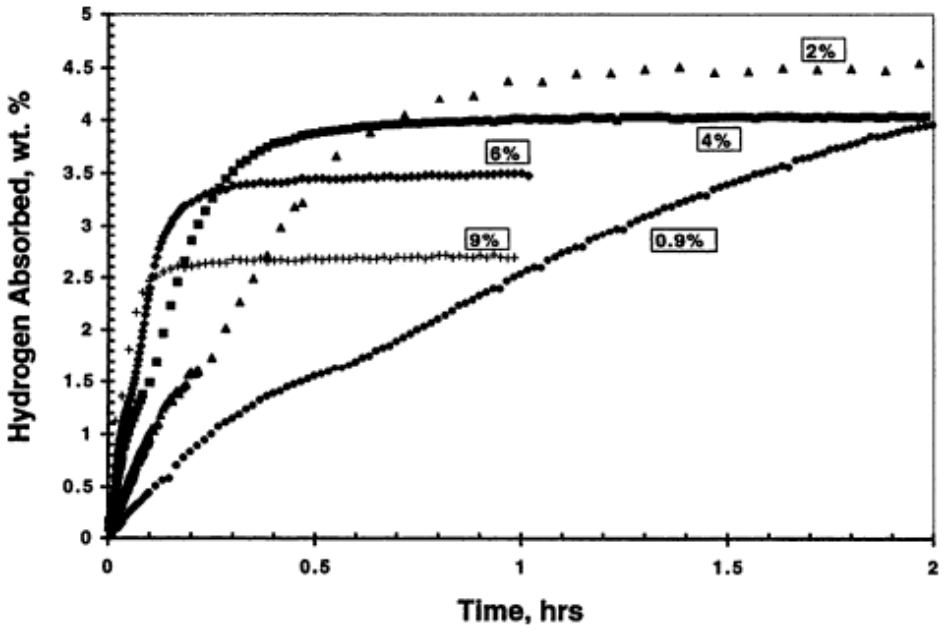

Figure 23 Influence of Dopant ratio[2]

Figure 23 shows the adsorption behavior of different samples depending on time. The samples are distinguished from each other by the amount of the dopant material. The dopant quantity was varied between 0.9% and 9.0%. With increasing dopant, a faster hydrogenation reaction is observable.

In addition, the total amount of adsorbed hydrogen is also depending on the dopant. It came out that 2% of dopant in the material showed improved reaction kinetics, but also the highest amount of adsorbed hydrogen [2, 7, 8].

1.7. Summary

The transition to an alternative fuel based infrastructure depends on many major aspects. Hydrogen as a fuel for mobile and portable application seems to be a promising alternative to fossil fuels, due to its favorable physical and chemical properties. Main challenges for hydrogen based application are the hydrogen production as well as

hydrogen storage. Therefore, the Department of Energy set guidelines and requirements to each field to establish the systems as a serious alternative to existing technologies.

Among all hydrogen storage systems, metal hydride based storage systems are seen to be the most promising systems for mobile applications. Metal hydrides consist of metal-hydrogen compounds, which share the ability to ad- and desorb hydrogen under certain condition. Guidelines, given by the Department of Energy, require the material to store at least 6.5wt % hydrogen reversible and to desorb hydrogen in a temperature range of 30-90℃. Current research focuses on eithe r sodium based alanates or boron based boranates, where both seem to be the best fitting materials referring to the guidelines and requirements.

The synthesis of these materials can either be done in a chemical reaction under controlled conditions or in a mechanochemical synthesis method, where the precursor material is charged with grinding balls in a vial and milled. Parameters, such as milling time and the amount of grinding balls play a crucial role for the material characteristics and need to be chosen carefully for each material. The current study focuses on the synthesis of materials and characterization of their hydrogen desorption dynamics.

2. Experimental Methods

2.1. Validation of the Synthesis Method

2.1.1. Objectives

The synthesis and characterization of an unknown material requires a preceding validation of the synthesis method and the performed analysis. Therefore, Li_3AlH_6 was chosen, synthesized and compared with published data. This particular system was chosen as a reference system because this material is well known and a multiplicity of data exists which makes a comparison easy. This method ensures the accuracy of later results and prevents errors in the course of research. Furthermore, a validation of the method enables eliminating flaws during the synthesis process. In the course of research, new materials are produced and analyzed in terms of hydrogen desorption temperature and desorption kinetics. In addition, dopants such as titanium chloride can be embedded into the material structure in order to change physical and chemical properties. The overall aim of this project is to synthesize a material which fulfills all the requirements given by both, DoE and industry [7, 8, 12].

2.1.2. Synthesis Methodology and Characterization

Metal hydrides and their precursors have a high affinity to react with oxygen and moisture. Therefore, the whole preparation process needs to be done under a controlled

atmosphere in a glove box. Typical values for residual oxygen and moisture are below 1ppm (parts per million). The glove box enables a safe and clean synthesis of the materials. Furthermore, it acts as a storage container, since the products cannot be stored under conventional conditions. Tools and devices must be baked out before they can be moved into the glove box. This process should remove moisture on their surface, which could cause a contamination of the inert atmosphere and the materials. Once all materials and devices are in the glove box, the preparation of the material can proceed. Based on the reaction equation, precursors are weighted and mixed in a fixed molecular ratio and charged into a vial. The vial for the ball milling consists of either tungsten carbide or stainless steel process and contains 6 steel balls. The choice of the vial material is important because it keeps contaminations of the material at less than 0.3mol %.

The vial, containing precursors and steel balls, is closed and moved out of the glove box and fixed in the ball mill. Since the phase formation and the material properties are related to the ball milling time, the process itself is an important and sensitive part of the material synthesis. Choosing too short of a ball milling time will lead to an incomplete phase formation and an impure sample. Milling the material too long will also have effects on the phase formation. At a certain point, the material starts to decompose, and impurities in the sample similar to a short milling time are observable. Depending on the material, typical values for milling times vary between 3 and 12 hours.

When the milling process is finished, the vial is moved back to the glove box. The only critical point during the synthesis is the milling process itself and needs special attention.

Once the material is synthesized, it needs to be analyzed in terms of its structure and hydrogen desorption kinetics. Since all materials are highly reactive with air and moisture, samples for the analysis need special treatment. A commonly used technique to protect the samples from ambient atmosphere during the structural analysis is to cover

them with Kapton foil. This foil protects the sample from moisture while only having a minor influence on the results. A structural analysis of the material is performed by X-ray diffraction (XRD), where X-rays hit the surface of the sample and measure the intensity of the reflected beam dependent on the angle.

$$n * \lambda = 2 * d * \sin\theta \qquad 2.1$$

This technique is governed by Bragg's law, which links the distance between two crystal layers and the angle of the X-ray beam to create a characteristic intensity pattern of the material. Each material has its own characteristic pattern and can be identified by this. Comparing results with data from a database allows for the determination of the existing phases in the sample. Another advantage of this technique is the possibility to receive information about the purity of the sample. As mentioned, the ball milling process has strong influence on the phase formation. Therefore, it is of major interest to determine the optimal ball milling time.

Besides a structural analysis, additional thermogravimetric analysis (TGA) and differential scanning caliometry (DSC) are performed. Both analyses enable a prediction about the reaction behavior and the hydrogen desorption of the material. The principle of a thermogravimetric analysis is based on the weight loss of the sample by increasing its temperature. In the beginning of the analysis, the material is put on a microbalance and the initial weight is measured. Then the sample is heated in the desired interval with a chosen heating rate under purge gas flow. The argon purge gas flow rate at the sample is 60mL/min ±0.02mL/min and avoids contaminations and unintentional reactions during the analysis. The weight change of the sample is a function of temperature. Depending on the strength of the bonds and the involved elements, a change in weight can be proved at a critical temperature. In the case of metal hydrides, the weight loss appears

when metal- hydrogen bonds split under the release of hydrogen. This information is of major interest because the critical temperature is an indicator to whether the material is practicable for mobile application or not. In addition, TGA analysis also shows the relative weight loss which is correlated with the amount of desorbed hydrogen. This aspect enables a prediction about storage density of the material, which is also a major criterion for their applicability.

The other analysis method is called differential scanning caliometry (DSC), where the amount of energy is measured to keep the sample in equilibrium with a reference sample as a function of temperature. Therefore, the sample and a reference are put on a balance, and the whole system is heated to a desired temperature with a fixed heating rate. At a critical temperature, the material starts to alter chemically, what is connected with either energy adsorption or desorption. Depending on the bond characteristics, this alteration is of heat absorbing or heat releasing character.

In the present study, this knowledge is important because the analysis gives important information about the sample characteristics. Materials with a high grade of stability are unfavorable for industrial application because of the high amount of energy that is required to desorb the hydrogen. These three analyses enable a clear overview of the structure, the chemical and physical properties of the sample, and allow for the decision over the industrial practicability of the material [1-3, 7, 9].

2.1.3. Analysis

The synthesis of Li_3AlH_6 was undertaken based on the following chemical reaction equation.

$$2LiH + LiAlH_4 \rightarrow Li_3AlH_6 \quad 2.2$$

The precursors were weighted and mixed in a molar ratio of 2:1 under argon atmosphere in a glove box. The powder was charged with 6 steel balls in a stainless steel vessel and milled in a SPEX 8000 planetary ball mill for 3 hours. After the synthesis, the formation of the Li_3AlH_6 phase from its precursors, $LiAlH_4$ and LiH, is confirmed by x-ray powder diffraction with a CuK_α source. Balema et al. [13] proved the mechanochemical synthesis of Li_3AlH_6, based on Equation 2.2.

XRD Analysis

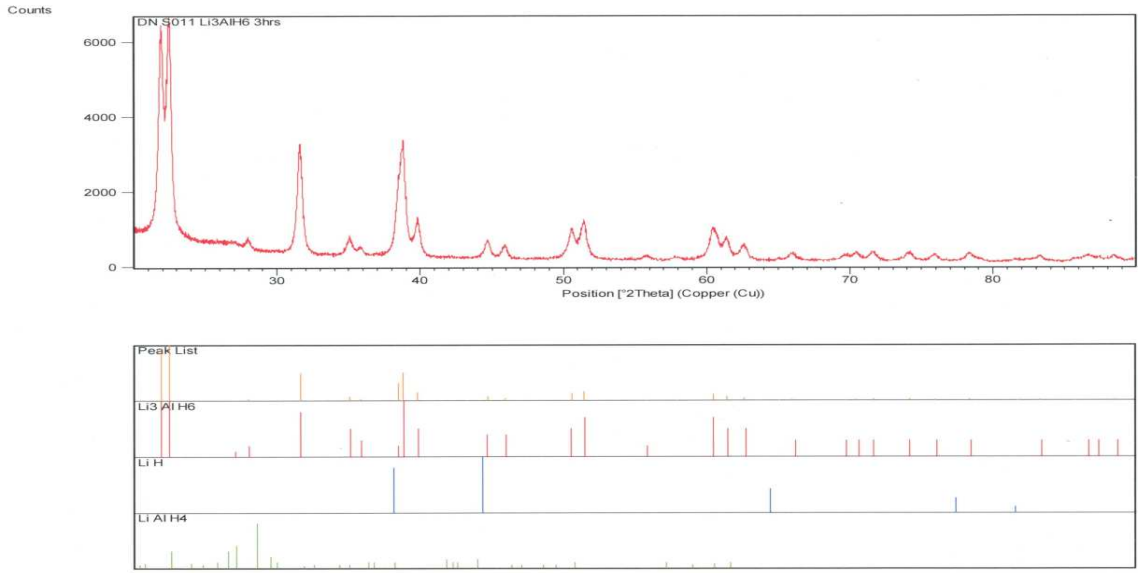

The result of the XRD analysis is presented in Figure 24 and is in good agreement with published literature [14-16].

Figure 24 XRD pattern of Li_3AlH_6, 3 hrs. ball milled

A comparison of the results with peaks from the JCPDF file indicates the formation of a Li_3AlH_6 phase with a high purity. However impurities from precursor material LiH and $LiAlH_4$ are still present in few quantities.

TGA Analysis

The sample holder without the sample need to be tare weighted in order to measure the net weight of the sample. Afterwards, the sample holder is moved into the glove box where the sample is prepared for the analysis. In this process, the sample is put on the microbalance and the automatic analysis is initiated by the experimenter. The time interval between putting the sample on the microbalance and starting the analysis is and needs to be as short as possible because the sample is exposed to air during that time. A temperature interval from ~25- 450℃ was chosen w ith a heating rate of 10℃/min. The result of the TGA analysis of Li_3AlH_6 is presented in Figure 25.

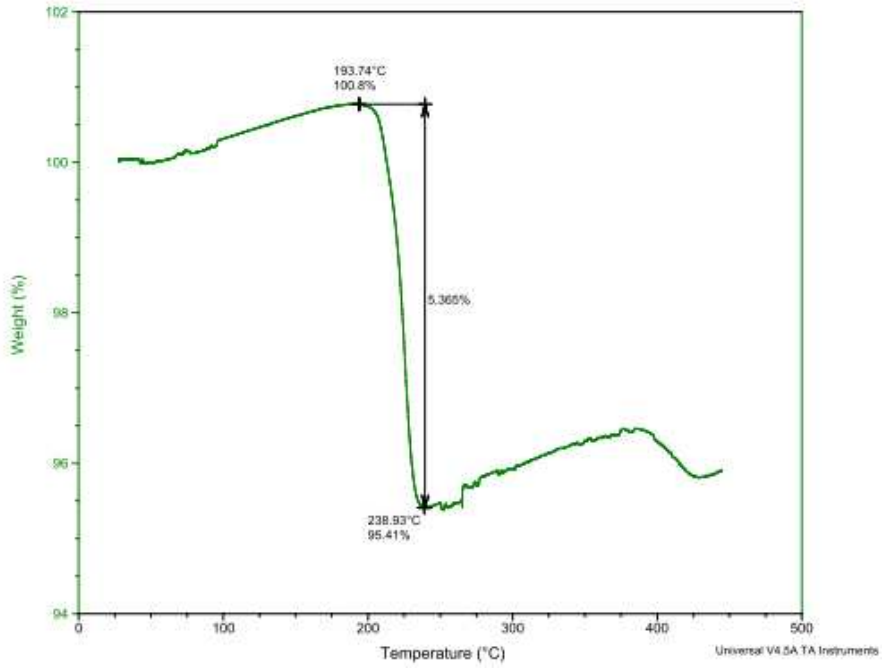

Figure 25 TGA analysis of Li_3AlH_6

The TGA analysis provides two main pieces of information. The hydrogen desorption takes place in an interval between 193- 240℃, whic h is marked with two cross points. Furthermore, the TGA analysis provides information about the relative weight loss during

the hydrogen desorption. The sample lost ~5.3wt %, which fits well with the theoretical value of 5.5wt % reversible storage density [13, 17-20].

DSC Analysis

The preparation of the sample holder is undertaken in the glove box under inert atmosphere due to the high affinity of the sample to react with moisture. Therefore, ~10mg of material are put into the lower pan cup and then covered with the upper pan cup. After the cups are mechanically pressed with each other, the sample was tested for its hydrogen desorption behavior. The sample is heated from ~25- 400℃ with a heating rate of 10℃/min, where the heat flow is recorded in dependency of time. The sample shows the following result, presented in Figure 26.

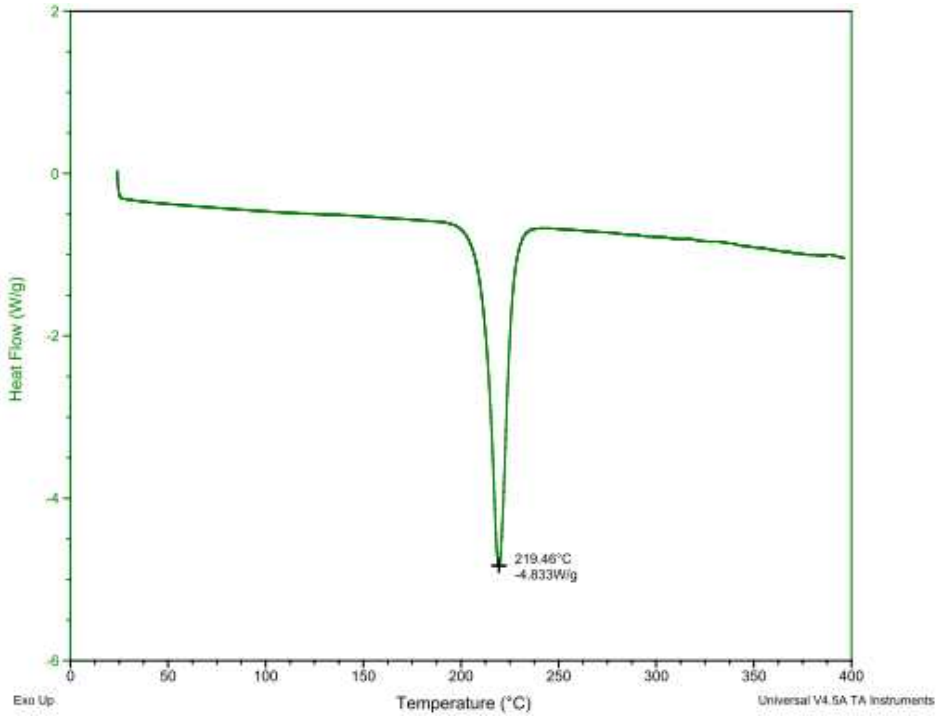

Figure 26 DSC analysis of Li_3AlH_6

The result of the DSC analysis shows an endothermic phase transition in the temperature range from 190- 240℃. This result stands in good agreement with the result

of the TGA analysis. The DSC analysis proves that the hydrogen desorption is an endothermic process which consumes an energy amount of 4.8$\frac{W}{g}$ [13, 18-20].

Discussion

The material was tested for its hydrogen desorption behavior. TGA and DSC analysis provided detailed information about desorption temperature and reaction characteristics. In the temperature range of 25- 190℃, the material gains weight (approximately 0.8wt %) due to reactions of the sample with ambient air and moisture. These reactions cannot be avoided because the material is, prior to the analysis and in the beginning phase, exposed to air. The possible reaction during that time can be expressed in the following.

$$Li_3AlH_6 + 6H_2O \rightarrow 3LiOH + Al(OH)_3 + 6H_2 \quad 2.3$$

For the reaction with moisture

$$Li_3AlH_6 + 2O_2 \rightarrow 3LiOH + Al(OH)_3 \quad 2.4$$

For the reaction with oxygen

At a temperature range of 190- 240℃, the material starts to decompose under hydrogen release. The total amount of desorbed hydrogen is 5.3wt %, which is close to the theoretical value of 5.5wt % and is more than in published data [13, 21], which stated a hydrogen desorption of 2.5wt % for undoped material.

This result is underlined with the results of the DSC analysis, where an endothermic peak of -4.8$\frac{W}{g}$ at a temperature of 200℃ was proven. The peak indicates that the desorption process is of endothermic character, which coincides with theoretical assumptions and published data [13].

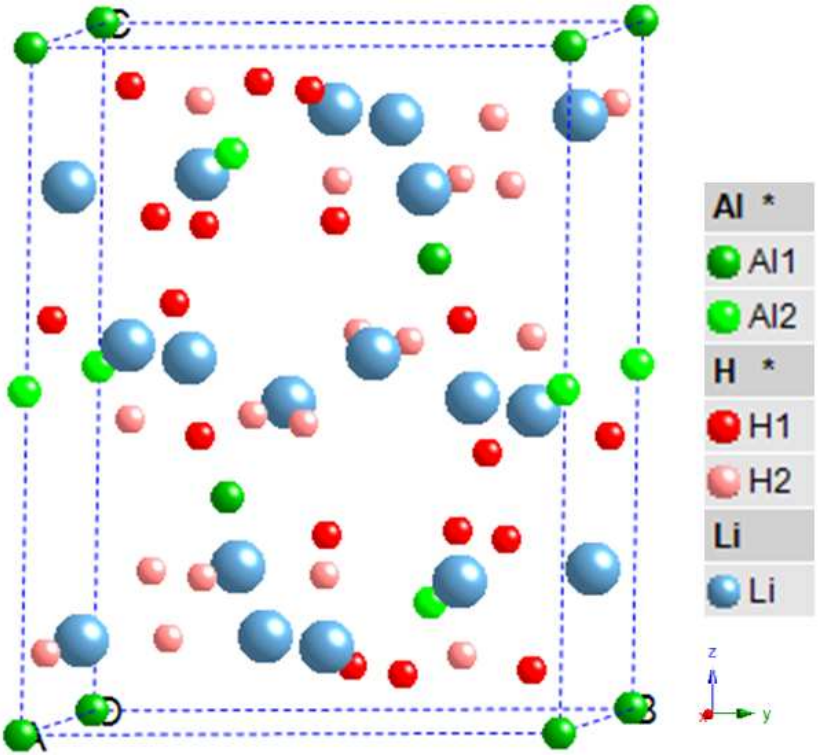

Figure 27 Crystal structure Li_3AlH_6

Figure 27 shows the crystal structure of Li_3AlH_6, which has a space group of $R\bar{3}$ with lattice parameters “a”= 5.667Å, “b”= 8.107Å, and “c”= 7.917Å. The bond length between the aluminum atom and the hydrogen atoms is 1.74Å. The crystal has monoclinic symmetry, but the overall crystal structure remains unclear due to its rhombohedral pseudo symmetry [13, 22].

Two main factors are responsible for the hydrogen desorption temperature, the Al- H bonds and the enthalpy, ΔH, of the reaction. The bond strength depends on factors such as bond nature, bond length and crystal structure. In case of Li_3AlH_6, the bond is assumed to be of ionic character [22], with bond parameters mentioned above. The enthalpy, which describes the heat that needs to be induced to split the bond, is another major factor. For Li_3AlH_6, ΔH= -102.8kJ/mol. This value is correlated with the height of the peak from the DSC analysis, where the peak stands for the heat flow into the sample

during the phase formation. This value matches published data, where similar peaks are proved [13, 23, 24]. At temperatures beginning at 200℃, enough energy is induced in form of heat to split the bond under hydrogen release and the formation of LiH.

2.1.4. Conclusion

In conclusion, this experiment should primarily be used as a means to validate the synthesis method. In the sample preparation, the influence of the ball milling time on the final product becomes visible. The results of the structural analysis were compared with reference data from the JCPDF file and with results from published articles [1, 2]. This validation process was successfully proven. The results of the XRD analysis indicate that the phase formation of the material Li_3AlH_6 is from 90% - 95% purity, which is a good result for this synthesis method. The variation of the ball milling time during the synthesis process yielded good results for 3 hours of ball milling. This result leads to the decision for choosing a similar milling time for other materials as well.

The hydrogen desorption kinetics are tested by TGA as well as DSC analyses. The pattern of the TGA analysis indicated within a temperature interval of 25- 190℃, an increase in weight due to reactions with the ambient atmosphere based on chemical reactions given in Equation 2.3 and 2.4. The hydrogen desorption process starts at a temperature of 190℃ where the ionic Al- H bonds are split by inducing energy in the form of heat, equivalent to a value of ΔH= -102.8 kJ/mol [13, 23, 24]. The total amount of released hydrogen is 5.3wt %, which is close to the theoretical value of 5.5wt %. This result indicates the complete hydrogen desorption of the material. During this process the crystal structure with the space group $R\bar{3}$ and monoclinic symmetry is broken into face-centered cubic LiH and molecular H_2 [22, 25, 26]. The decomposition process is underlined by the results of the DSC analysis, where an endothermic peak with its

maximum at 200℃, indicates the phase transition. The peak shows a negative (endothermic) peak with its maximum value at $4.8\frac{W}{g}$, which correlates with the value for ΔH.

2.2. Singularly and Binary Hydrides: MH and MH_2

2.2.1. Objectives

The key conditions that will allow a material to act as a potential candidate as a storage medium is the amount of adsorbed hydrogen in respect to its molecular weight. Additionally, desorption kinetics have to be favorable in regards to desorption- pressure, temperature and desorption rate. Logically, the simplest materials are singularly and binary light weight hydrides. These hydrides consist of one alkali or earth alkali metal and one and two hydrogen atoms, respectively. The following materials were tested in the present study:

- Singularly Hydrides: KH, LiH and NaH
- Binary Hydrides: MgH_2, CaH_2 and TiH_2

Even though, the results of these analyses are known in most cases, it is important to validate the results. One of the objectives is to synthesize composites of these hydrides. Later attempts to synthesize new materials on the basis of these singularly and binary hydrides need to have an established understanding of the precursors behavior and characteristics. The aim of this study is the synthesis of a material which shares the advantages of each precursor while eliminating each individual's drawbacks. There are two possibilities for the material synthesis, formation of a new compound and the formation of a composite. The materials mentioned above were analyzed according to

their composition and their hydrogen desorption kinetics. Structural analyses are performed by an XRD technique, whereas desorption kinetics are determined by TGA and DSC analyses methods.

2.2.2. Characterization

High quality materials are purchased and used as received. Analyses are performed by following the procedure described before. The preparation of the material is done in a glove box under an argon atmosphere due to the high affinity of metal hydrides to react with moisture. The structural analysis is done by an XRD technique, utilizing CuK_{α} source with a voltage of 45kV and a current of 40mA. The scanning range was chosen to $20° \leq 2\Theta \leq 90°$.

The storage density and the desorption temperature were analyzed with a TGA apparatus. Due to their affinity to moisture, two main aspects have to be taken into account. Commonly used nitrogen purge gas was changed into argon purge gas due to its unfavorable thermal characteristics. The sample was transported in a small plastic box from its point of preparation to the analysis apparatus in order to avoid contamination. Because of this, it was not possible to avoid all contamination, and there is a time frame of approximately 60 seconds when the sample might have reacted with moisture. The purge gas flow rate was adjusted to 60mL/min in the chamber, which implies an overall flooding of the chamber. In order to avoid interactions between residual gas and sample, purge gas right above the sample with a rate of 40mL/min is adjusted. Furthermore, samples were analyzed in a temperature range of 25- 400℃ and 800℃, respectively, depending on nature of samples being tested.

Main chemical characteristics, such as bond strength and desorption characteristics are analyzed by DSC. Results of the analysis provide information about the amount of

energy required to hold the sample in equilibrium. Related to that is the strength of the bonds between hydrogen and the host material. Results will also detect if the phase formation is of endothermic or exothermic character. As mentioned, samples are highly air sensitive, so that preparation of the pans is done in a glove box under an argon atmosphere. Unlike TGA analysis, the samples are placed in a closed pan, in order to eliminate contaminations during the transport. The apparatus is set on the same settings as at TGA analysis. According to the guidelines set by the DoE as well as the settings of the apparatus, the upper temperature value is limited to 400℃.

2.2.3. Analysis

2.2.3.1. Singularly Hydrides MH (M= K, Li, Na)

2.2.3.1.1. Material 1: LiH

Lithium hydride is one of the basic precursors of complex hydride structures. Due to its favorable molecular weight ratios between the two elements, the material has theoretical storage density of 12.7wt %, which is more than the other singularly hydrides. Further analysis will depict the reason for its impracticability as a storage material in its origin form.

XRD Analysis

The XRD analysis will show the characteristic peak pattern of this material. Therefore, the sample was prepared in a glove box and tested under standard conditions. The characteristic lithium hydride XRD pattern is presented in Figure 28.

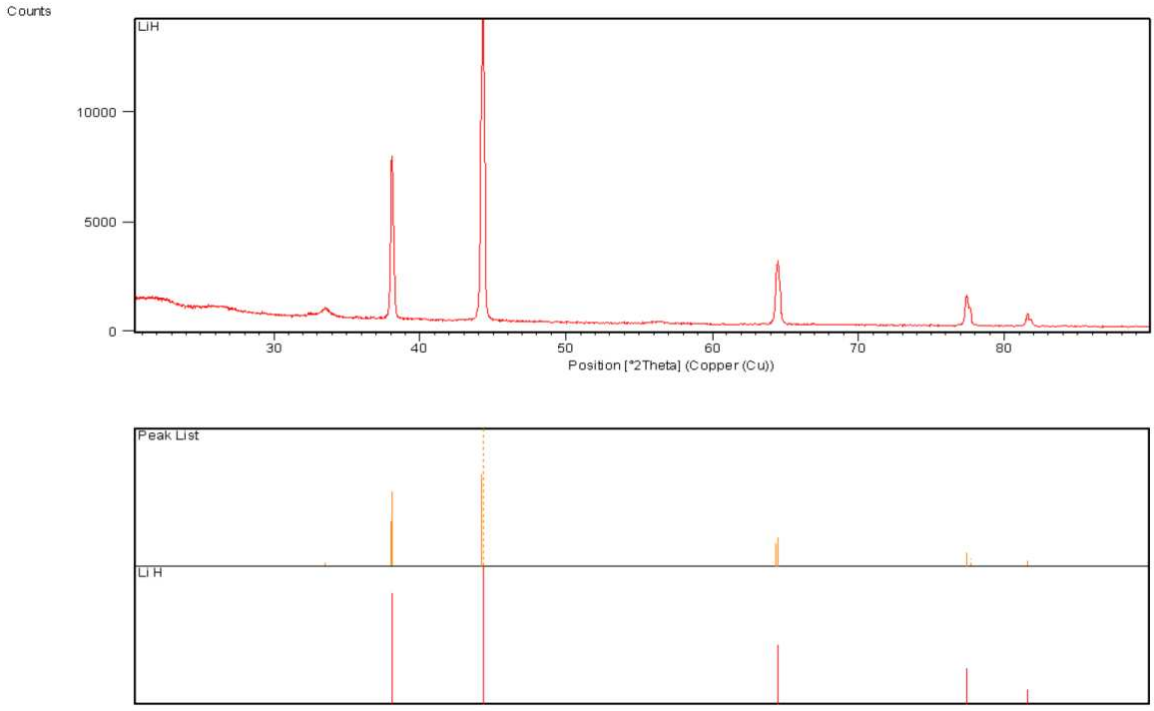

Figure 28 XRD analysis of LiH

The XRD pattern of the sample correlated well with the reference pattern and identifies the material itself as well as the high purity of the material.

TGA Analysis

The TGA analysis is performed in order to receive information about the desorption temperature of the material. According to previous descriptions, the sample is prepared for the analysis and tested for its hydrogen desorption characteristics. The results of the analysis are given in Figure 29.

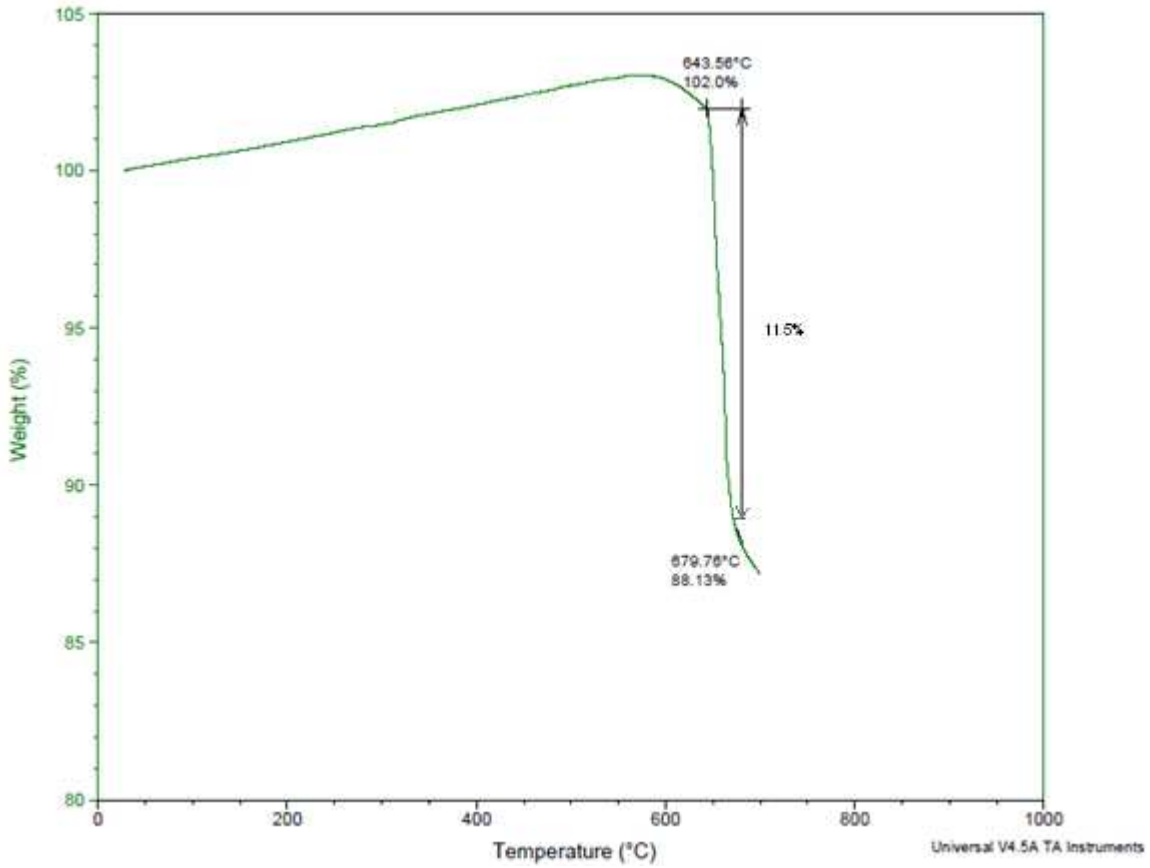

Figure 29 TGA analysis of LiH

The TGA analysis provides information about the hydrogen desorption temperature and the amount of desorbed hydrogen in the interval of 25- 640℃. Starting at a temperature of 640℃, the material begins to decompose under hydrogen adsorption until approximately 680℃. The total amount of desorbed hydrogen is 11.5wt %, which is lower than the theoretical value of 12.7wt %. Based on experiences gained, later experiments with this material are limited to 680℃ [27].

DSC Analysis

As the TGA analysis already showed, hydrogen desorption takes place in a temperature interval of 640- 680℃. The DSC analysis is performed in order to provide information

about the chemical bond characteristics. Therefore, the material is prepared for the analysis as described previously. The results of the DSC analysis are given in Figure 30.

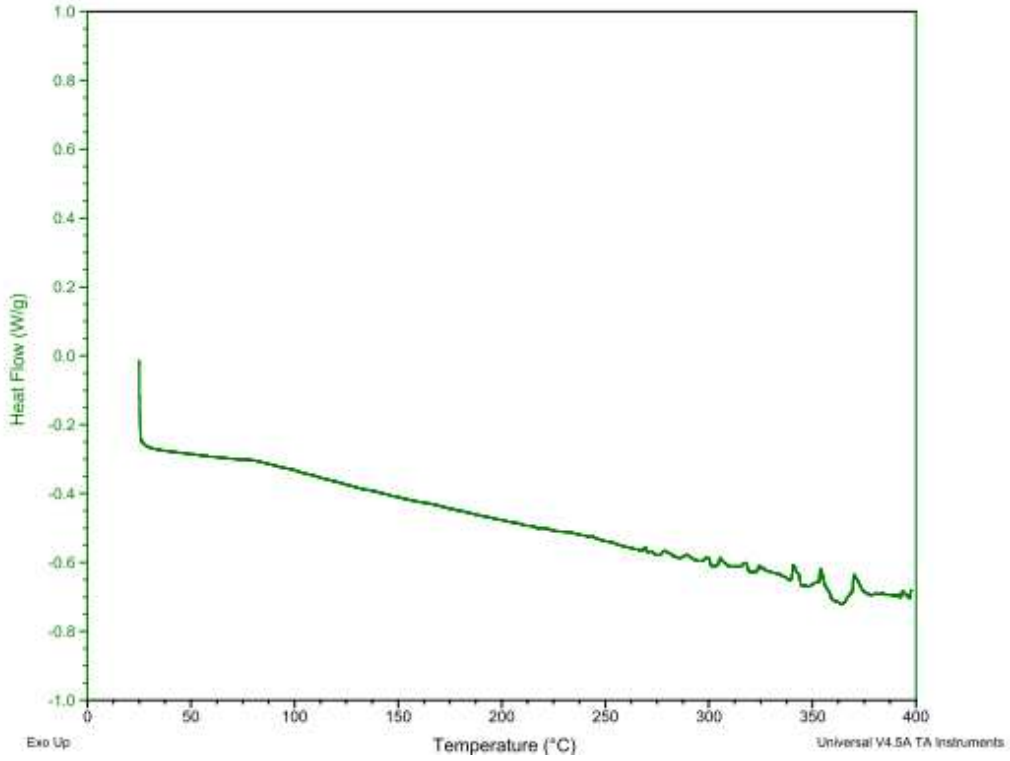

Figure 30 DSC analysis of LiH

As previously mentioned, the analysis does not yield any unexpected results. The initial drop at 25℃ results from the calibration process a nd is not from interest in the course of analysis. The following steady decrease of the curve results from the reaction caused by uncontrollable side effects. The TGA analysis already showed a weight increase of the sample in this temperature interval. Those reactions are of endothermic character, which leads to a decreasing DSC signal. Those reactions are ignored as well because they are not related to the hydrogen desorption reaction. The DSC and the TGA result matches well since the TGA analysis showed a desorption reaction at 640℃ and the DSC result do not prove any reaction until 400℃.

Discussion

The TGA analysis of the material shows within the temperature range of 25-640℃, a weight increase of approximately 2.5wt %. This behavior can be explained of interactions between the material and oxygen in the following way:

$$LiH + 0.5O_2 \rightarrow LiOH \quad (2.5)$$

or

$$2LiH + 0.5O_2 \rightarrow Li_2O + H_2 \quad (2.6)$$

$$Li_2O + H_2O \rightarrow 2LiOH \quad (2.7)$$

and moisture

$$LiH + 0.5H_2O \rightarrow 0.5Li_2O + H_2 \quad (2.8)$$

$$Li_2O + H_2O \rightarrow 2LiOH \quad (2.9)$$

or

$$LiH + H_2O \rightarrow LiOH + H_2 \quad (2.10)$$

during the preparation for the analysis and within the analysis [28]. Both the reaction with moisture and the reaction with oxygen can potentially occur during the exposure to air. As shown in the Equation 2.2 or 2.7, respectively, the reactions can go directly to LiOH or get there with a two step reaction as shown in Equation 2.3 and 2.4 or 2.5 and 2.6, respectively. Recent studies have shown [28, 29] that the increase in weight (~2.5wt %) is caused by the oxidation of 0.4vol % of the LiH sample via reaction 2.2 or 2.7. This reaction takes place during the heating of the sample with residual oxygen and moisture and is linked with a weight increase of ~2.5wt %.

At a temperature of 640℃, the weight of the sample decreases by 11.5wt %, which is related to hydrogen desorption. This value matches with the theoretical value of

12.7wt % and other published data, which proved hydrogen desorption of approximately ~11.5wt % [28, 29].

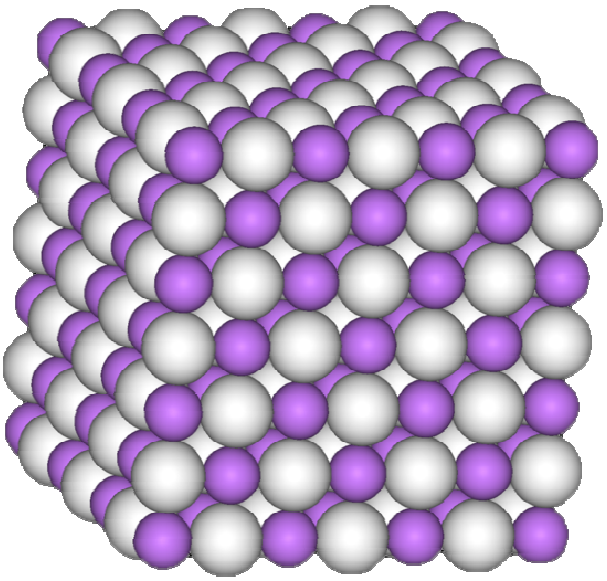

Figure 31 Crystal Structure LiH

Figure 31 shows the crystal structure of LiH, where in purple the lithium atoms and in grey the hydrogen atoms are presented. It is a face centered cubic structure with lithium and hydrogen ordered next to each other with a lattice parameter of "a"= 4.055Å and a bond length of 1.629Å. The bond characteristics are dependent on different factors, such as electronegativity, bond length and bond strength. Based on the parameters and values for LiH, the bond consists of a mixture of 60% covalent bonds and 40% ionic bonds [30]. The strong bonds of covalent and ionic character are responsible for the high desorption temperatures. The heat of the hydride formation is ΔH= -92.1kJ/mol. This amount of energy needs to be induced into the system so that the bonds can break and the hydrogen can decompose. At high temperatures, enough energy is provided to split the bond between the lithium and the hydrogen atom in a hemolytic dissociation reaction [30]. Due to their partially ionic character, Li^+ and H^- ions are formed [31, 32]. The

hydrogen desorption takes place at temperatures above 400℃, no additional information from the DSC analysis can be provided concerning the hydrogen desorption reaction.

2.2.3.1.2. Material 2: NaH

A special group of metal hydrides are the so called alanates. These materials consist of sodium and aluminum atoms included in their structure. The standard precursor for the synthesis of an alanate is sodium hydride. The material itself has a theoretical storage density of 4.3wt %. NaH in combination with $NaAlH_4$ is often used as precursors for more complex alanates, which are seen as potential candidates in industrial applications. For a successful synthesis of these complex alanates, an established understanding of the chemical and physical characteristics of their precursors is required.

XRD Analysis

The preparation for the XRD analysis of the material is done as described previously. The results of the XRD analysis are shown in Figure 32, below.

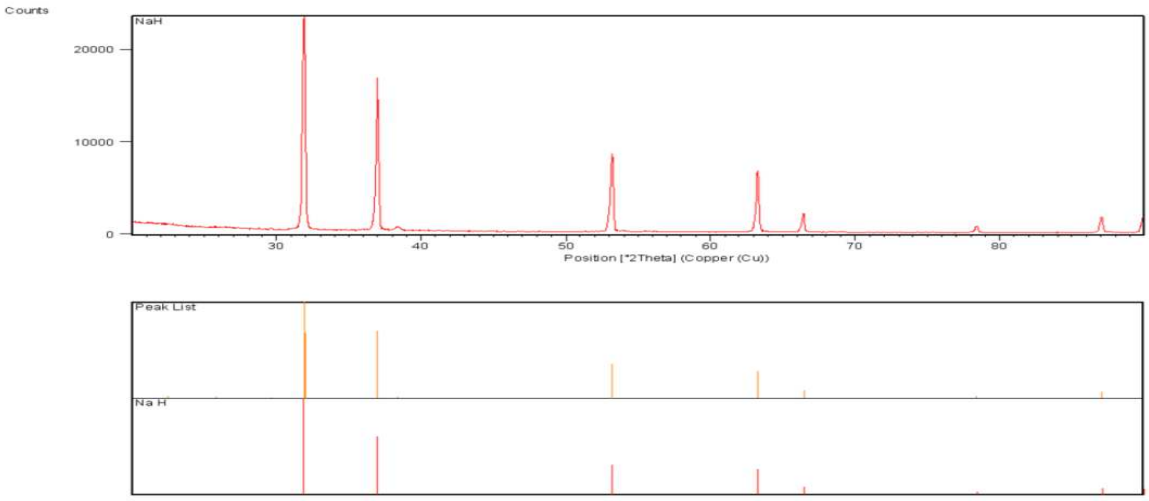

Figure 32 XRD analysis NaH

The XRD pattern shows the characteristic peaks at discrete angles. A comparison with the JCPDF patterns, verified the material as sodium hydride. Furthermore, the analysis indicates the high purity of the sample.

TGA Analysis

The TGA analysis was performed in order to provide an overview of the amount of desorbed hydrogen and the critical temperature when the hydrogen desorption begins. Therefore, the sample was prepared for analysis according to the procedures described in a previous chapter. Figure 33 depicts the result of the analysis.

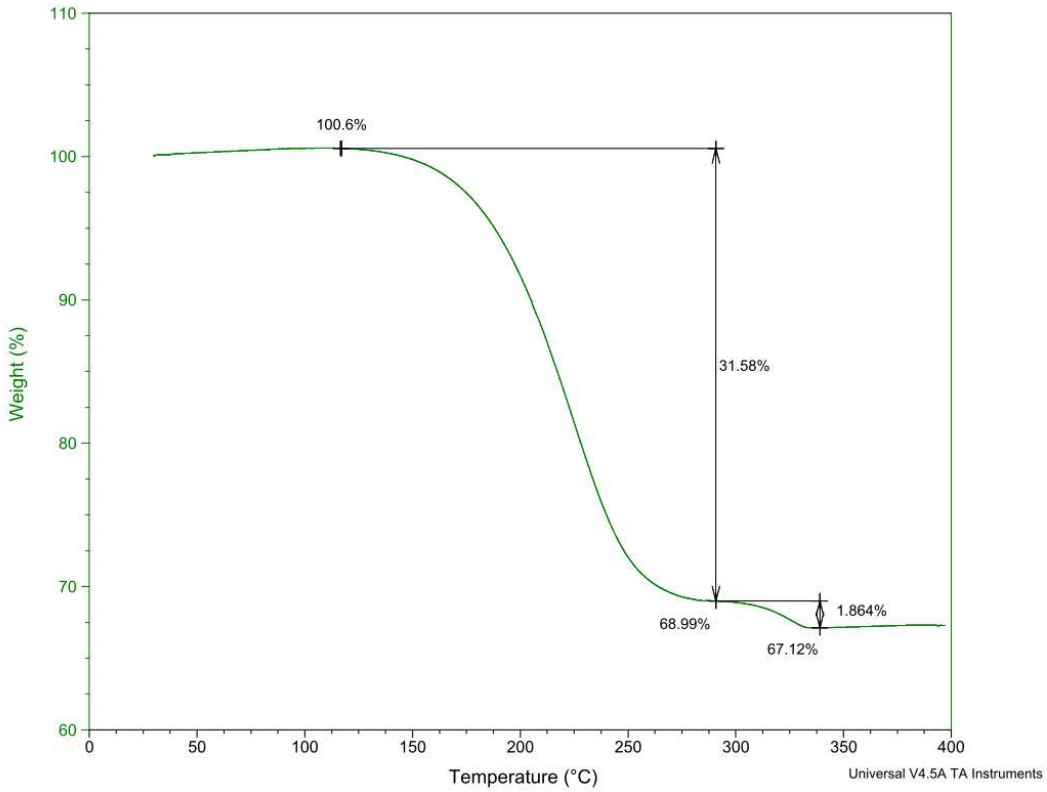

Figure 33 TGA analysis of NaH

The sample shows two plateaus: The shift, which is related to the hydrogen desorption occurs at a temperature of 300℃ and is followed by a weight loss of approximately

1.8wt %, which is lower than the theoretical value of 4.3wt %. The analysis indicates an incomplete desorption reaction, which can be related to the heating rate of 10℃/min connected with weak desorption behavior of the material. The pattern indicates that only 50% of the hydrogen is released, which can be improved by choosing a heating rate of 1- 2℃/min. During the preparation for the TGA anal ysis, the material is exposed to air, which causes a reaction between moisture and the material, where NaOH is created [27]. At 150℃, NaOH decomposes and causes the shif t in the sample.

DSC Analysis

The DSC analysis can provide information about the bond and desorption characteristics of the sample. The strength of the bond is of major interest because it characterizes the desorption temperature of the material as well as the desorption kinetics. A strong bond between the metal atom and the hydrogen atom, results to a high desorption temperature and slow reaction kinetics. Results of the DSC analysis will provide information about the strength of the bond. The sample was prepared in a glove box under standard conditions. The results are presented in Figure 34 below.

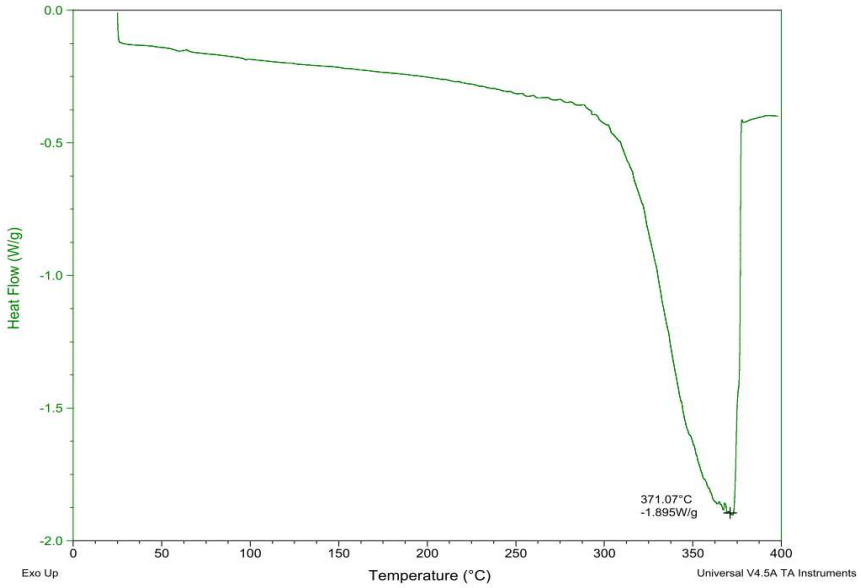

Figure 34 DSC analysis of NaH

The results match to the TGA pattern. The first shift, which is related to melding and vaporizing of the material, does not affect the DSC measurement. However, the second shift, which is linked with 2wt % loss, is identified in the DSC pattern. The pattern shows a endothermic reaction with a heat flow of -1.9 $\frac{W}{g}$. This fact is evidence of the hydrogen desorption.

Discussion

NaH shows, in the temperature range of 25- 150℃, a weak weight increase of approximately 0.6wt %, which can be related to a minor reaction of the sample with residual oxygen or moisture in the chamber. Similar to the reaction of LiH with oxygen and moisture, the following reaction could have taken place during the heating process.

$$NaH + 0.5O_2 \rightarrow NaOH \quad (2.11)$$

or

$$2NaH + 0.5O_2 \rightarrow Na_2O + H_2 \quad (2.12)$$

$$Na_2O + H_2O \rightarrow 2NaOH \quad (2.13)$$

and moisture

$$NaH + 0.5H_2O \rightarrow 0.5Na_2O + H_2 \quad (2.14)$$

$$Na_2O + H_2O \rightarrow 2NaOH \quad (2.15)$$

or

$$NaH + H_2O \rightarrow NaOH + H_2 \quad (2.16)$$

Literature research revealed that no information about of the reaction of NaH with moisture or air exist, however it can be assumed that NaH has a similar behavior to LiH

and reacts with oxygen and moisture in a single step reaction, as described in Equation 2.11 and 2.16.

At a temperature range beginning at 150℃, a drop of the sample weight related with 30wt % of the sample is recognizable. The weight loss is caused by the decomposition of NaOH, a product formed when the material was exposed to air, based on Equations 2.11- 2.16. At temperatures beginning at 250℃, the material starts slowly to decompose under hydrogen release. The TGA results matches well with the results from the DCS analysis, where an endothermic peak of -1.8$\frac{W}{g}$ at a temperature of 370℃ indicates the hydrogen desorption. The desorption is linked with a weight loss of 1.8wt %, which is significantly lower than the theoretical value of 4.3wt % and also lower than other published data [33]. In their experiments, Xu et. al. could reach hydrogen desorption rates of 3.9wt %, which is significantly more than in current results.

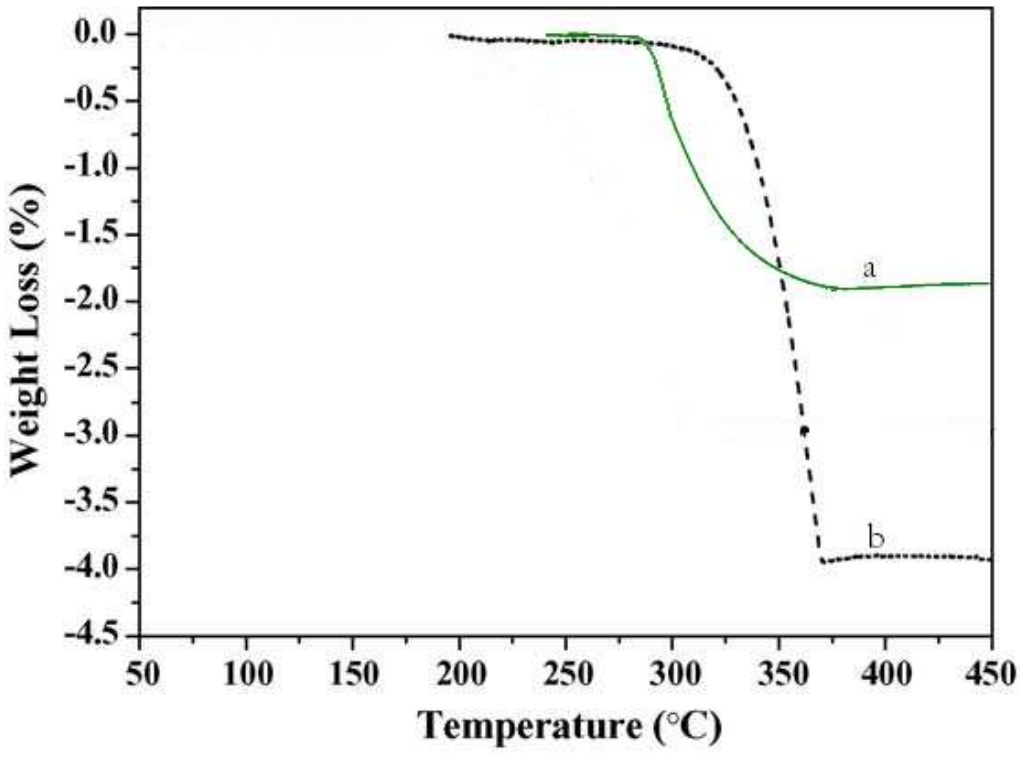

Figure 35 Comparison hydrogen desorption

Figure 35 presents the TGA results of the current study in comparison with published data [33], where curve **a** represents results for currents research, and curve **b**, those of published data. Xu et. al. chose a heating rate of 5℃/min, whereas current experiments were performed with a heating rate of 10℃/min. Sin ce other parameters were similar to each other, it can be assumed that the heating rate plays a significant role in the adsorption rate.

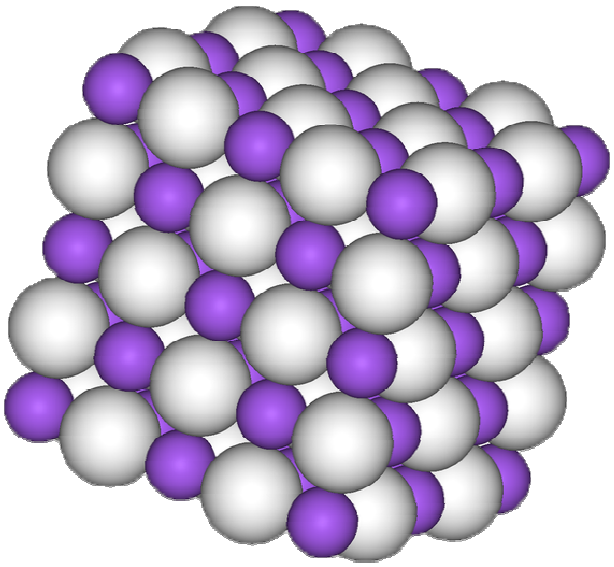

Figure 36 Crystal Structure NaH

Figure 36 shows the crystal structure of NaH, where in purple the sodium atoms and in grey the hydrogen atoms are presented. The structure of NaH is a face- centered cubic crystal structure with a lattice parameter of "a"= 4.84Å and a Na- H bond length of 1.935Å [31, 32, 34]. The bond characteristics are of major importance to the hydrogen desorption process because it is mainly responsible for the desorption temperature, combined with the heat of the formation. The type of the bond is dependent on different factors such as bond length, electro negativity and crystal structure. In the case of NaH, a mixture of covalent and ionic bonds with the ratio 75:25 [31, 32] is present and mainly determines the desorption temperature. The heat of the hydride formation is ΔH= -59.8

kJ/mol [33], which is significantly lower than that of LiH. This value matches with the experimental data of the DSC analysis, where the heat flow was measured to -1.8$\frac{W}{g}$ for NaH, whereas published data indicated a heat flow of more than -5.0$\frac{W}{g}$ for LiH [28]. As a result, NaH desorbs hydrogen at a temperature of 250℃ in a homolytic dissociation reaction, where the ions Na^+ and H^- are formed due to the partially ionic bond character.

2.2.3.1.3. Material 3: KH

Potassium hydride in its natural form cannot be used as a storage medium in commercial scale due to its theoretical storage density of 2.5wt %. However it is used as a precursor for other complex hydrides. Therefore knowledge about its physical and chemical characteristics is from high importance. Potassium hydride is usually stored in mineral oil in order to avoid its natural decomposition into its elements. As a consequence, the material needs to be washed and filtered several times with hexane before further treatment can begin. Afterwards the powder is prepared under conventional conditions for the analyses [35, 36].

XRD Analysis

The structural analysis is performed with a XRD measurement and leads to results resented in Figure 37.

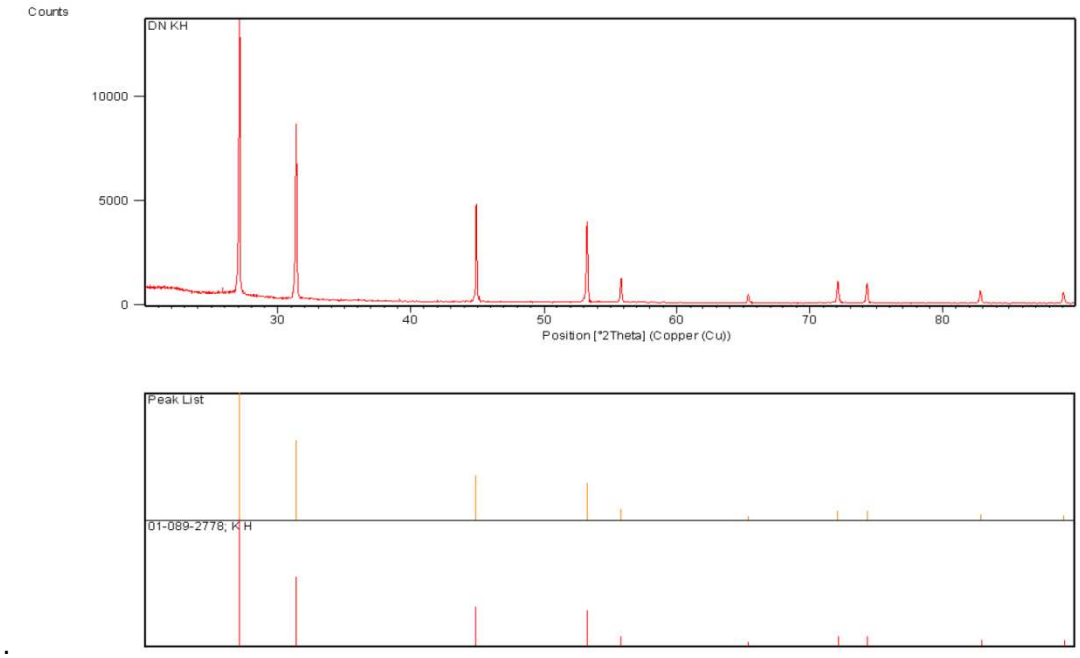

Figure 37 XRD analysis of KH

The XRD pattern proves clear peaks at discrete values for 2Θ, which coincide with the reference JCPDF pattern. This result identifies potassium hydride as the material itself; it also indicates the high purity of the material.

TGA Analysis

By performing the TGA analysis, the temperature at which the material decomposes into its elements, potassium and hydrogen can be determined. Publications have already shown that the material decomposes at temperatures above 400℃ [35, 36]. Therefore, a temperature range of 25- 800℃ with a heating rate of 10℃/min was chosen. Figure 38 depicts the results of the analysis.

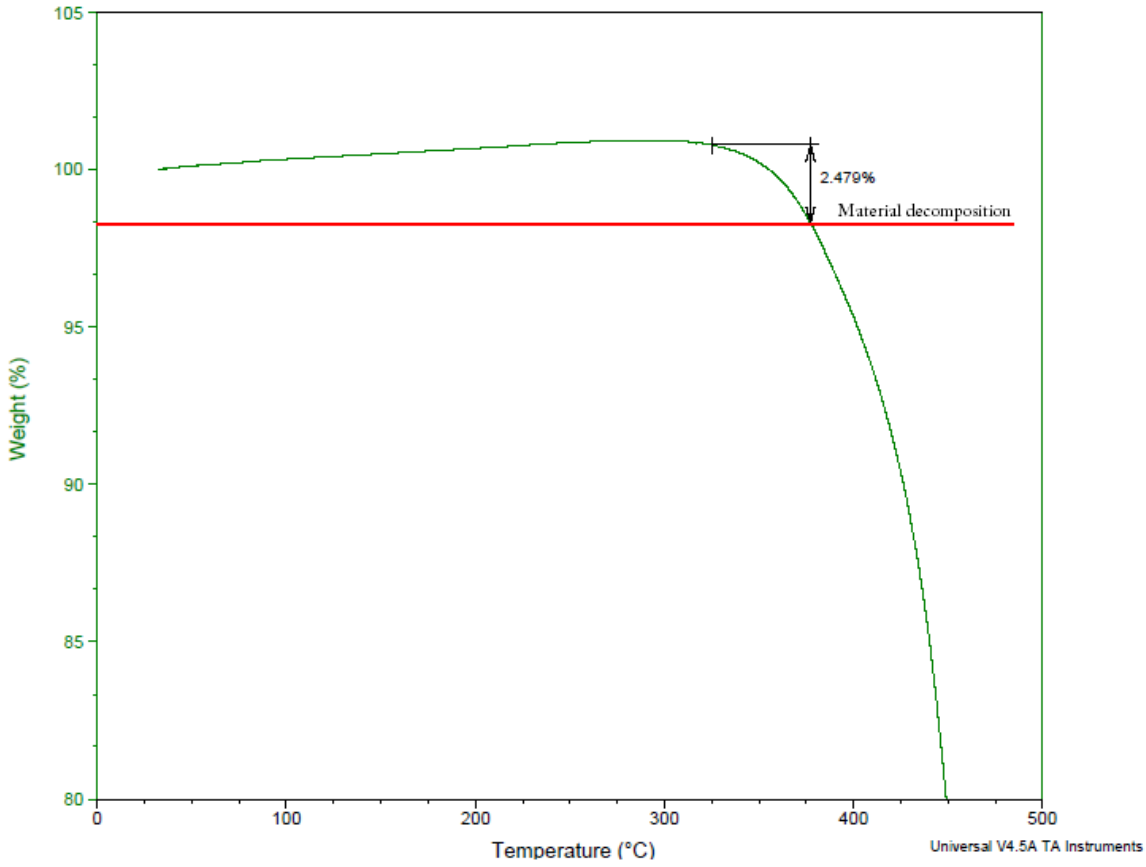

Figure 38 TGA analysis of KH

This curve shows the thermal behavior of the material in the tested temperature interval. The material starts desorbing hydrogen at a temperature of approximately 300℃. The end of the curve is marked at 450℃ by the failure of the material. At this point, almost all of the material is vaporizes and the junction between hydrogen desorption and material decomposition is hardly to distinguish. However, it can be noted that the slope of the curve changes slightly. This point might indicate the end of hydrogen adsorption and the decomposition of the material. At this point, the material desorbs 2.5wt %, which coincides with its calculated theoretical value.

DSC Analysis

The DSC analysis should determine the thermodynamic characteristics of the hydrogen desorption process. The TGA analysis already showed that hydrogen desorption takes place within the temperature range of 300- 400℃. S ince the upper temperature limit of the DSC apparatus is set to 400℃, it is not possib le to determine the whole desorption process and data from outer publications have to be considered, [35, 36] which proved an endothermic peak at a temperature of 410℃. The results of the DSC analysis are presented in Figure 39.

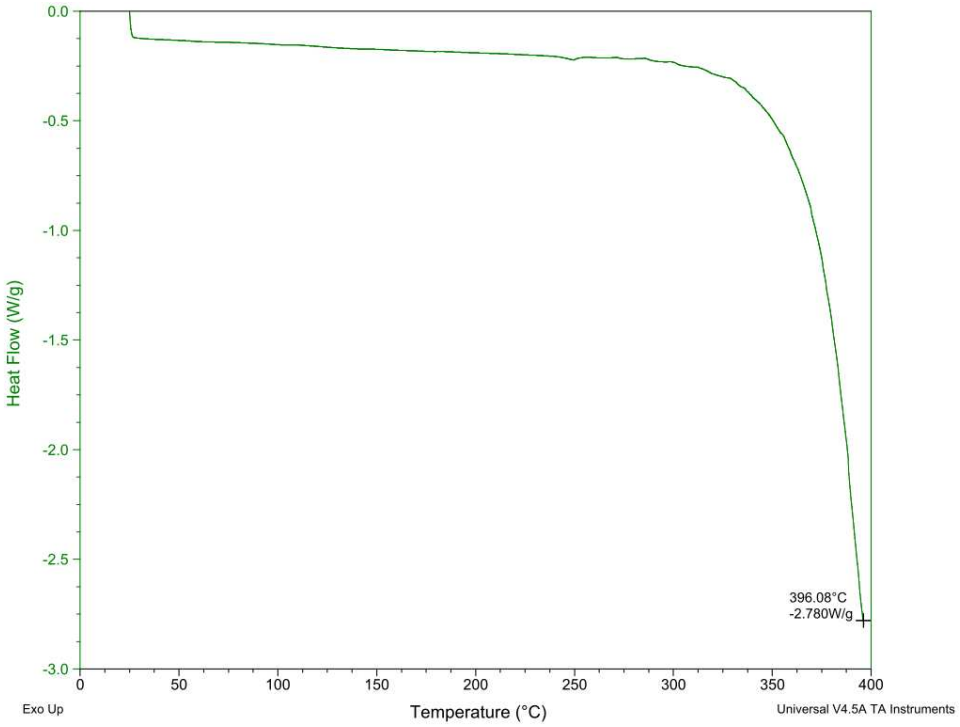

Figure 39 DSC analysis of KH

The DSC results coincide with the TGA results. The fluctuations of the signal until 350℃ can be ignored due to their small maximum value of 0.25$\frac{W}{g}$. At 320℃, the curve begins to decrease steadily, which indicates an endothermic reaction. The exact value of the peak cannot be determined because the maximum is reached at a temperature of 410℃, which is beyond the temperature range of the DSC measurement.

Discussion

Similar to LiH and NaH, KH shows an initial weight increase before the hydrogen desorption takes place. In the temperature interval of 25- 330℃, the sample gains approximately 1wt % of weight, which can be related to an interaction between the sample and residual air and moisture. Based on the reaction equations, the following reactions with oxygen and moisture can take place.

$$KH + 0.5O_2 \rightarrow KOH \quad (2.17)$$

or

$$2KH + 0.5O_2 \rightarrow K_2O + H_2 \quad (2.18)$$

$$K_2O + H_2O \rightarrow 2KOH \quad (2.19)$$

and moisture

$$KH + 0.5H_2O \rightarrow 0.5K_2O + H_2 \quad (2.20)$$

$$K_2O + H_2O \rightarrow 2KOH \quad (2.21)$$

or

$$KH + H_2O \rightarrow KOH + H_2 \quad (2.22)$$

Regarding the chemical reactions, the interactions can take place in a single or in a double step reaction. Since no data about the analysis is available, it only can be assumed that the direct transition from KH to KOH took place, based on Equation 2.17 and 2.22.

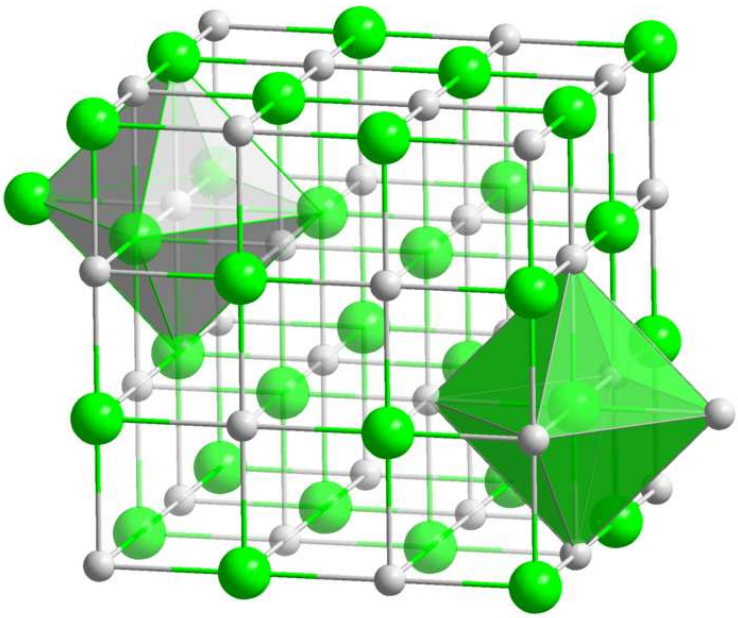

Figure 40 Crystal Structure of KH

Figure 40 shows the crystal structure of KH, where in green the potassium and in grey the hydrogen atoms are presented. It has an orthorhombic face- centered cubic unit cell and is in the space group Fm m with potassium and hydrogen as crystal atoms. The lattice parameter of the crystal is “a”= 5.71Å, with a bond length of 2.31Å between each hydrogen and potassium atom [31, 32, 37]. The crystal structures, as well as the bond characteristics, are mainly responsible for the hydrogen desorption characteristics. A present study could show the hydrogen desorption in a temperature range beginning at 320℃, followed by a total decomposition of the material when reaching the melting point [38][38]. The TGA analysis can only predict the total amount of desorbed hydrogen, since the hydrogen desorption and decomposition of the material merge together and are not distinguishable from each other. Therefore, the DSC analysis provides important information. An endothermic peak, beginning at ~320℃ with a maximum heat flow of -2.7— indicates the hydrogen desorption. Similar results are published from Bastide et. al., where hydrogen desorption of 2.5wt % could be proved.

As mentioned, the characteristics of the K- H bonds are responsible for the desorption dynamics of the material. The bond is characterized by different factors such as electro negativity and bond length. Based on values for potassium hydride and hydrogen, KH consists of a mixture of ionic and covalent bonds between the atoms in a ratio of approximately 60:40. Another important factor that determines the hydrogen desorption temperature is the heat of the formation ΔH= -70.4kJ/mol [34]. This value describes the energy required to split the bonds between the hydrogen and the potassium atoms. At temperatures of 330℃ and higher, enough energy (in form of heat) is induced in the system to split the bonds. Due to their partially ionic character [34, 37], K^+ and H^- ions are formed in the homolytic dissociations reaction in addition to atomic hydrogen and potassium. This aspect, that heat needs to be induced in the system coincides with the result of the DSC analysis, where an endothermic peak is measured, indicating an endothermic reaction.

2.2.3.2. Binary Hydrides NH_2 (N=Mg, Ti, Ca)

2.2.3.2.1. Material 4: MgH_2

Magnesium as a host material is preferred due to its light weight and its ability to bind two hydrogen atoms. Thus, its theoretical storage density is 8.2wt %, which would fulfill one aspect of the requirements given by the DoE. Further analyses will detect desorption kinetics, which are the reason for the impracticability of this material as a commercial storage material [39, 40].

XRD Analysis

For structural analysis, a discrete amount of material is put on a sample holder and covered with Kapton foil, which prevents a contamination of the material during the analysis. The results of the XRD analysis are presented in Figure 41.

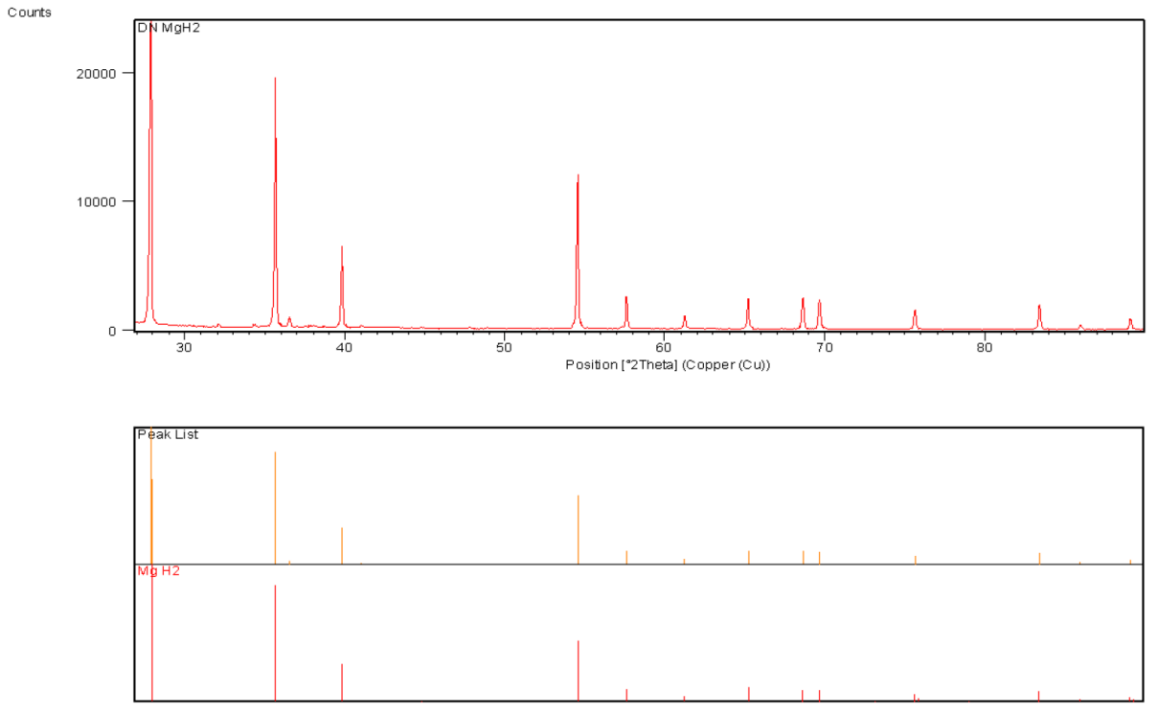

Figure 41 XRD analysis of MgH_2

The resulting peak pattern of the analysis and the JCPDF pattern from the data base match well with the sample and can be clearly identified as magnesium hydride. Similar to other materials, magnesium hydride is of high purity and can be used as a precursor for the synthesis of new materials.

TGA Analysis

The temperature where the magnesium and hydrogen split their bonds and hydrogen becomes free can be determined by a TGA analysis. Therefore, the material is prepared for the analysis as discussed previously. Based on external information, the temperature interval was set at 25- 600℃ with a he ating rate of 10℃/min. The result of the analysis is shown in Figure 42.

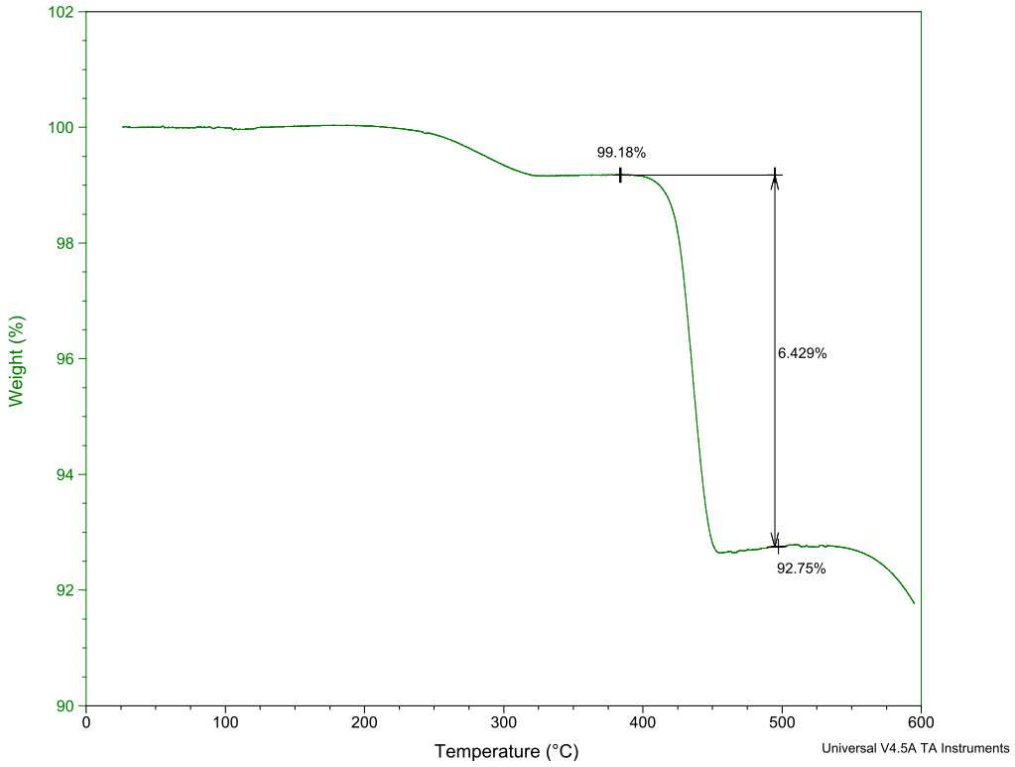

Figure 42 TGA analysis MgH_2

In general, the TGA pattern shows two events. The first event begins at a temperature of 240℃ and is linked with a weight loss of ~1wt %. T he second event is much stronger and takes place in a temperature range of 400℃- 45 0℃. The first shift might be caused by either hydrogen desorption or reactions between the material and residual air in the chamber. Since the hydrogen adsorption is a single step process, one can assume that the first shift is caused by residual air. The second shift, which is linked with a weight loss of ~6.5wt %, is identified as the hydrogen desorption process.

DSC Analysis

The DSC analysis provides information about the strength of the bonds between the two involved elements. Since the analysis is limited to a temperature interval with an upper limit of 400°, one recognizes that the DSC analysis will have no significant effects. Figure 43Figure 1 shows the result of the DSC analysis.

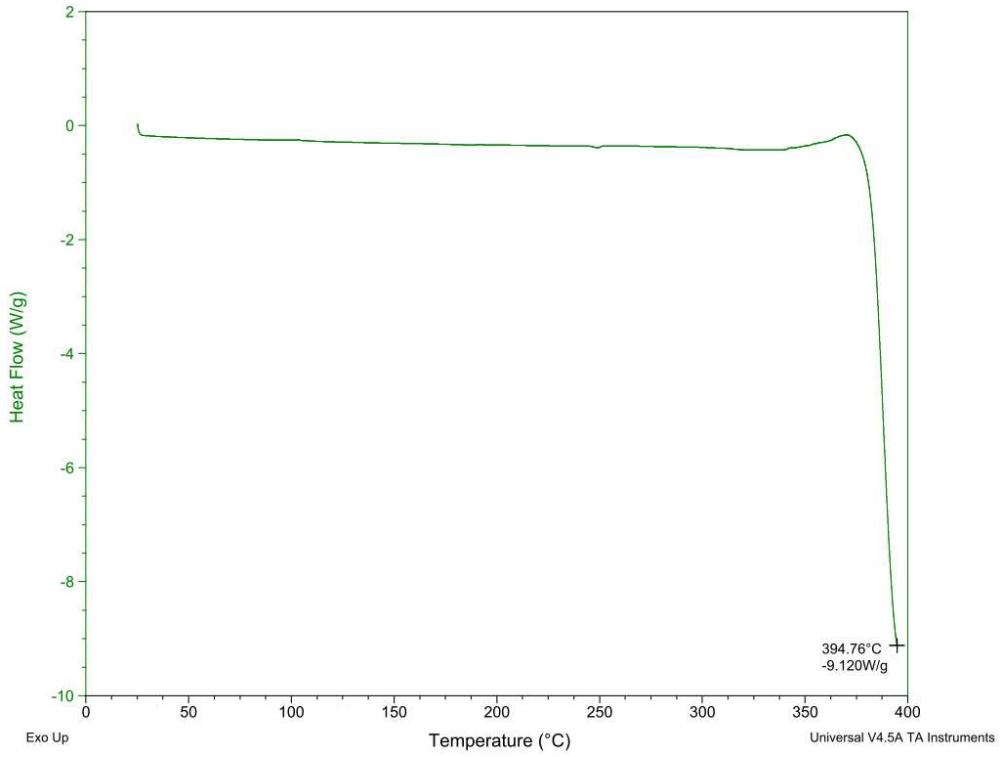

Figure 43 DSC Analysis of MgH_2

The DSC analysis shows no significant events in the interval from 25℃ to 400℃. This result matches well with the result from the TGA analysis since the hydrogen adsorption begins at temperatures above 400℃. The peak indica tes an endothermic reaction with a heat flow of $9.1\frac{W}{g}$. The high value for the heat flow indicates the covalent bond between the metal atom and the hydrogen atom. He covalent character is also responsible for the high desorption temperature. The initial assumption that the first shift is caused by residual air is verified by the DSC analysis. If the shift is of hydrogen desorption nature, it would also be observable in the DSC pattern. However, no shift at a temperature of

240℃ can be proven so that the shift must be caused by interaction between residual air and the material.

Discussion

The TGA analysis as well as the DSC analysis provided basic information about the hydrogen desorption process while heating the sample. The initial drop of 0.9wt % at a temperature of 250℃ can be related to reactions with air and moisture, and will be neglected in the course of the study since the byproducts do not affect the hydrogen desorption behavior of the material. At a temperature range of 400- 440℃, the material starts to desorb hydrogen, which is connected with a weight loss of 6.5wt %. This amount lays approximately 1wt % below the theoretical value of 7.4wt %. Comparisons with published data show a similar behavior. The amount of desorbed hydrogen is significant higher than in the resent study [41-43]. One possible reason for that might be the heating rate, which is with 10℃/min higher (5° C/min) than in published data [41-43].

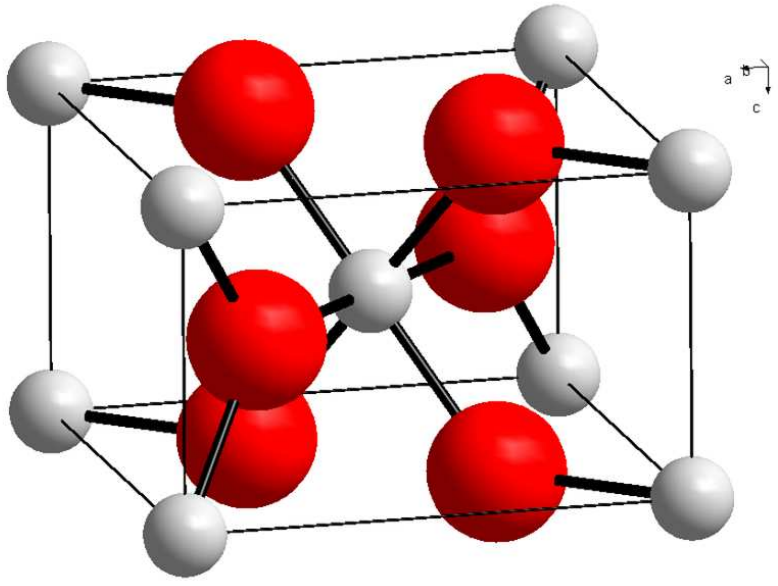

Figure 44 Crystal Structure of MgH_2

Figure 44 shows the crystal structure of MgH_2, where in red the Mg atoms and in grey the hydrogen atoms are presented. It is a tetragonal face centered cubic structure with a $P4_2/mnm$ space group consisting of magnesium and hydrogen atom. The lattice parameters of the tetragonal face- centered cubic unit cell are “a”=”b”= 4.5025Å and “c”= 3.0123Å, with a Mg- H bond of 1.704Å. The bond characteristics, the crystal structure and the heat of the hydride formation are all important aspects because they mainly affect the hydrogen desorption temperature. The bond character is dependent on parameters, such as the electro negativity of the atoms, bond length and crystal structure. MgH_2 consists of a mixture of ionic and covalent bonds in the ratio of approximately 80:20 due to the specific bond characteristics [31, 32]. Even though the majority of the Mg-H bonds are of ionic character, some bonds show covalent characteristics and influence the macroscopic behavior of the material.

Another main aspect that influences the hydrogen desorption temperature is the enthalpy of the material, in the case of MgH_2 ΔH= -75kJ/mol. This value describes the amount of heat that becomes free during the hydride formation. The same amount of heat must be introduced into the system to split the Mg-H bond. At a temperature of approximately 400℃, enough energy is added in the system to split the bond, leading to gaseous hydrogen. The DSC analysis underlines this assumption. The pattern shows a strong endothermic peak beginning at a temperature of 370°C with a peak at -9.1$\frac{W}{g}$, indicating the hydrogen desorption. The height of the peak correlates with the strength of the bond because it describes the heat flow per mass into the sample. The value coincides well with published data, where comparable values for the heat flow were proved [42, 44-47]. Due to their partially ionic character, Mg^{2+} as well as $2H^-$ becomes free.

2.2.3.2.2. Material 5: CaH_2

Calcium hydride has a similar structural buildup to that of magnesium hydride. Both materials have one earth alkali metal as a host, which is bonded with two hydrogen atoms. Its theoretical storage density is approximately 5wt %, which excludes this hydride as a storage material in its original form as well. However, it is used as a precursor to form more complex hydride structures [27].

XRD Analysis

The XRD analysis is done to resolve the structural composition and to get an idea of the XRD pattern of this material. As described previously, the material is prepared for the analysis and tested under defined conditions. Results are illustrated in Figure 45 below.

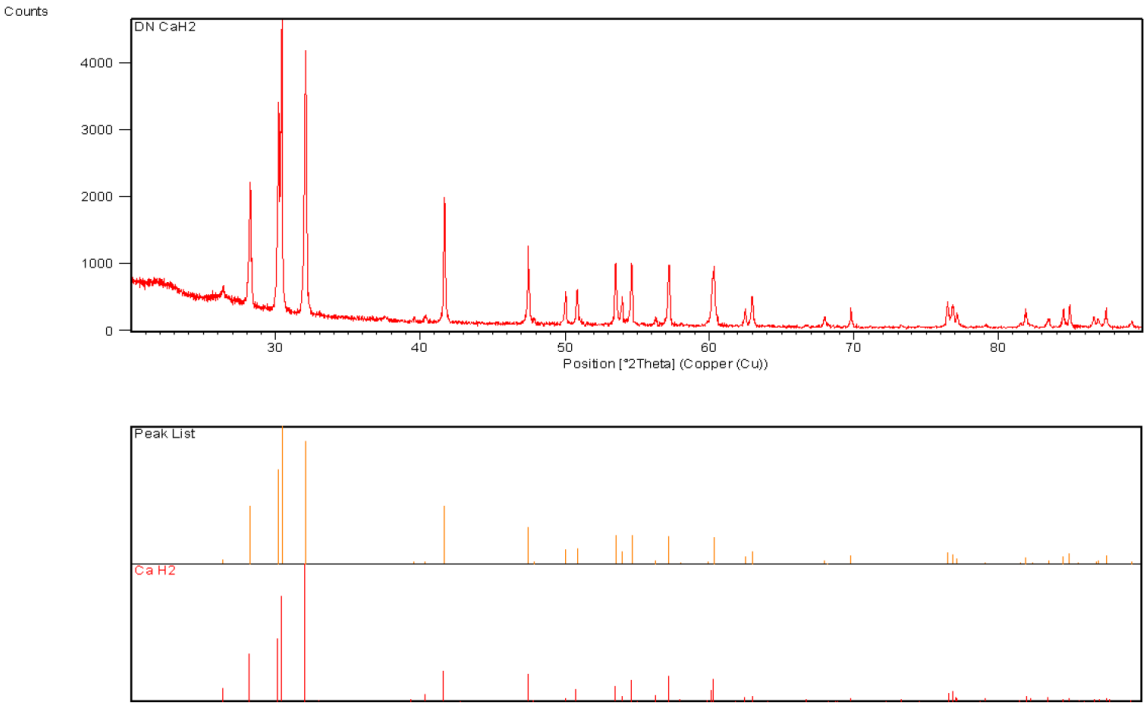

Figure 45 XRD Analysis CaH_2

The XRD results identify the sample as the desired material. Peaks and individual peak intensity correlate with the reference pattern from the data base. Additionally, this material is similar to all other materials of high purity.

TGA Analysis

One of the most significant pieces of information for later synthesis of new materials is the decomposition temperature of calcium hydride. Hence, the TGA analysis provides information about the amount of desorbed hydrogen in regards to the material weight and desorption temperature. Figure 46 depicts the results of the TGA analysis.

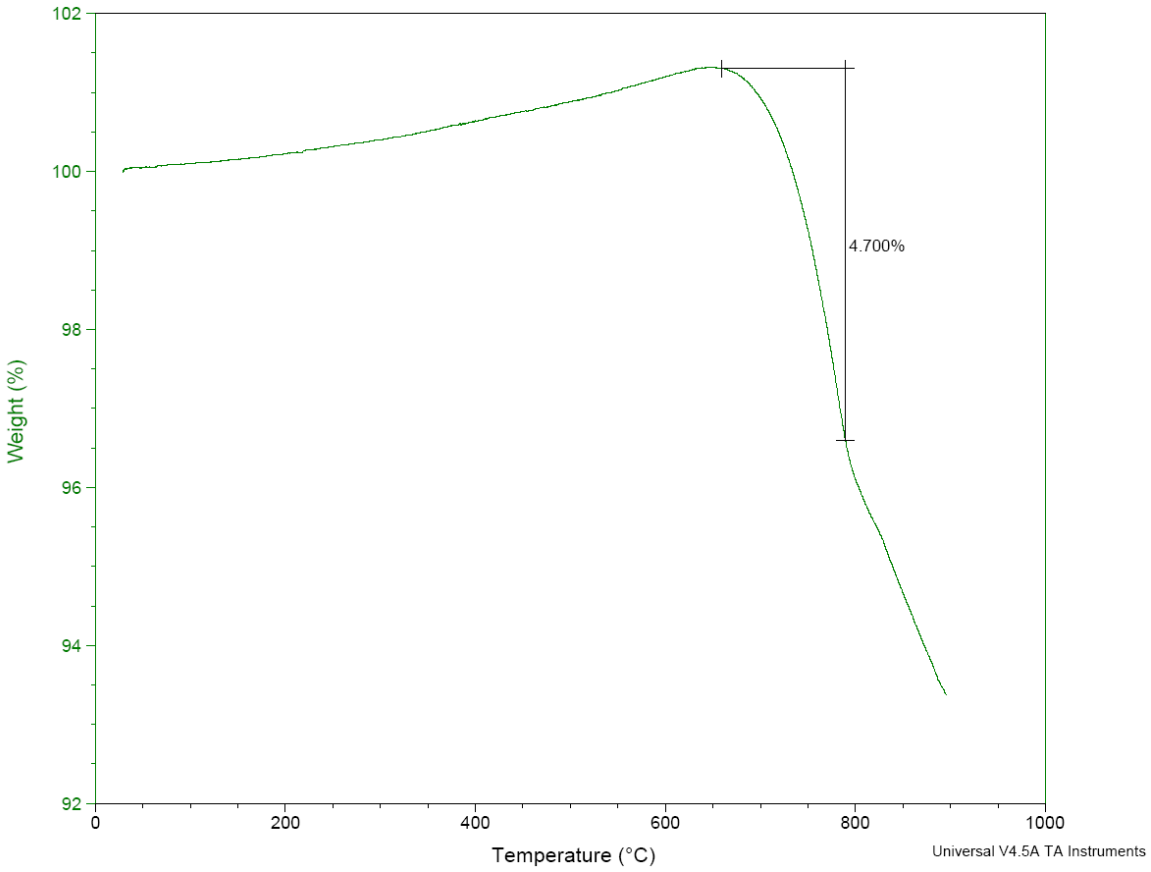

Figure 46 TGA analysis of CaH_2

Based on prior information, the temperature interval for the analysis was set from 25℃ to 900℃ with a heating rate of 10℃/min. The mater ial shows no significant change until

approximately ~650℃. Beginning at this temperature , the material starts to decompose through hydrogen release until almost the whole hydrogen is desorbed at 800℃. At this temperature, the material starts to melt and to vaporize, which will lead to a total decomposition of the sample with increasing temperatures.

DSC Analysis

The TGA analysis already showed that the phase transition from the calcium hydride phase to atomic calcium and hydrogen phase occurs at temperatures above 600℃. As a consequence, the hydrogen desorption occurs beyond the measuring range of the apparatus. The results are shown in Figure 47 below.

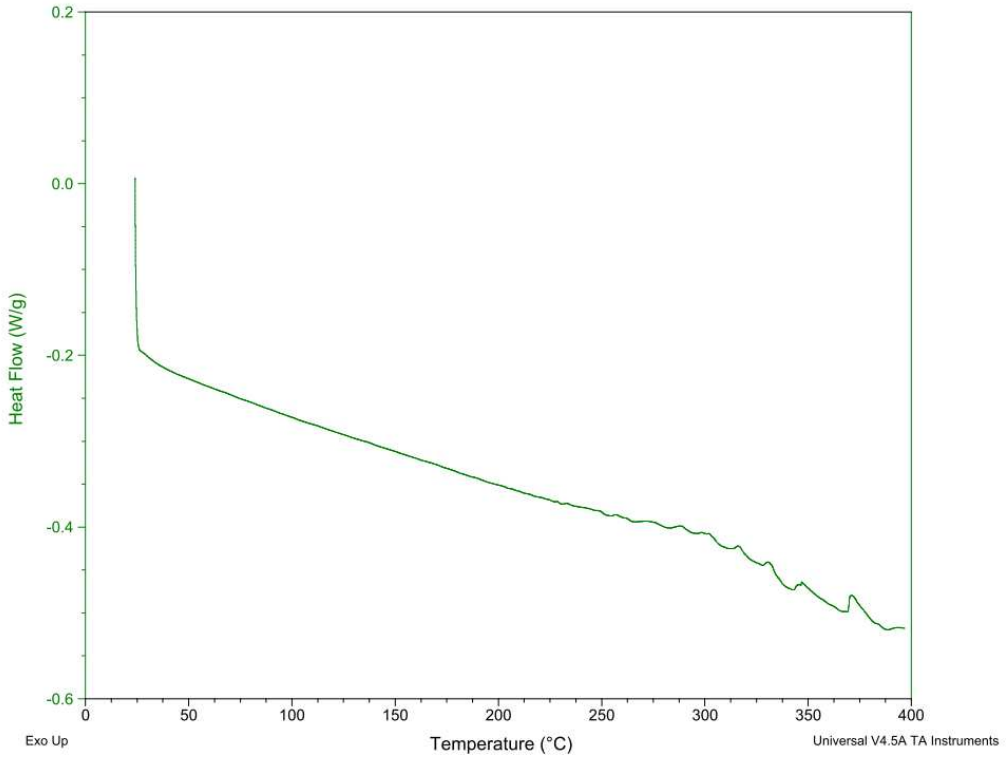

Figure 47 DSC analysis of CaH_2

The curve looks surprising due to the initial drop and the overall negative slope. The initial drop is caused by equilibrating the system to 25℃. Furthermore, the negative slope describes the occurrence of an endothermic reaction, which seems to refute the

assumption that the hydrogen desorption begins at a temperature of 650℃. However, the TGA pattern shows a steady weight increase until 650℃ that is caused by reactions with moisture and oxygen, which can be neglected in the study. As the DSC pattern shows, these effects are of endothermic character. Comparing these results to the results of the TGA analysis, it turns out that the sample gains weight until 400℃.

Discussion

The TGA analysis of the sample shows, within the temperature range of 25- 650℃, a steady weight increase of approximately 1.2wt % before the material starts to decompose hydrogen at 650℃, followed by the materi al decomposition at temperatures of 800℃.

The initial weight increase during the heating of the sample can be related to interactions between the sample and residual air and moisture, respectively, in the following way [42, 45] equivalent to MgH_2.

$$CaH_2 + 2H_2O \rightarrow Ca(OH)_2 + 2\mathrm{H}_2 \qquad 2.23$$

or

$$CaH_2 + 2O_2 \rightarrow Ca(OH)_2 + H_2 \qquad 2.24$$

Depending on the outer condition, air and moisture concentration, both reactions could possibly take place. Further analysis need to show which reaction is preferred, since no experimental data is available. However, the reaction with the ambient atmosphere during the synthesis is responsible for the weight increase of the material. At a certain temperature, the material starts to desorb hydrogen, which is followed by a weight loss of 4.7wt %. This experimental value coincides well with the theoretical value of approximately 5wt %, and also with experimental data from Li et al. [48]. Performing

similar analysis at the same parameters, this research group was able to prove the desorption of 4.5wt % hydrogen from CaH_2.

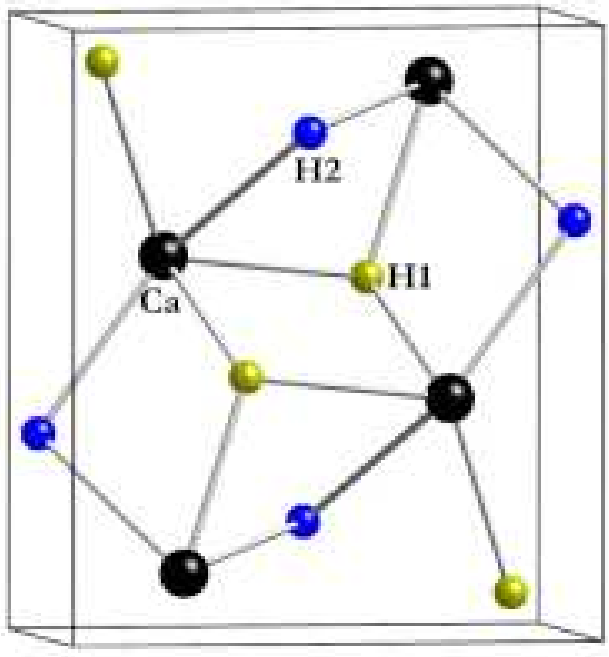

Figure 48 Structure of CaH_2

Figure 48 shows the primitive orthorhombic crystal structure of the material with the lattice parameters “a”= 6.137Å, “b”= 3.694Å, and “c”= 7.098Å [49-52], where the bond length between the hydrogen atoms and the calcium atoms is 2.045Å. Aspects such as bond length and crystal structure are influencing factors for the hydrogen adsorption as well as the heat of the hydride formation. The bond character is determined by different factors, such as electro negativity and crystal structure. However earth alkali metals bonded with hydrogen generally consist of more ionic bonds due to the higher electro negativity values for earth alkali metals [48, 53]. Even though the majority of the bonds are of ionic character, covalent bonded Ca- H occurs as well. Another major factor of the desorption temperature is the heat of the hydride formation. The value describes the amount of heat that is generated during the hydride formation, which in the case of CaH_2, is ΔH= -45kJ/mol. The same amount that becomes free during the hydride formation

needs to be induced in order to split the hydrogen bonds again. The DSC analysis could not provide information about the reaction equation because the desorption is beyond the range of the apparatus. Data from published experiments verified the endothermic character of the reaction [48]. At temperatures of 650°, enough energy is induced into the system in the form of heat to break the ionic/covalent bonds and release hydrogen in form of H^- ions. Due to their partially ionic character, Ca^{2+} and H^- ions are formed during the desorption process in addition to Ca and H in an atomic state.

2.2.3.2.3. Material 6: TiH_2

Similar to both previous binary hydrides, titanium hydride consists of one metal atom, which is covalently bonded to two hydrogen atoms. Due to the high molecular weight of titanium, its maximum theoretical storage density is limited to 4wt %, which makes it undesirable as a storage medium for commercial application. Similar to calcium hydride and magnesium hydride, this hydride is a commonly used precursor for complex hydrides as well as doping material. Therefore, it is analyzed by its structural composition and its hydrogen desorption behavior [54-56].

XRD Analysis

The XRD analysis will provide important information about the composition of the material as well as the determination of the purity of the sample. Therefore the sample is prepared for the analysis as described in a previous chapter and tested under defined conditions.

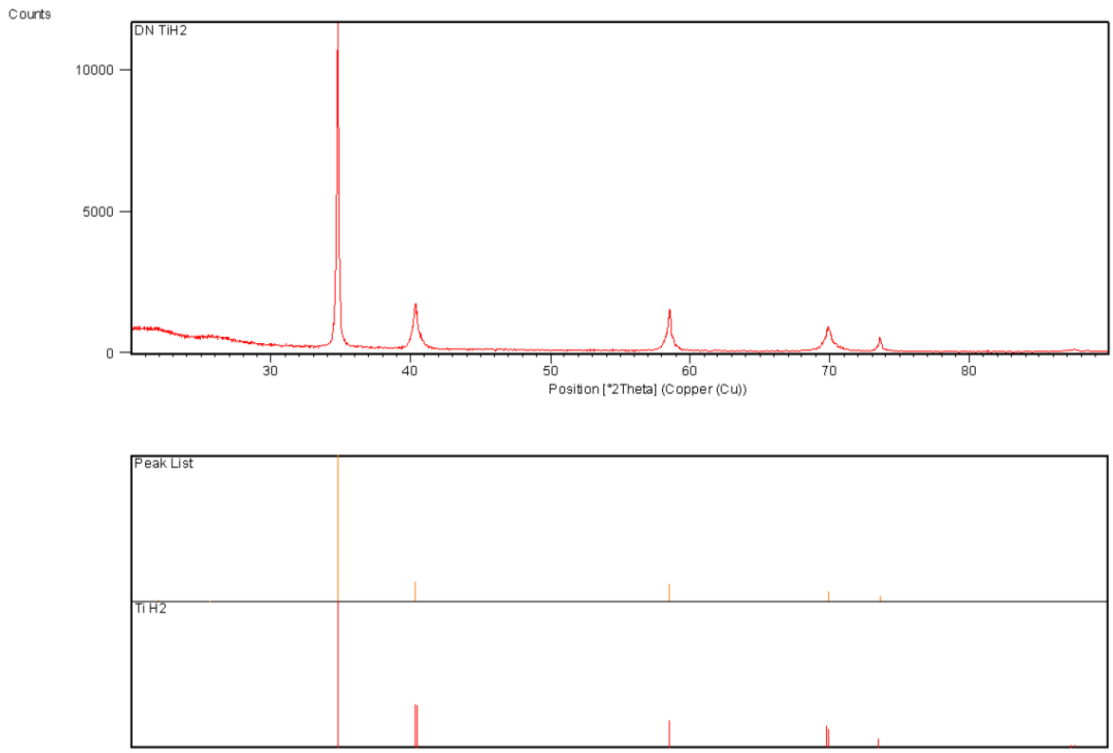

Figure 49 XRD analysis of TiH_2

Figure 49 above presents the results of the analysis. The comparison of the peak list with the data base verified the material and indicated the high purity of the material. Throughout the course of research, this material has also been used as a precursor to synthesize new compounds and composites.

TGA Analysis

In order to get a better understanding of the hydrogen desorption behavior, the material was analyzed by TGA. The determination of its characteristics is of major interest and is the basis for the success of the synthesis of new materials. The material is prepared for the analysis and tested under defined conditions and parameters. The result of the TGA analysis is presented in Figure 50.

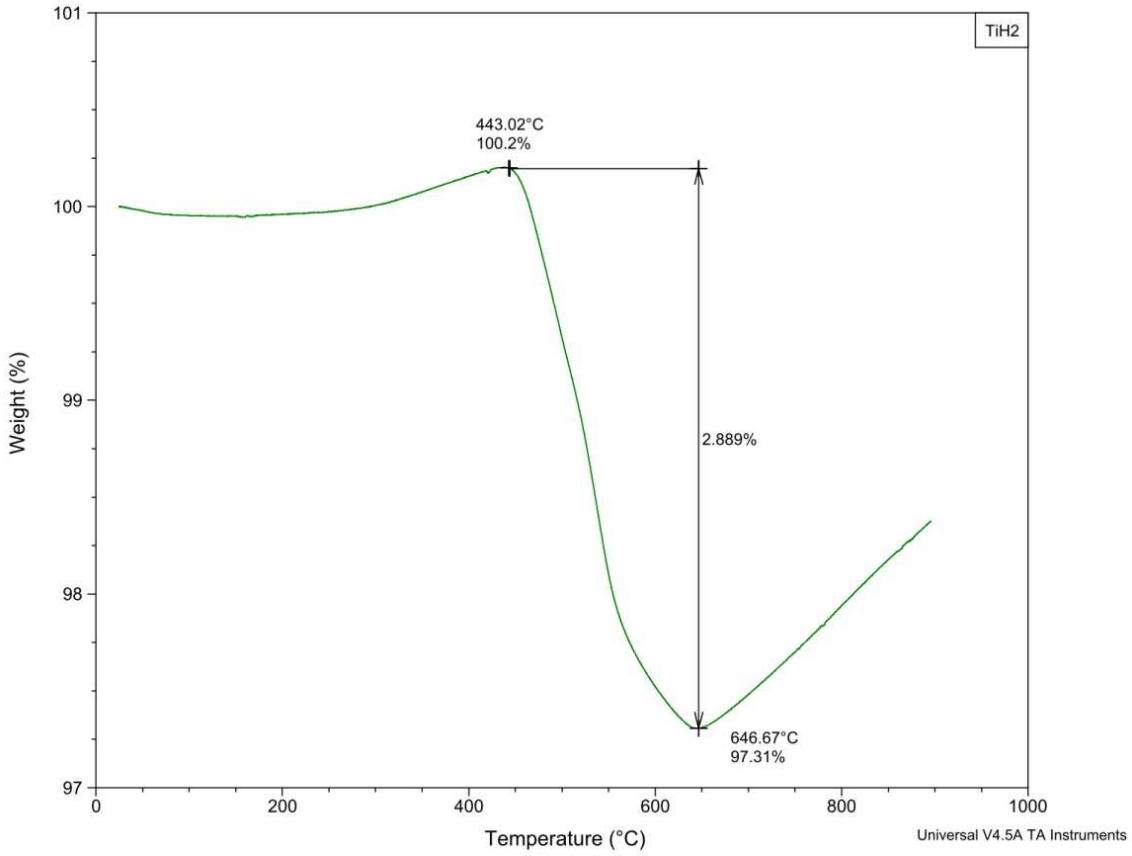

Figure 50 TGA analysis of TiH_2

This analysis provides two important sets of information. First, the desorption temperature begins at 440℃ and ends at 650℃. Seco nd, approximately 2.9wt % hydrogen was desorbed, which leads to the assumption that the hydrogen desorption was not complete since the theoretical amount of hydrogen desorption is 4.0wt %. The high desorption temperature of this material can be mainly referred to the bond characteristics between the calcium atom and the hydrogen atoms. These covalent bonds are strong which requires a high amount of energy to split them. At high temperatures, enough energy is introduced in the system, which leads to hydrogen desorption.

DSC Analysis

The DSC analysis has been designed in order to get information about the bond characteristics. Therefore the sample is prepared and tested under defined conditions mentioned previously.

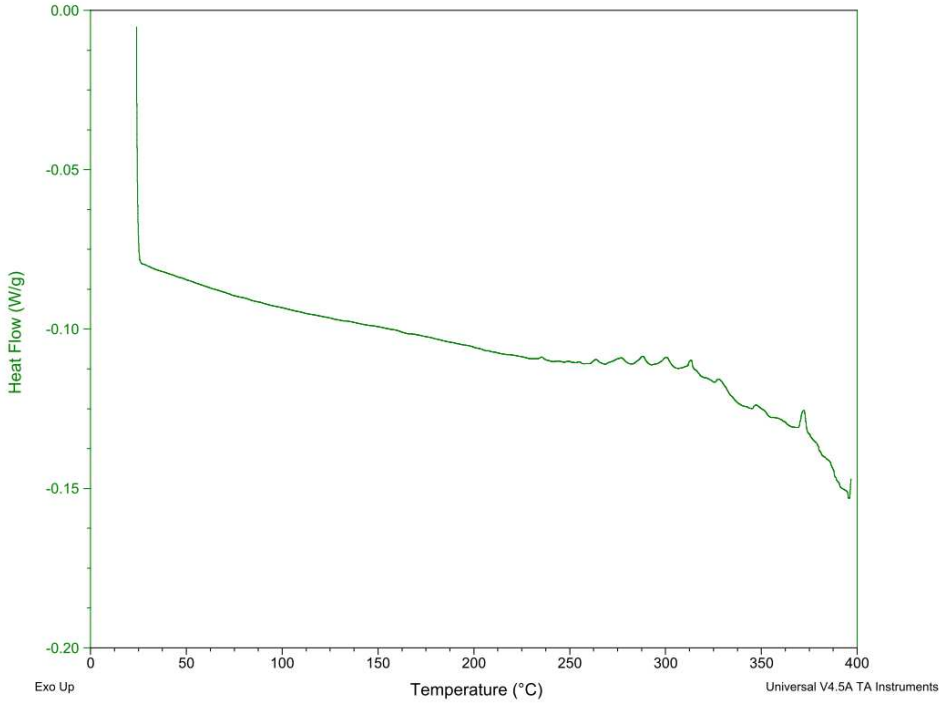

Figure 51 DSC analysis of TiH_2

The DSC pattern looks similar to the pattern of calcium hydride. Similar to the other pattern, two unexpected events occurred. An initial drop can be observed as well as a steady decrease of the curve can be recognized. Both events can be explained in the same way as in the DSC pattern of calcium hydride where the drop is caused by a calibration process of the sample whereas the decrease is caused by reactions of the sample with residual air.

Analysis and discussion

The hydrogen desorption behavior of titanium hydrides was examined by a TGA analysis as well as a DSC analysis. The results of the TGA analysis show, in the temperature range of 25- 440℃ a steady increase in weight of a pproximately 0.2wt %. This increase in weight can be related to minor reactions of the sample with residual moisture and oxygen. However, these side effects are weaker than in all other tested materials.

The TGA pattern shows a hydrogen desorption behavior in a temperature range of 440-640℃, linked with a total amount of desorbed hydro gen of ~2.9wt %, which is less than the theoretical value of 4.0wt % and other published results [57, 58]. Published experiments show a hydrogen desorption rate close to the theoretical value, which is approximately 1wt % more than current results. Comparing the analysis parameters and system parameters of each measurement with each other, it points out that the heating rate during TGA and DSC was chosen to rates as low as 2-5℃/min instead of 10℃/min for current measurements. Since all other parameters are similar to each other, it can be assumed that weak reaction dynamics, connected with a unfavorable heating rate, result in the decreased amount of desorbed hydrogen. The DSC analysis could not provide information about the temperature of desorption, because the desorption is out of the analysis range. The increase in weight of the sample at temperatures as high as 650-800℃ can be related to high energy reactions betwe en Ti and Argon.

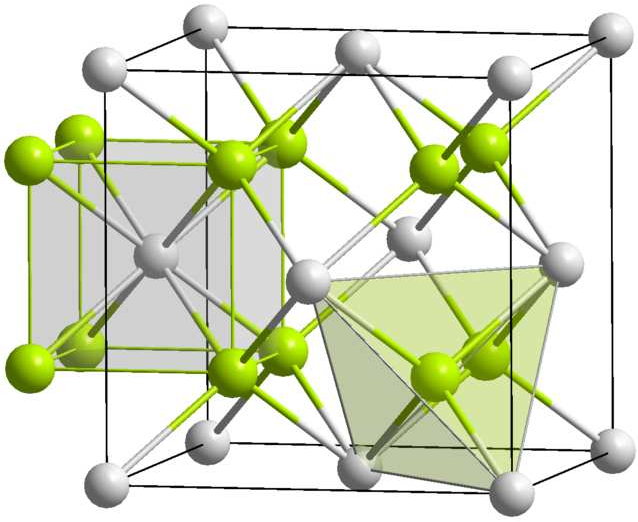

Figure 52 Crystal Structure of TiH_2

Figure 52 shows the crystal structure of the TiH_2 crystal, which is a tetragonal face centered cubic crystal with a space group of Fm3m with titanium and hydrogen in the unit cell. The lattice parameters of the tetragonal- face-centered cubic crystal are "a"= 4.47Å and "c"=4.4Å, with a bond length between the titanium atom and hydrogen atoms of 1.8Å [59, 60]. The strength of the bond is dependent on two main aspects, the bond characteristics and the heat of the formation ΔH. Due to their values for bond length and crystal parameters as well as the position of titanium in the periodic table (electro negativity), the Ti- H bonds are of covalent character.

The hydrogen desorption takes place in a multi step reaction in the form of

2.25

Behavior cannot be proved in the TGA analysis because both reaction processes are overlapping each other. Recent study found and verified this behavior through DSC analysis, where two different reaction peaks were proved [57, 58, 61]. The hydrogen

desorption is beyond the range of the DSC apparatus so that no DSC analysis is performed.

The heat of the hydride formation is another important factor for the determination of the hydrogen desorption temperature. The heat of the formation, ΔH= -72kJ/mol determines the amount of energy that needs to be induced into the system to split the Ti-H bonds [59, 61]. In the case of TiH_2, enough energy is introduced at 440℃ to split the bond under hydrogen release.

2.2.4. Summary

Both the structural analysis and the hydrogen desorption analyses of singularly and binary hydrides are of basic interest in further material synthesis. The thermal behavior and the desorption kinetics of the materials are already well tested in a multitude of experiments and did not provide new basic knowledge. However, these analyses were important throughout the course of the study because a deep knowledge about the material's behavior is important to the quality of further analyses. Since all materials mentioned in this chapter can be used as precursors for new compounds and composites, having a basic knowledge of their chemical and physical behavior is essential. Based on these results, decisions about new compositions and compounds are made.

Table 1 Summary of Singularly/Binary Hydrides

	Decomposition Temperature [℃]	Theoretical Storage Density [wt %]	Experimental Storage Density [wt %]
Singularly Hydrides			
LiH	640-680	12.7	11.9
NaH	300	4.3	1.8
KH	375	2.5	2.4
Binary Hydrides			
MgH_2	400-450	8.2	6.5
CaH_2	650	5.0	4.7
TiH_2	440-650	4.0	2.8

Table 1 provides an overview of the experimental results of the hydrogen desorption behavior of the material. Values for the desorbed amount of hydrogen lie, in most cases, near the theoretical value, which indicates the complete hydrogen desorption. In the example of NaH and MgH_2, values for the hydrogen desorption are low compared to the other materials. The reason for that is the weak reaction kinetics of the material caused by the strength of the bond between the metal atom and the hydrogen atom. Connected with the unfavorable heating rate of the sample, which is, for these particular materials too high.

Furthermore, almost all the materials showed interactions between moisture and air during the heating process. Singularly hydrides can potentially react with air as well as moisture in the general form of:

$$MH + 0.5O_2 \rightarrow MOH \tag{2.26}$$

or

$$2MH + 0.5O_2 \rightarrow M_2O + H_2 \tag{2.27}$$

$$M_2O + H_2O \rightarrow 2MOH \quad (2.28)$$

and moisture

$$MH + 0.5H_2O \rightarrow 0.5M_2O + H_2 \quad (2.29)$$

$$M_2O + H_2O \rightarrow 2MOH \quad (2.30)$$

or

$$MH + H_2O \rightarrow MOH + H_2 \quad (2.31)$$

where M stands for Li, Na, K. Basically, the reaction with air and moisture can take place either in a single step reaction or in a double step reaction. Comparisons with published data indicate that the single step reactions are preferable over the double step reactions [51].

Similar to the singularly hydrides, binary hydrides showed these interactions with the ambient atmosphere as well. The materials reacted with air and moisture in the following way

$$XH_2 + 2H_2O \rightarrow X(OH)_2 + 2H_2 \quad (2.32)$$

or

$$XH_2 + 2O_2 \rightarrow X(OH)_2 + H_2 \quad (2.33)$$

where X stands for Ca, Mg, and Ti. Unlike singularly hydrides, the reaction only takes place in a single step. These reactions mentioned above cannot be eliminated in the TGA analysis and need to be considered in the analysis of the results. The side reactions do not affect the hydrogen desorption behavior of the tested material.

Another important outcome of the analysis of the materials is the unexpected two-step desorption reaction of TiH_2, where in a first step, a structural change takes place, and in

a second step, the hydrogen bond splits. This behavior is especially for the composite formation and its hydrogen desorption of interest.

In conclusion, the analyses of the material gave a basic overview of the hydrogen desorption temperature and its kinetics. Furthermore, information about the structure of the material, their bond characteristics and their specific values for the heat of the hydride formation, were provided. All materials except of TiH_2, where the bond is of metallic character, show a mixture of ionic and covalent bonds within their structure. This information is of major importance understanding the desorption kinetics of each material.

2.3. Mixture of TiH_2 and CaH_2

2.3.1. Objectives

Previously it has been shown that both singularly and binary hydrides are not applicable as hydrogen storage systems due to their high desorption temperatures or their inadequate storage densities. All tested materials showed hydrogen desorption temperatures of above 300℃, which is about 200℃ more than what is accepted in storag e densities of 4-5wt %. Therefore, attempts to synthesize composites of these materials are done. Singularly and binary hydrides have favorable storage densities so that improved decomposition temperatures can be expected by forming a composite. This chapter deals with the mixture of materials, when two precursor materials are taken and mixed in different ratios with each other. Depending on their structural composition and their chemical behavior, either new compounds or composites can be formed with the potential for improved desorption kinetics. By having six precursor materials available and mixing just two with each other, 15 possible mixtures can be formed. In the present case, weight mixtures of 25:75, 50:50, 75:25, and a mixture based on the molar ratio of 95:5 were chosen. Furthermore, titanium dioxide, titanium chloride and aluminum chloride are available as doping materials.

All these combinations add up to a multitude of possible variations of mixtures. Hence, one needs to focus on certain materials and compositions which seem to have favorable characteristics and desorption behavior [1, 62, 63].

2.3.2. Synthesis Methodology and Characterization

In a first attempt, calcium hydride and titanium hydride are chosen as precursor material. Even though their individual desorption kinetics may not be favorable, a compound or composite of these materials can yield completely different characteristics. As a result, materials should never be excluded as precursors due to their individual characteristics.

The first series of experiments consist of the materials which are mixed in a titanium hydride to a calcium hydride mass ratio of 25:75, 50:50, and 75:25. Additionally, a mixture of these materials with a molar ratio of 95:5 was synthesized. The preparation of the material is performed in a glove box under an argon atmosphere in order to avoid contaminations of both the precursor material, and the final product. 1g of each sample is produced. Then, the precursors are weighed, mixed and charged together with 6 steel balls in a stainless steel vial. The steel balls have a diameter of 10 mm and 5 mm, respectively. The vial is adjusted to a planetary ball mill and the mixture is mixed for 3 hours. After that process, the vial is moved back into the glove box and the product is prepared for the structural and desorption analyses. The structural composition of the composite is analyzed by an XRD technique. Parameters and sample preparation are discussed in previous chapters and are valid for the composite testing as well.

The hydrogen desorption behavior is analyzed by both the TGA and DSC apparatus. The preparation of the sample is done in the glove box and then moved to the location of analysis. Both apparatus run with an argon purge gas flow of 60mL/min and a heating rate of 10℃/min [1, 2].

2.3.3. Analysis

2.3.3.1. Mixture 1: TiH_2 + CaH_2 mass ratio 25:75

The precursors were mixed in TiH_2 :CaH_2 mass ratio of 25:75 in order to form a compound of the general form $TiCaH_4$ or a composite in the general form of TiH_2:CaH_2 with different mass ratios. After weighing, mixing and charging the materials in a vial, the mixture is milled and the product tested for its structural and desorption characteristics.

XRD analysis

The sample is prepared under an argon atmosphere to avoid contamination. There, the material is placed on a sample holder and covered with Kapton foil. The analysis of the material is done under a standard set up, as mentioned above. The results of the analysis are given in Figure 53.

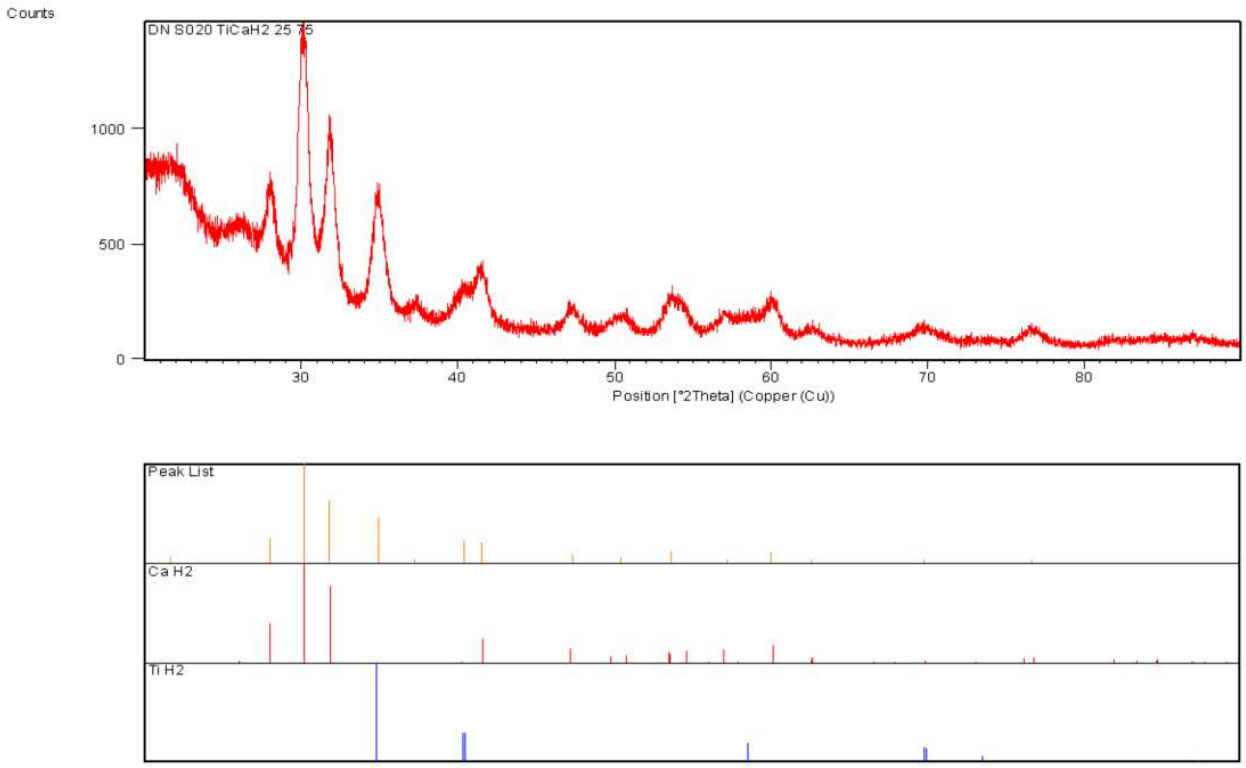

Figure 53 XRD analysis of TiH_2 :CaH_2 Composite 25:75

The peak pattern identifies the two precursor materials and a few peaks which, can be related to new a composite of titanium hydride and calcium hydride. The structural analysis showed that the formation of a new compound was unsuccessful. A formation of the compound is from a chemical point of view not possible. Recent experiences have shown that after 3 hours of ball milling, the formation of at least traces of new material should occur. This expectation leads to the assumption that a solid state reaction is not favorable for this combination. Hence, the peak pattern clearly differs from the two precursor pattern. This indicates that a structural change in the sample during the ball milling process has occurred, which implies a success in the synthesis itself.

TGA and DSC Analysis

The new composite is analyzed in terms of its hydrogen desorption behavior. Both precursor materials show hydrogen desorption at temperatures of 400℃ and 600℃, respectively. It is of interest to see, how the desorption temperature improved by using a composite of these materials. In the present case, the TGA analysis was performed within a temperature interval of 25℃- 400℃. Two reasons for that are following:

- Desorption temperatures above 400℃ are not of int erest
- Risk for damaging pan and weighting plate are high at temperatures above 600℃.

The result of the TGA analysis is shown in Figure 54

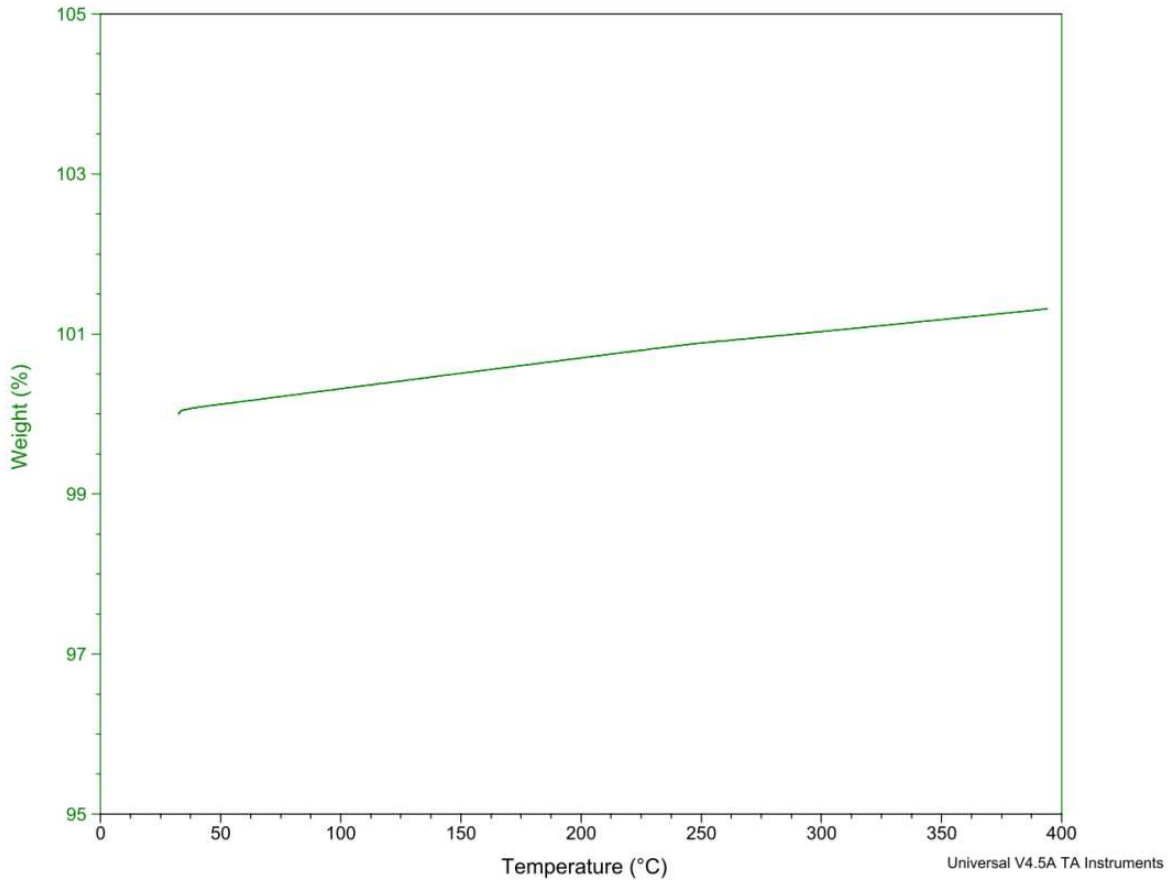

Figure 54 TGA analysis of TiH_2 :CaH_2 Composite 25:75

The result of the TGA analysis showed that no hydrogen desorption within the tested temperature interval occurred. It is still being analyzed, where desorption takes place, even though this information is of minor interest in the present study. Because the desorption does not take place within the desired temperature interval, and the DSC analysis is limited to a maximum temperature of 400℃.

2.3.3.2. Mixture 2: TiH_2 + CaH_2 mass ratio 50:50

In a second attempt, a mixture with a TiH_2 :CaH_2 mass ratio of 50:50, was chosen. Previous analysis has shown that the formation of a compound will not occur, and instead, a composite formation will form.

XRD Analysis

The mixture of titanium hydride and calcium hydride is ball milled for 3 hours, similar to previous attempts. After the synthesis, the material is prepared for a structural analysis in a commonly used procedure. The results of the structural analysis are given in Figure 55.

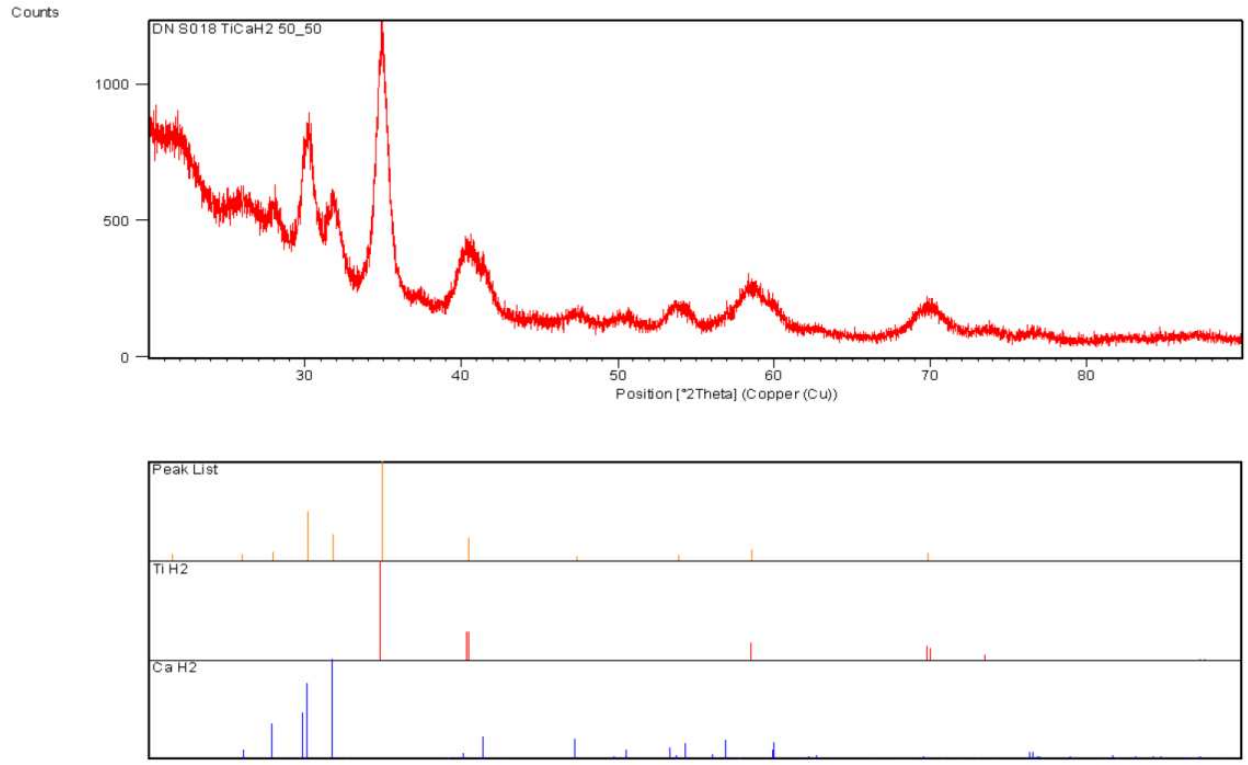

Figure 55 XRD analysis of TiH_2 :CaH_2 Composite 50:50

Similar to the previous sample, a change of the pattern in comparison to the precursors was proven. This behavior indicates a change in the structure of the material, which is linked to the formation of a composite.

TGA and DSC Analysis

Hydrogen desorption behavior of the composite should be proven by a TGA and DSC analysis, respectively. Therefore, the material is prepared in the glove box for the TGA analysis. The analysis itself is done under standard conditions within a temperature interval of 25℃ to 400℃. The results of the analysis are presented in Figure 56 below.

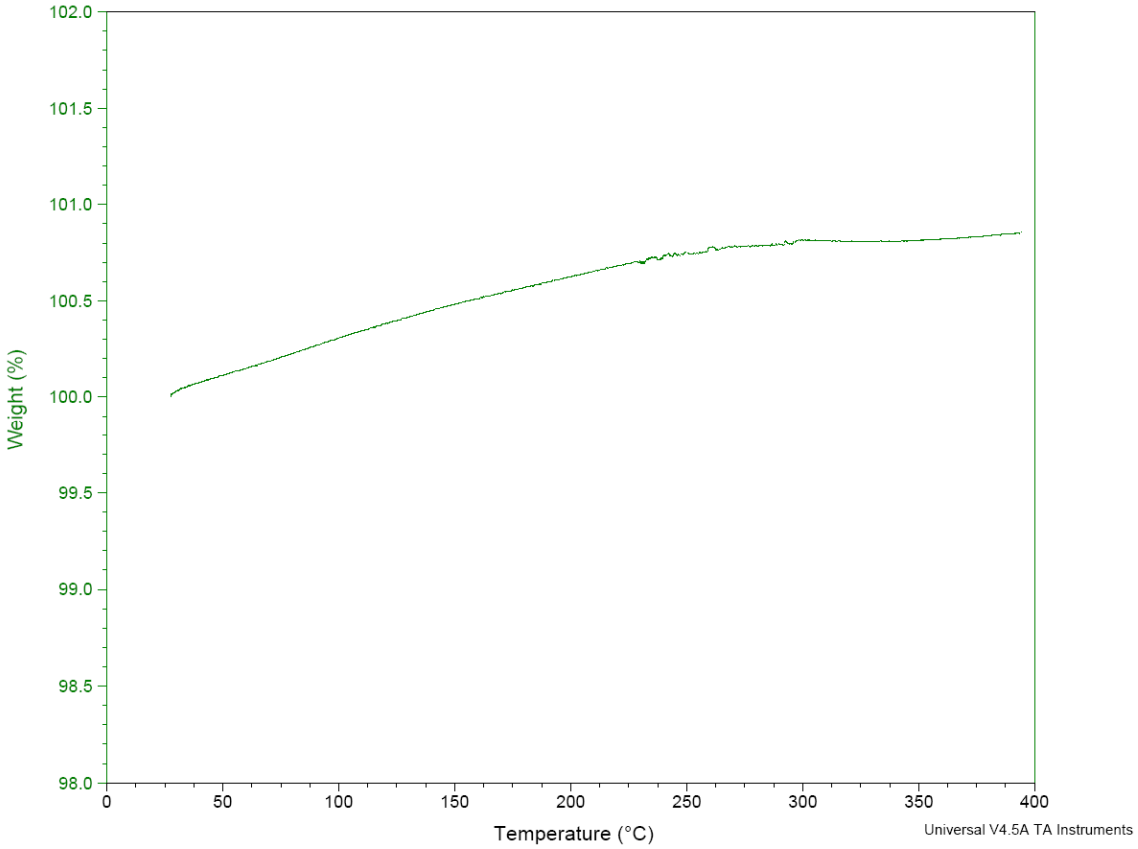

Figure 56 TGA analysis of $TiCaH_2$ Composite 50:50

The pattern indicates the absence of hydrogen desorption in the tested interval. However, no statement implying improved reaction kinetics can be made. This outcome needs to be tested for further analyses.

2.3.3.3. Mixture 3: TiH_2 + CaH_2 mass ratio 75:25

In a third attempt, the mass ratio of the TiH_2 :CaH_2 is varied again to a value of 25:75. Similar to other samples, the XRD, TGA and DSC analyses should provide basic information regarding the composite characteristics. Based on previous experiments, it is not anticipated that a new compound will be formed. However, the formation of a composite is expected.

XRD Analysis

The two precursors are mixed and charged in a vial and then milled for 3 hours. Afterwards, the resulting product is analyzed based on its structural characteristics using common techniques. As usual, the sample is prepared in the glove box and moved to the place of analysis, where it is analyzed under standard conditions. The results are presented in Figure 57 below.

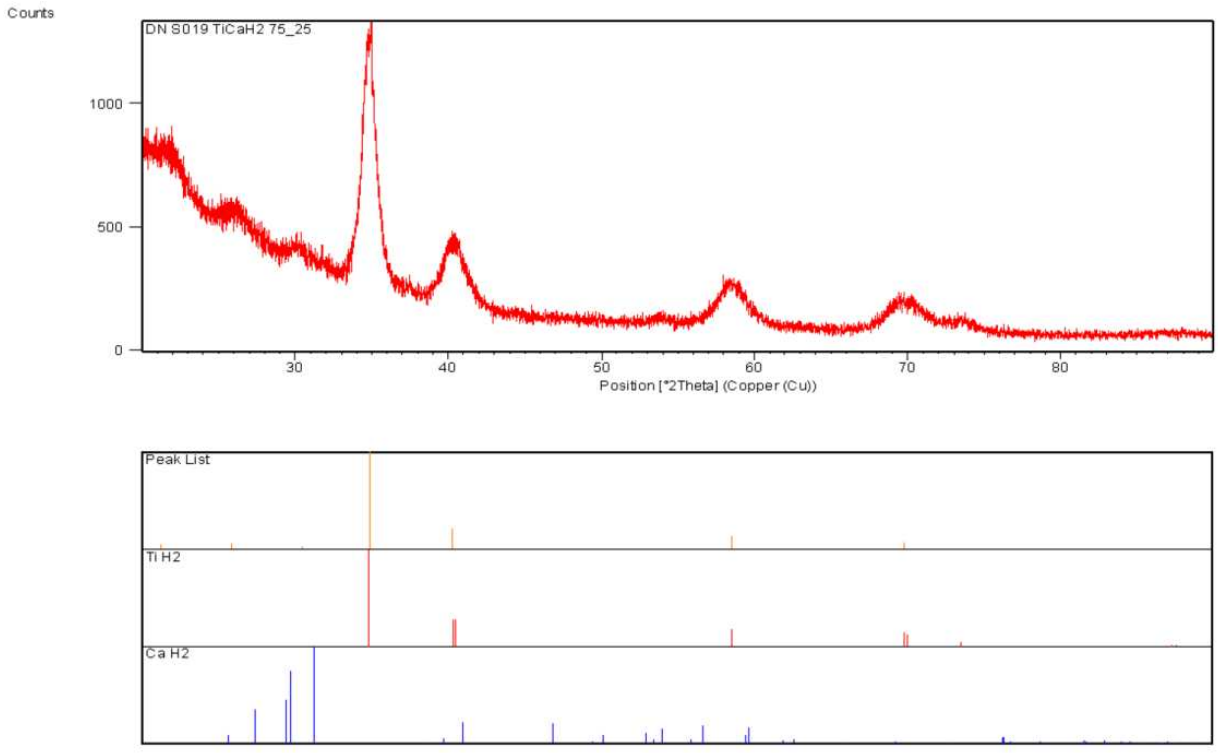

Figure 57 XRD analysis of TiH_2 :CaH_2 Composite 75:25

As expected, the XRD pattern does not indicate the formation of a new compound. However, it could be proven that a composite from the two precursor materials has been formed. The pattern shows main peaks of the titanium hydride precursor, but also significant peaks of the calcium hydride precursor, which leads to the assumption of the formation of a new composite.

TGA and DSC Analysis

TGA and DSC analysis should provide information concerning hydrogen desorption kinetics. The sample is prepared in the glove box for the analysis and tested under the common used techniques and parameters. The analysis was performed and yielded the following results.

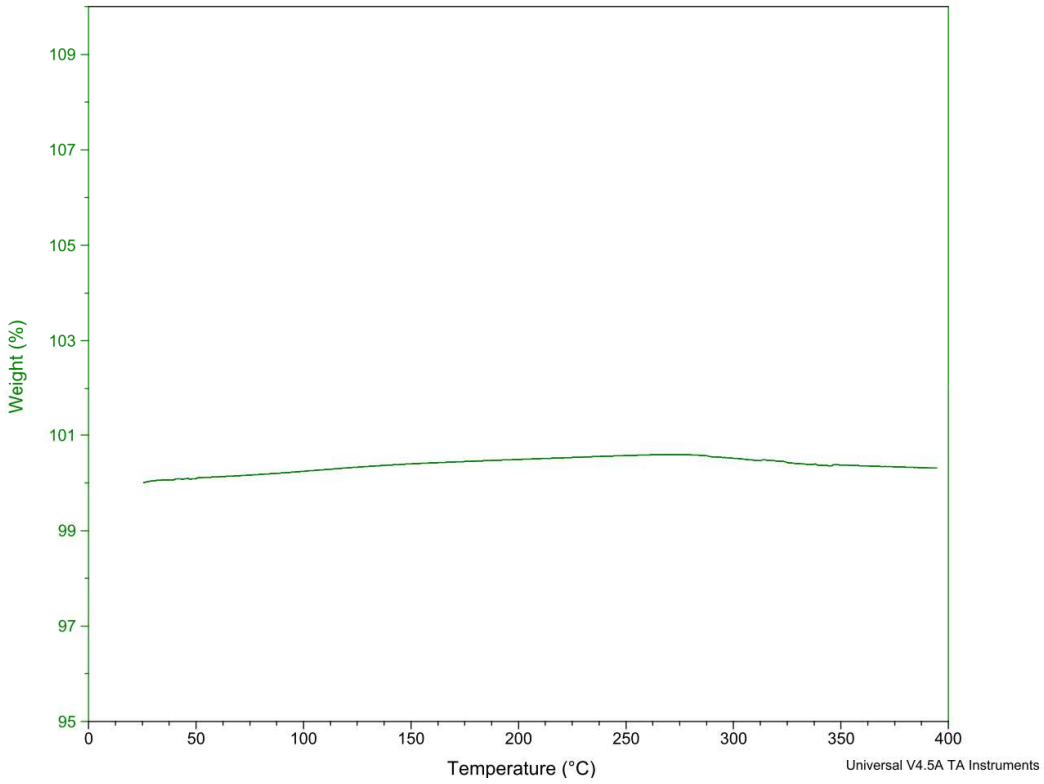

Figure 58 TGA analysis of TiH_2 :CaH_2 Composite 75:25

The results clearly support the assumption that no hydrogen desorption occurs within the given temperature interval. Furthermore, it is not possible to predict the hydrogen desorption temperature. In order to attain information about improved desorption dynamics, further analysis must to be done.

2.3.3.4. Mixture 4: TiH_2 + CaH_2 molar ratio 95:5

In a last experiment of this system, a composite with a molar ratio of TiH_2 :CaH_2 of 95:5, was tested. This mixture results in a small amount of calcium hydride in the material, so that this material acts more like a dopant than as a precursor.

XRD Analysis

The material is weighed and mixed dependent on its molar ratio. The mixture is then milled by a planetary ball mill for 3 hours. The product is prepared and analyzed for its structural properties by a XRD technique. The results of the analysis are presented in Figure 59 given below.

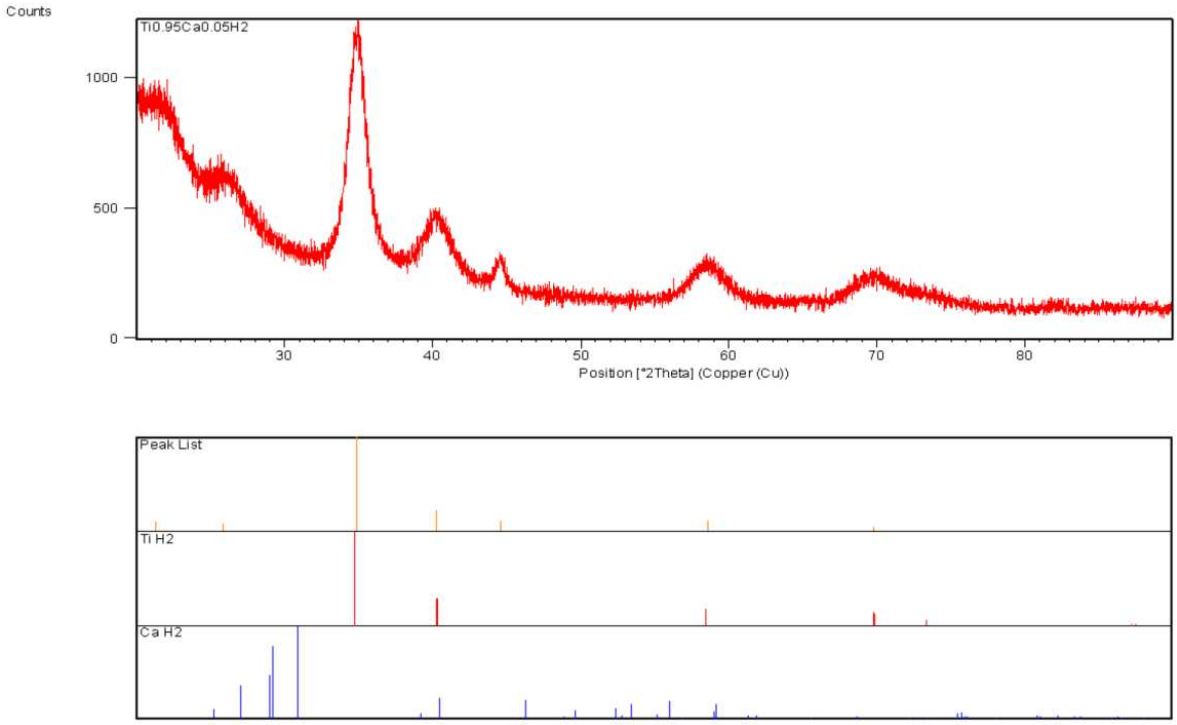

Figure 59 XRD analysis of $Ti_{0.95}Ca_{0.05}H_2$ composite

The pattern provides a clear overview of the structural composition of the material. Main peaks of both the titanium hydride precursor, as well as the calcium hydride material, can be observed.

TGA and DSC Analysis

The TGA analysis of the sample should provide information about the desorption characteristics of the material. Therefore, the samples are prepared for the analyses and tested under the common used conditions. The result of the analysis is shown in Figure 60 mentioned below.

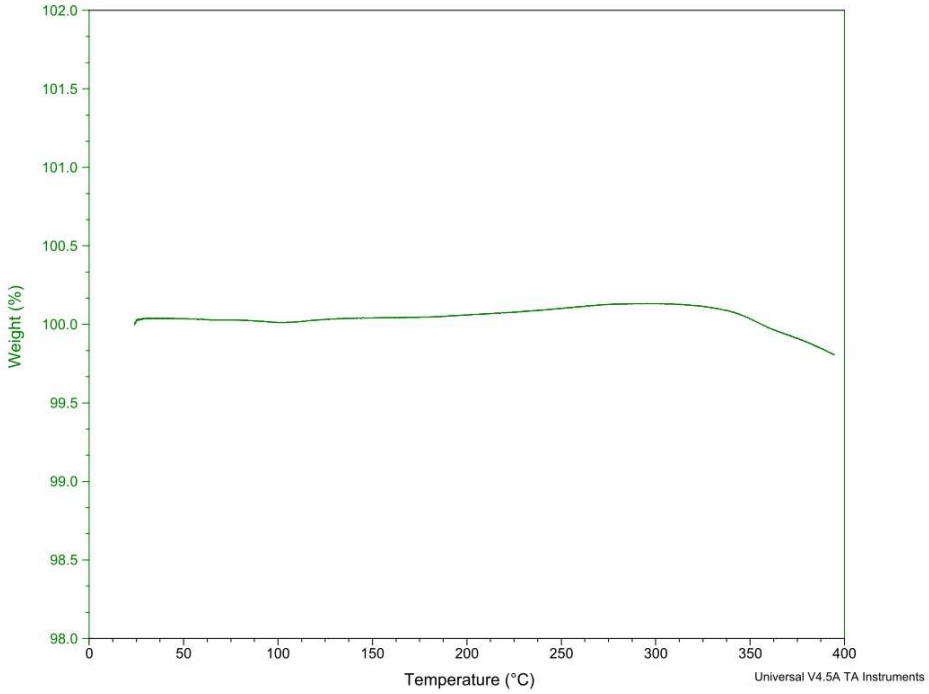

Figure 60 TGA analysis of $Ti_{0.95}Ca_{0.05}H_2$ Composite

The analysis is performed in a temperature interval of 25℃ to 400℃, and under standard condition. The TGA curve does not show any significant change, which leads to the conclusion that the hydrogen desorption lies above 400℃. As a consequence, no additional DSC analysis was performed.

2.3.4. Discussion

In this series of experiments, different mixtures of titanium hydride and calcium hydride were made and tested. Even though the desorption behavior of each component is unfavorable due to their high desorption temperatures, the composite can yield improved reaction kinetics. Mixtures of different mass ratios were formed in order to see the influence of each precursor on the reaction behavior. Results of this series are given in Table 2.

Table 2 Overview of results of the Composite

Material	Material Specifications				TGA				DSC					XRD
	molar weight [g/mol]	theoretical storage density [wt %]	chem. Reaction	reversible storage density [wt%]	experimental [wt%; ℃]		published [wt, ℃]		experimental [W/g, ℃]		theoretical [W/g]	published [W/g, ℃]		
					without catalyst	with catalyst	without catalyst	with catalyst	without catalyst	with catalyst		without catalyst	with catalyst	x
$TiCaH_2$ 25:75	43.8039	4.6	Data n.a.	Data n.a.	no desorption Until 400°C	-	Data n.a.	-	beyond range	-	-	Data n.a.	-	x
$TiCaH_2$ 50:50	45.6587	4.4	Data n.a.	Data n.a.	no desorption Until 400°C	-	Data n.a.	-	beyond range	-	-	Data n.a.	-	x
$TiCaH_2$ 75:25	47.6775	4.2	Data n.a.	Data n.a.	no desorption Until 400°C	-	Data n.a.	-	beyond range	-	-	Data n.a.	-	x
$Ti_{0.95}Ca_{0.05}H_2$	49.4936	4.0	Data n.a.	Data n.a.	no desorption Until 400°C	-	Data n.a.	-	beyond range	-	-	Data n.a.	-	x

n.a.= not available

The XRD analysis of the samples provides information about the structural composition of the samples dependent on the mixtures of the precursors. As a general conclusion, it can be stated that composites were formed independent of the mixture. Comparing the pattern of the precursor materials with the product, a clear phase formation took place during the synthesis process. Significant peaks for the new phase are at angles of $2\Theta_1 = 32.1°$ and $2\Theta_2 = 45.5°$. Since the synthesis of that mixture is not yet published, no references to the current results can be made.

Based on the results of the structural analysis, the hydrogen desorption behavior of the samples was tested. The TGA experiments were performed until a temperature of 400° because hydrogen desorption above that temperature range is not of interest for further analysis.

Depending on the ratio of the precursors, a theoretical storage density of 4.0wt % and 4.6wt % is expected. All samples showed a thermodynamic stable behavior in the temperature range until 400° and did not desorb any hydrogen. Further analysis need to be performed to determine the temperature of desorption and the possible amount of desorbed hydrogen.

2.4. Doping of Materials

2.4.1. Objectives

The analysis of all systems, lithium- sodium alanate, lithium hydride and the composite of titanium hydride and calcium hydride, indicate either unfavorable desorption kinetics or insufficient storage densities. In order to improve at least the reaction kinetics, catalysts are implemented into the material structure. In the present study, materials such as titanium chloride, aluminum chloride or titanium dioxide are used as precursors for this process. Only titanium and aluminum act as the catalyst, while the dioxide and chlorine molecules act as host materials of the catalysts. These materials do not influence the chemical and physical properties of the material. As mentioned in previous chapters, different methods for the implementation of these catalysts can be distinguished. In the present study, the catalyst is embedded into the material structure after the synthesis process itself. During the mechanochemical treatment, titanium and aluminum, respective split up their existing bonds and generate new bonds with the host atom of the metal hydride.

Many different materials have been found that have the potential to act as a catalyst. Besides the materials mentioned above, nickel, vanadium, as well as compounds of these materials are commonly used catalyst materials. The catalyst itself, along with the milling method, milling time, and the amount of dopant are critical factors influencing the materials behavior. Previously published data portrays good results for the catalysts titanium chloride, aluminum chloride and titanium dioxide. Based on this knowledge, analyses were performed on the synthesized materials in order to gain new information about the reaction kinetics and desorption behavior of different materials [16, 19, 39, 54-56, 62, 64-69].

2.4.2. Synthesis Methodology and Characterization

Many hydrides do not fulfill the guidelines, such as reversible storage density of 6wt %, working temperatures in the temperature interval of -30-100℃, or cost of the material, given by the DoE. Therefore, the material is doped with a catalyst material. The doping process can be performed by either a chemical or mechanochemical reaction. In the present study, a mechanochemical process, ball milling, is used to implement the catalyst into the structure. Similarly, it is possible to dope a material. To do this, the material and the dopant are mixed in a fixed molar ratio and charged with several steel balls into a vial.

The amount of dopant, milling time and the amount of steel balls have a significant influence on the hydrogen desorption characteristics of the resulting material. Previous analyses have determined that 2 mol% of dopant material optimizes results in terms of reaction kinetics and storage density and that a milling time of 30 minutes is seen as an adequate milling time in order to receive a proper implementation of the catalyst material into the host structure. In addition to the production process and the hydride to dopant ratio, the dopant material is a significant component of this process. In general, many different materials can be used as dopants, primarily nickel, titanium, vanadium and aluminum. During the milling process, these atoms form complex structures with the hydride, which results in improved reaction dynamics. In the present study, $TiCl_3$, $AlCl_3$, and TiO_2 have been selected as doping materials due to their favorable effects on hydrides in previous studies.

The general reaction that occurs during the hydrogen desorption process in the case of sodium aluminum hydride and titanium chloride can be written as

$$3NaAlH_4 + TiCl_3 \rightarrow 3NaCl + Al + Ti + 6H_2 \qquad 2.34$$

Even though this example describes only one possible hydride to dopant combination, processes using other combinations can be derived from this reaction equation, as well.
This reaction equation shows that the dopant material reacts with the hydride in order to form sodium chloride, atomic titanium and molecular hydrogen. This process is thermodynamically easier than the processes required by the hydride in its original form. As a result, the hydrogen release takes place under more moderate conditions.

The analysis of the doped material is similar to the analysis of all other materials. The structural analysis is performed by an XRD apparatus under standard conditions, mentioned in a previous chapter. The scanning range was chosen based upon previously published results and experience gained throughout the study. It is adjusted to an angle range of $20° \leq 2\Theta \leq 90°$. In this range, characteristic peaks of the hydride/dopant mixture can be proven and a clear identification of the doped hydride is possible. Furthermore, the hydrogen desorption behavior is analyzed by the TGA and DSC apparatus. Both methods combined, enable a precise prediction about the bond characteristics and the desorption dynamics. These analyses are performed under standard conditions [2, 9].

2.4.3. Analysis

2.4.3.1. $NaAlH_4$

The manipulation of sodium aluminum hydride, with a structural composition of $NaAlH_4$, is an important precursory step for the analysis of unknown samples. Published data using doped materials can be compared with current data to validate the doping process. Similar to the synthesis validation, this aspect is important for the validation of later results [62, 67, 68, 70-72]. Previously mentioned in Chapter 3.1, a prior validation of the doping method is crucial for the interpretation of later results and the prevention of flaws in the doping process. For each sample 0.2g of the hydride was mixed with 2mol % of dopant.

Table 3 Mixture of $NaAlH_4$ and Dopants

	Matrix Material	**Dopant**		
Name of Material	$NaAlH_4$	$TiCl_3$	TiO_2	$AlCl_3$
Molecular weight [g/mol]	54.00	154.23	79.866	133.34
Sample weight [g]	0.2	-	-	-
mole% of dopant [%]	-	2	2	2
mole of Matrix Material [mol]	0.00370	0.00007	0.00007	0.00007
Amount of Material [g]	**0.2**	**0.0114**	**0.0059**	**0.0099**

The components are mixed and charged with 6 steel balls in a tungsten carbide vial and then milled for 30 minutes. Afterwards, the doped samples are prepared for the analyses.

XRD analysis

The preparation for each material is done in a glove box due to their high affinity to react with moisture. The analysis itself is done under standard conditions mentioned earlier. Figure 61 gives an overview about the XRD spectra of each doped material as well as the undoped material.

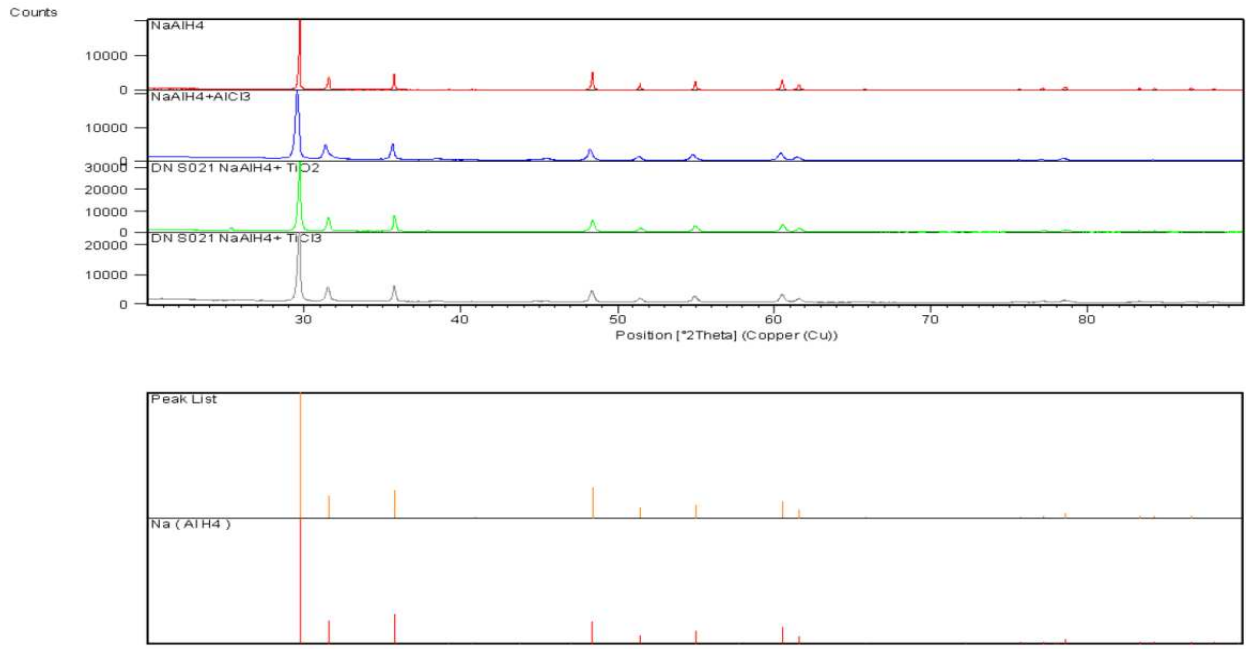

Figure 61 XRD analysis of doped $NaAlH_4$

The collection of the XRD pattern clearly shows the impact of the dopant on the material structure. The XRD pattern shows no indication of precursor material. This fact is a strong indication of the implementation of dopant material in the hydride structure.

TGA Analysis

The TGA analysis is performed to clarify the impact of different dopants on the desorption characteristics of the material. Therefore, the samples are prepared in the glove box similar to all other previously prepared samples and tested in the TGA apparatus. The results of the TGA analyses are presented in Figure 62 shown below.

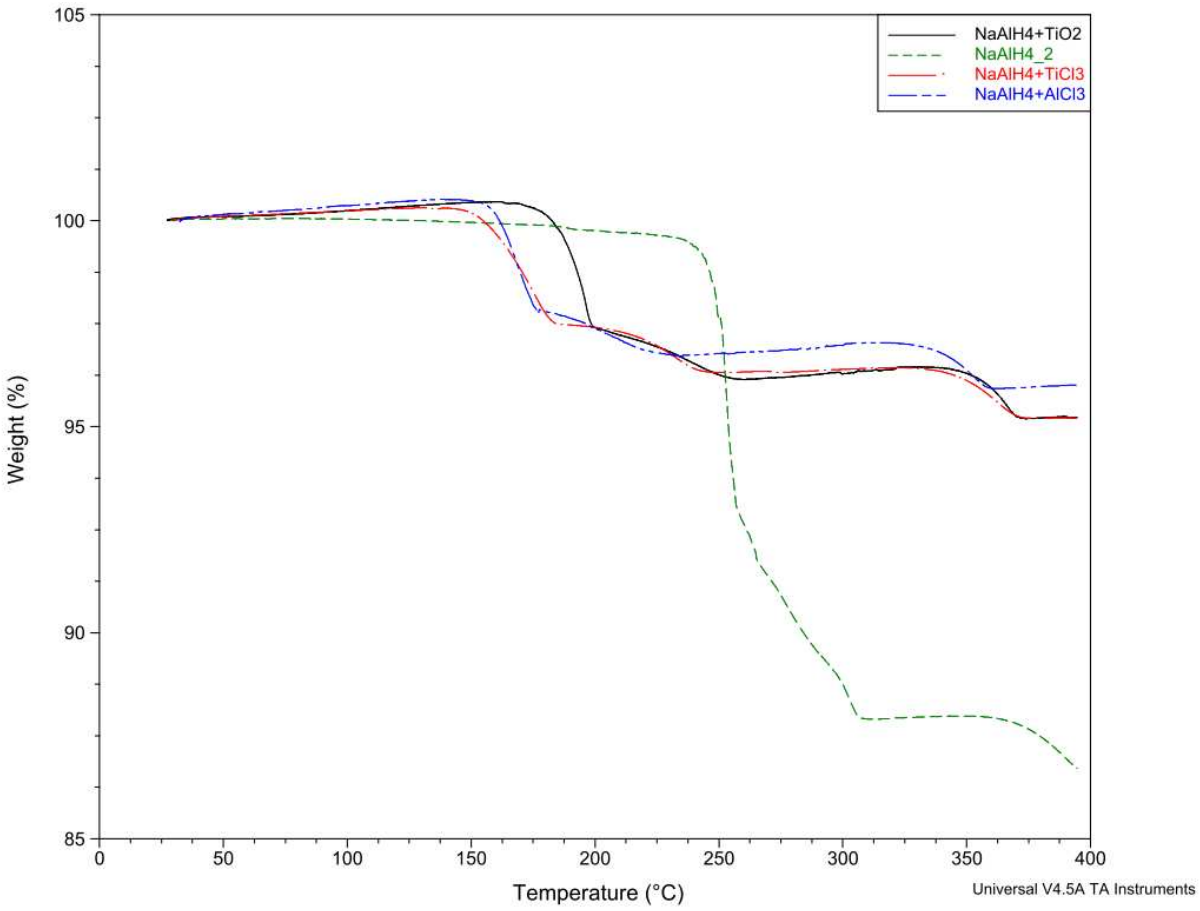

Figure 62 TGA analysis of doped $NaAlH_4$

The results of the TGA analyses provide three main sets of information. The temperature of desorption is lowered with all dopants. Depending on the dopant, temperature shifts of 70℃ (TiO_2) to 95℃ ($TiCl_3$) are reached. This fact is an important step towards a material that fulfills the requirements given by the DoE.

A known chemical reaction with the dopant included is still a 3 step reaction in the form of

$$3NaAlH_4 \rightarrow Na_3AlH_6 \rightarrow 3NaH \rightarrow 3Na \qquad 2.35$$

where each step is linked with hydrogen desorption. The total amount of desorbed hydrogen significantly decreases. All doped samples show an overall weight loss of approximately

2.5wt %, whereas the undoped sample stars a weight loss of 6wt %. Excluding the increase in the molecular weight of the material, many other assumptions about this behavior can be made. Further analyses have to be done in order to provide a clear explanation for this behavior. [2, 64, 73, 74].

DSC Analysis

The DSC analysis of the samples provides additional information about the bond characteristics of the samples and the reaction dynamics during the phase transition. Therefore, the sample is prepared in the glove box, adjusted in the DSC apparatus and tested under standard conditions mentioned previously. The results of the DSC analysis are shown in Figure 63.

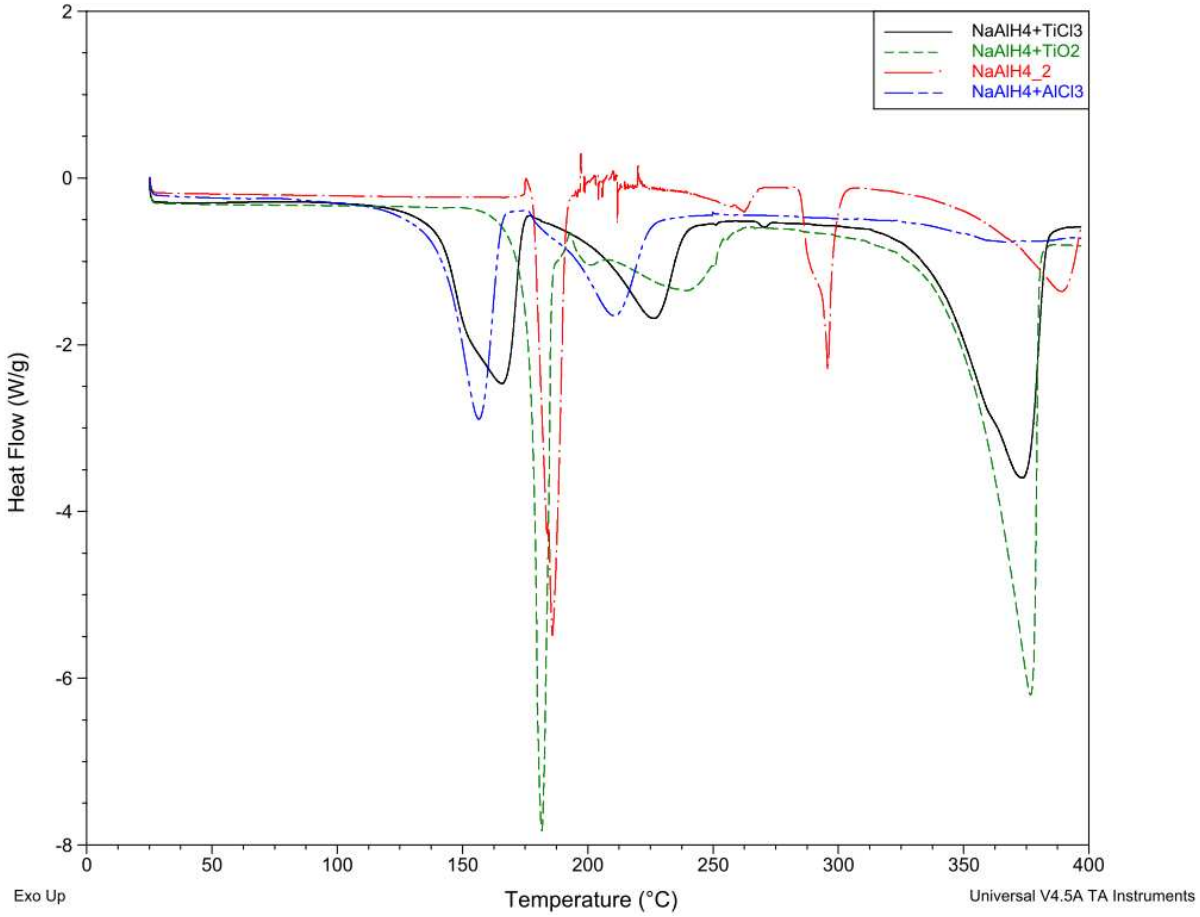

Figure 63 DSC analysis of doped $NaAlH_4$

The results of the DSC analysis stand in good agreement with the results of the TGA analysis. The DSC pattern shows endothermic peaks at discrete temperatures, which indicates the phase transition mentioned in Equation 2.34. The temperature shift of the doped materials compared to the peaks of the undoped materials coincides with the results from the TGA analysis and verify their accurately [16, 75-77].

Analysis and Discussion

This series of experiments was originally performed in order to validate both the doping, and the analysis method. In the course of research, it was discovered that no published data about the dopant being used in the present study was available. As a consequence, this system gained interest in current study. Results of this series are listed in Table 4.

Table 4 Overview of the results $NaAlH_4$

Material	**Material Specifications**			
	molar weight [g/mol]	theoretical storage density [wt %]	chem. Reaction	reversible storage density [wt %]
$NaAlH_4$	54	7.4	1. $NaAlH_4 \rightarrow Na_3AlH_6 + Al + 3H_2$ 2. $Na_3AlH_6 \rightarrow 3NaH + Al + 1.5H_2$ 3. $NaH \rightarrow Na + 0.5H_2$	1. 3.7 2. 1.85 (3. 1.85)
$NaAlH_4+TiO_2$	54	7.4	$6NaAlH_4 + 3TiO_2 \rightarrow 3Na_2O + 6Al + Ti + 12H_2$	7.4
$NaAlH_4+TiCl_3$	54	7.4	$3NaAlH_4 + TiCl_3 \rightarrow 3NaCl + Al + Ti + 6H_2$	7.4
$NaAlH_4+AlCl_3$	54	7.4	$3NaAlH_4 + AlCl_3 \rightarrow 3NaCl + 4Al + 6H_2$	7.4

Continuation of the results of $NaAlH_4$

Material	TGA				DSC					XRD
	experimental [wt%; ℃]		published [wt, ℃]		experimental [W/g, ℃]		theoretical [W/g]	published [W/g, ℃]		
	without catalyst	with catalyst	without catalyst	with catalyst	without catalyst	with catalyst		without catalyst	with catalyst	
$NaAlH_4$	6.0; 240-260	-	rev. 3; 180-230	-	-5.5;190	-	-	- ;185	-	x
$NaAlH_4$+TiO_2	-	2.5; 160-200	-	3.8; 155-180	-	-7.7;180	-	-		x
$NaAlH_4$+$TiCl_3$	-	2.6; 150-180	-	3.8; 150-200	-	-2.5;165	-	-		x
$NaAlH_4$+$AlCl_3$	-	2.5; 155-175	-		-	-2.8;155	-	-		x

x= analysis performed

The structural analysis of the undoped material showed main characteristic peaks at angles of $2\Theta_1$= 29.85° and $2\Theta_2$= 48.31° and $2\Theta_3$= 45.88°. A comparison with the JCPDF data clearly indicates the material and also shows its high grade of purity. No additional peaks are recognizable which might indicate the existence of impurities or other byproducts. For the analysis of impact of dopants on the hydrogen desorption behavior, different dopants, such as TiO_2, $TiCl_3$ and $AlCl_3$ were embedded into the matrix material. The XRD analysis of the doped material showed besides the original peaks, no additional peaks. This behavior implies the fact, that the dopant and the matrix material reacted and formed new phases similar to the origin phase. Comparisons with published data underline this assumption and state that catalytic phases are formed [54, 55, 62, 68, 72]. In the example of $TiCl_3$ as dopant material, $L1_2$-$TiAl_3$ as well as TiH_2 and traces of NaCl are formed. The formation of catalytic phases with aluminum chloride and titanium dioxide can be explained in a similar way and coincide with published data [67, 70, 71, 77-79].

The hydrogen desorption behavior of the undoped sample, as well as the doped samples are tested and compared with each other. The results of the TGA analysis of the undoped sample showed hydrogen desorption at 240- 260℃, with a weight loss of 6.0wt %. This value is lower than the theoretical value of 7.4 wt and also lower than published data [16, 64, 73-76]. The difference between the theoretical value, other publication values and the value of the current analysis is caused by the high heating rate of 10℃/min compared to 2-5℃/min in other pub lications.

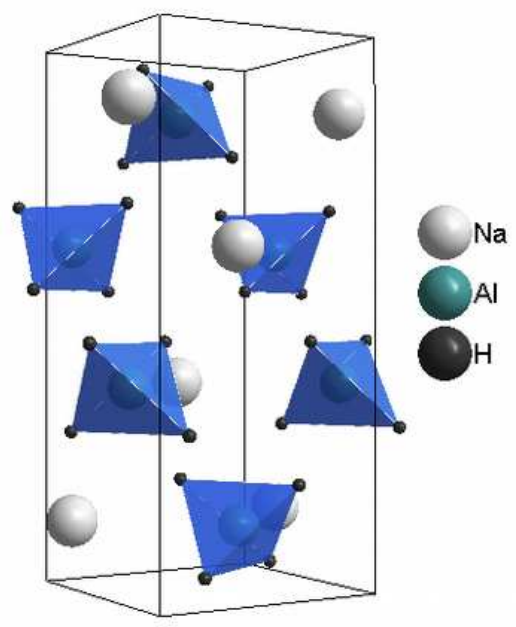

Figure 64 Crystal Structure of $NaAlH_4$

Figure 64 shows the tetragonal crystal structure of $NaAlH_4$ with the space group $I4_1/a$, where each sodium atom is surrounded by 12 H atoms and 3Al-H tetrahedrons, respectively, with lattice parameters of "a"= 5.08Å and "c"= 11.33Å, and a Al- H bond length of 1.54Å. The hydrogen desorption temperature is dependent on two main aspects, the bond characteristics and the heat of the hydride formation. The bonds in the tetra hydride need to be divided into Na^+- Al^- bond, which is of ionic character and the Al-H bonds. Even though these bonds show ionic characteristics, they are of covalent character with strong ionicity (polar covalent) [22, 26].

The other major aspect for the hydrogen desorption is the heat of the hydride formation, ΔH. This value describes the amount of heat that needs to be introduced into the system in order to break the bonds under hydrogen desorption. As seen in the TGA pattern, at temperatures of 200℃, enough energy is induced into the system to break the bonds, and the material starts desorbing hydrogen by decomposing into Na_3AlH_6. The crystal structure of Na_3AlH_6 differs from that of $NaAlH_4$. At low temperatures, it has a monoclinic

$P2_1/n$ symmetry, whereas at higher temperatures the symmetry changes to orthorhombic Immm,.

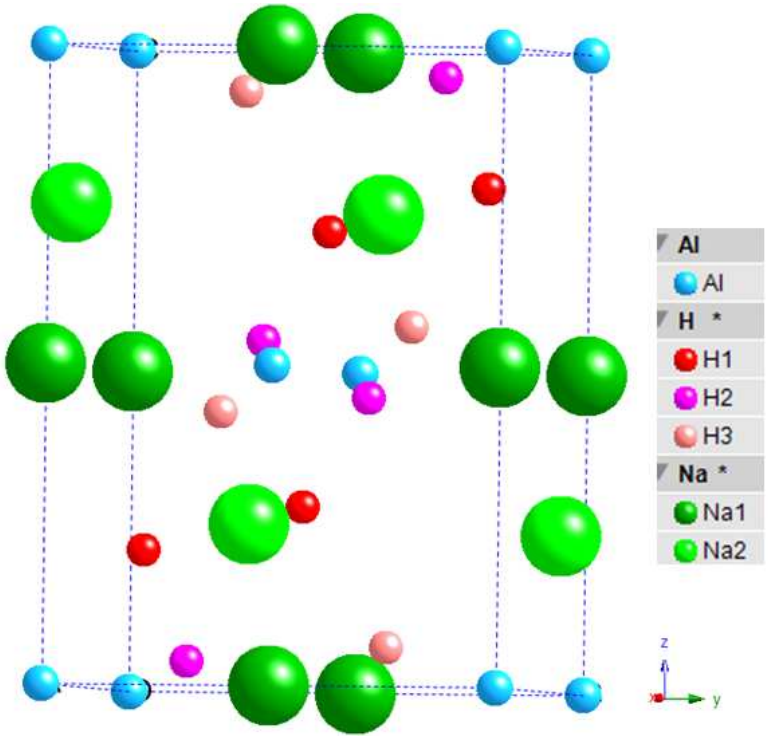

Figure 65 Crystal Structure of Na_3AlH_6

Figure 65 shows the crystal structure of Na_3AlH_6 with the lattice parameters of this structure are “a”= 5.322Å, “b”= 5.516Å, and “c”= 7.679Å, with a Al- H bond length of 1.77Å [22, 26]. As mentioned, the hydrogen desorption is dependent on the bond characteristics and ΔH. The Al- H tetrahedron remains a covalent bond with strong ionicity and splits when enough heat is induced into the system under hydrogen desorption. The amount of heat correlates with the value for ΔH= -69.8kJ/mol [22, 26], and is reached at temperatures of 250℃ when the ma terial starts to decompose to face-centered cubic NaH under hydrogen release. In a third decomposition step, the material decomposes to Na^+ and H^- , due to the ionic character of the Na-H bond, at temperatures of 350℃, where the material releases approximately 1,8wt %. Detailed descriptions of the desorption process are given in Chapter 2.2.3.1.2.

Regarding the doped samples, a general statement about the reaction dynamics can be made. The desorption temperature decreased independent of the dopant material, but simultaneously the total amount of desorbed hydrogen decreases as well. The titanium dioxide doped sample desorbed 2.5wt % in a temperature range of 160℃- 200℃, the titanium chloride desorbed 2.6wt % at a temperature range of 150℃- 180℃, and the aluminum chloride doped sample desorbed 2.5wt % at a temperature range of 155℃- 175℃.

Even though the temperature of desorption could be lowered with the addition of dopant material, a significant decrease in the amount of desorbed hydrogen was proven.

The reason for the weaker desorption value lies in the phase formation in the milling process. The formation of three main phases, $D0_{22}$-$TiAl_3$, NaCl, and TiH_2 could be proved during the milling process. $D0_{22}$-$TiAl_3$ acts as the catalyst and is mainly responsible for the shift of the desorption temperature, whereas TiH_2 is responsible for the decreased amount of desorbed hydrogen causes due to its thermal stability in the temperature range below 400℃. Current results agree with published data [55, 68, 71]. Furthermore no predictions about the atomic crystal structure and crystal change during the dopant implementation can be made.

Regarding the results of the DSC analysis of the undoped sample, peaks of endothermic character, which prove the different desorption steps, are observable. The position of the peaks are related to the desorption steps and coincide with published data [16, 54, 75, 76]. Besides the endothermic character of the reaction, the peaks provide information about the bond strength between the host atom and the hydrogen atom. The Al-H bond of the $NaAlH_4$ and Na_3AlH_6 material is of covalent character with strong ionicity, which results in high peaks and in characteristic decomposition temperatures.

As mentioned, the bond strength is also dependent on the entropy, ΔH, of the material. Therefore, values for the entropy of $NaAlH_4$ and Na_3AlH_6 are related to the height of the peak of the DSC analysis [66, 80, 81].

Comparing the results of the undoped sample with the results from the doped samples, the same outline becomes clear. The peaks of the doped samples are shifted to lower temperature values when compared to the undoped samples. This result indicates the improvement of the desorption kinetics by adding dopant materials. Similar to the TGA results, the DSC result matches well with published papers and verifies the doping process. Referring to the requirements given by the DoE, it becomes clear that the material cannot fulfill these guidelines, even if its kinetics are improved by implementing catalyst materials into the host structure. The fact that the desorption temperature is still too high for mobile application, where the guideline states a desorption below 100℃, excludes the material as potential candidate for mobile applications [16, 64, 73-77].

2.4.3.2. Li_3AlH_6

The material of the actual system is Li_3AlH_6 which showed in the undoped state a hydrogen desorption rate of 4.6wt % in a temperature range of 210- 240℃. A decrease in the temperature of desorption is expected by adding different catalysts into the material. The present study, will show the influence of the dopant on the temperature of desorption and the effect of the dopant on the amount of desorbed hydrogen. The materials are weighed and mixed based on the ratios presented in Table 5.

Table 5 Mixture of Li_3AlH_6 and Dopants

	Matrix Material	**Dopant**		
Name of Material	Li_3AlH_6	$TiCl_3$	TiO_2	$AlCl_3$
Molecular weight [g/mol]	53.85	154.23	79.866	133.34
Sample weight [g]	0.2	-	-	-
mole% of dopant [%]	-	2	2	2
mole of Matrix Material [mol]	0.00371	0.00007	0.00007	0.00007
Amount of Material [g]	**0.2**	**0.0115**	**0.0059**	**0.0099**

Doping precursors and matrix material are mixed, weighed and charged with 6 steel balls in a tungsten carbide vial and milled for 30 minutes [82-86].

XRD Analysis

The preparation of the samples for the XRD analysis is done in the glove box because of the materials' affinity to react with moisture. The results of the doped and undoped samples are shown in Figure 66.

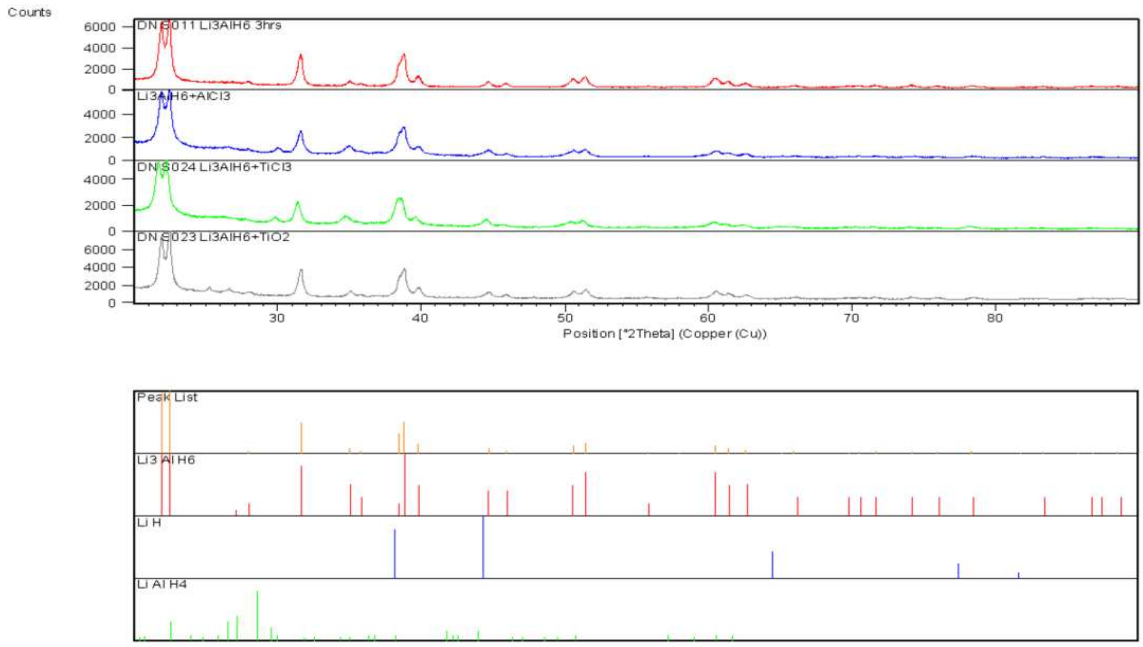

Figure 66 XRD analysis of doped Li_3AlH_6

The XRD analysis provides an overview of the doped and undoped samples. The comparison of the samples with the JCPDF file proves the existence of the Li_3AlH_6 phase and also shows the impact of the dopant on the structure. Besides the peaks of the hydride phase, no precursory dopant material can be seen, which indicates an implementation in the hydride structure.

TGA Analysis

The TGA analysis is performed to receive information about the impact of different dopants on the temperature of desorption and the amount of desorbed hydrogen. Figure 67 gives an overview of different doped materials and their impact on the material.

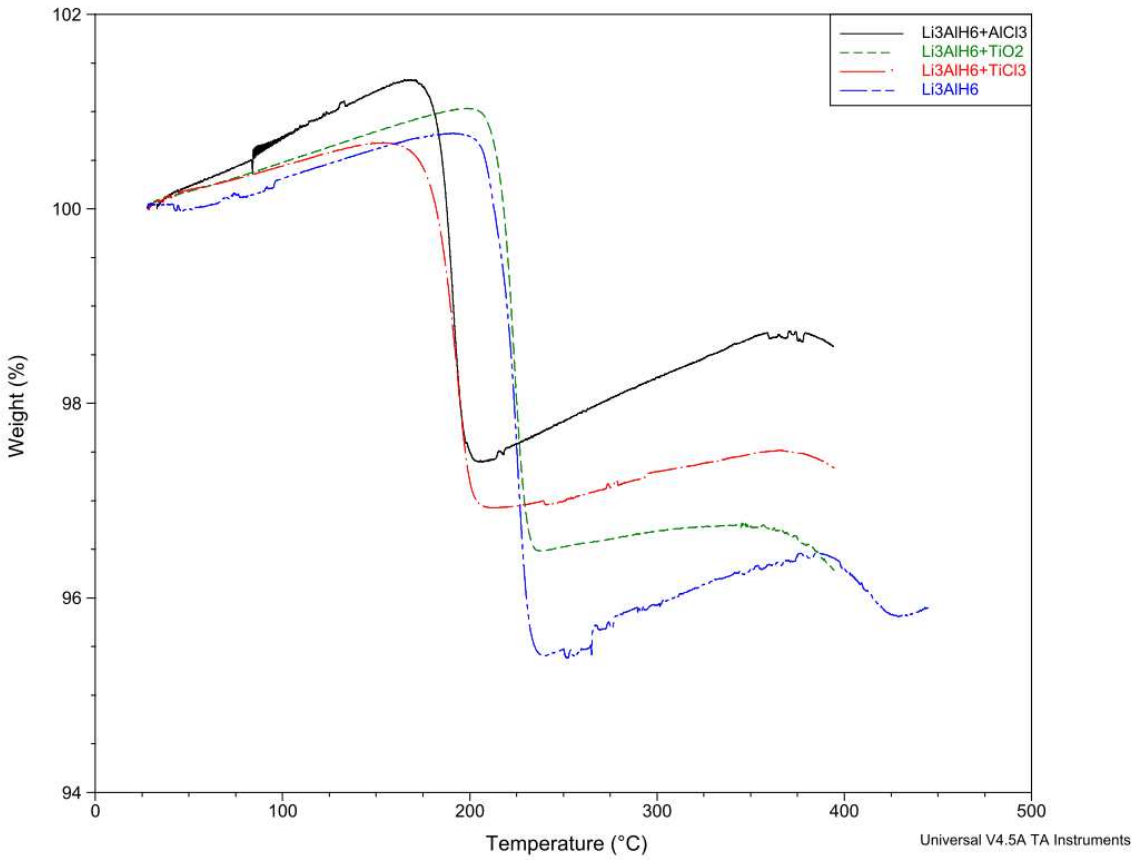

Figure 67 TGA analysis of doped Li_3AlH_6

The results of the TGA analysis provide two sets of information. That the hydrogen desorption temperature of the doped samples shifts to lower temperatures. The undoped sample releases hydrogen of 4.6wt % at a temperature of 240℃, whereas the doped materials release 3.5wt % hydrogen at 200℃ (TiO_2) and 2.6wt % hydrogen at 175℃ ($AlCl_3$). These results prove the positive impact of the dopants on desorption time but at the same time show the negative impact of the dopants on the amount of desorbed hydrogen. In all doped samples, a significant decrease of desorbed hydrogen of approximately 1.5- 2wt % is recognizable.

DSC Analysis

The DSC analysis of the samples provides additional information about the bond characteristics and the reaction dynamics during the phase transition. For the analysis, the samples are prepared and placed in the DSC apparatus. The preparation and the analysis are done under standard conditions mentioned in the beginning of the chapter. The results for the doped and undoped materials are presented in Figure 68.

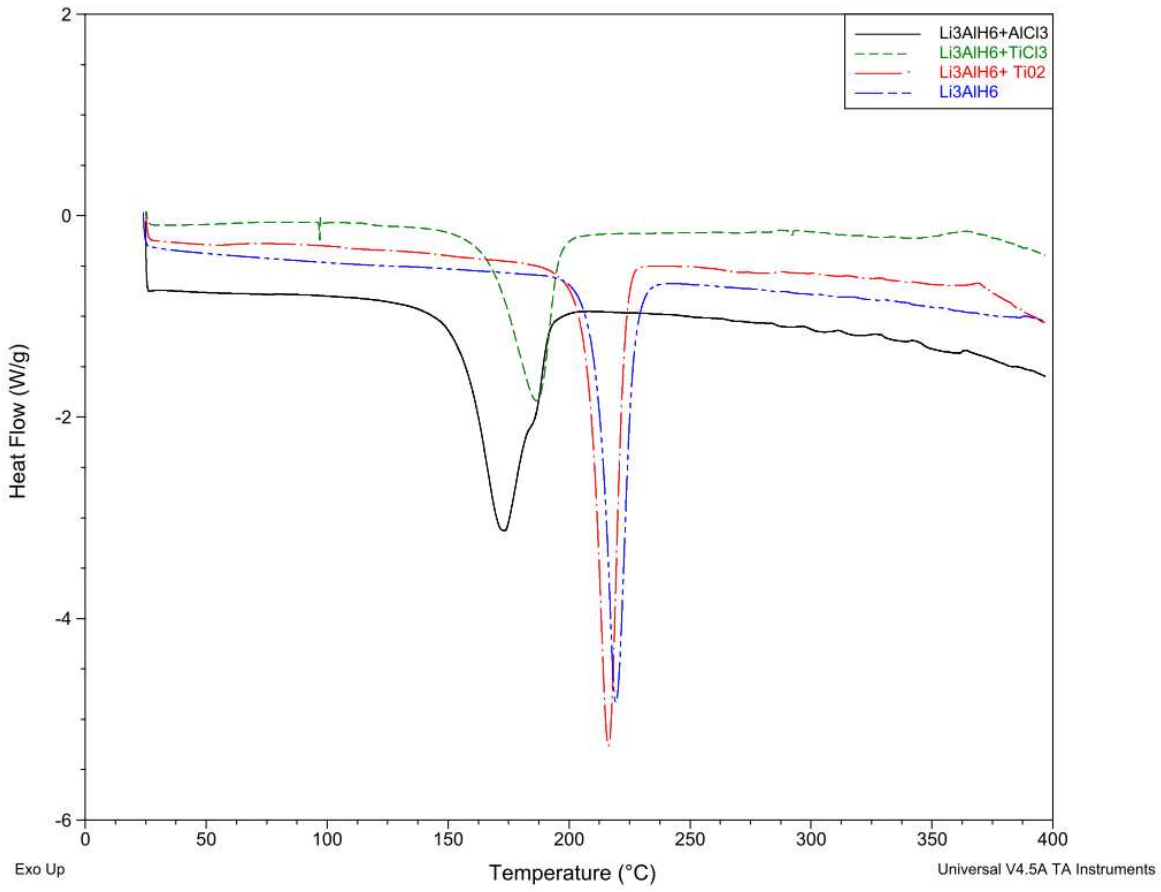

Figure 68 DSC analysis of doped Li_3AlH_6

The results of the DSC analysis show that the hydrogen desorption takes place in a single step transition, which directly correlates with theoretical assumptions and published data. Furthermore, the DSC analysis clearly identifies a shift of the peaks, which is related at a hydrogen desorption to lower temperatures. Even though the

temperature shift with the dopants is not as much as with sodium tetra hydride, a significant improvement of reaction kinetics is recognizable.

Analysis and Discussion

This particular material was formed from its precursors LiH and $LiAlH_4$. Its theoretical storage density of 11.1wt % makes it interesting for industrial application. Therefore it was tested for it hydrogen desorption kinetics in an undoped state as well as a doped material. Table 6 shows the results of the TGA and DSC analysis of each tested material.

Table 6 Overview of the results of Ni_3AlH_6

Material	**Material Specifications**			
	molar weight [g/mol]	theoretical storage density [wt %]	Chemical Reaction	reversible storage density [wt%]
Li_3AlH_6	53.852	11.1	1. $Li_3AlH_6 \leftrightarrow 3LiH+Al+1.5H_2$ 2. $3LiH \rightarrow 3Li+1.5H_2$	1. 5.5 (2. 5.5)
$Li_3AlH_6+TiO_2$	53.852	11.1	1. $Li_3AlH_6+TiCl_3 \leftrightarrow 3LiCl+Al+Ti+3H_2$	7.9
$Li_3AlH_6+TiCl_3$	53.852	11.1	1. $Li_3AlH_6+AlCl_3 \leftrightarrow 3LiCl+2Al+3H_2$	7.9
$Li_3AlH_6+AlCl_3$	53.852	11.1	1. $4Li_3AlH_6+TiO_2 \leftrightarrow 6Li_2O+Al+3Ti+12H_2$	7.9

Continuation of overview of results Li_3AlH_6

Material	TGA				DSC					XRD
	experimental [wt%; ℃]		published [wt, ℃]		experim ental [W/g, ℃]		theoretical [W/g]	published [W/g, ℃]		
	without catalyst	with catalyst	without catalyst	with catalyst	without catalyst	with catalyst		without catalyst	with catalyst	
Li_3AlH_6	4.6; 210-240	-	rev 2; 201-240	-	-4.8; 220	-	-	- ;227-247	-	x
$Li_3AlH_6+TiO_2$	-	3.5; 200-235	-		-	-5.2;215	-	-		x
$Li_3AlH_6+TiCl_3$	-	3.1; 160-210	-	2.0; 175-220	-	-1.9;188	-	-	-;175	x
$Li_3AlH_6+AlCl_3$	-	2.6; 175-210	-	1.0; 155-220	-	-3.2;175	-	-		x

x= analysis performed

The mechanochemical synthesis of the precursor lithium hydride and Li_3AlH_6 resulted in the product Li_3AlH_6, which was tested for its structural composition with an XRD apparatus. The main peaks were found at angles of $2\Theta_1$= 21.9°, $2\Theta_2$= 22.46°, $2\Theta_3$= 38.43° and $2\Theta_4$= 38.8° and are a clear indication for the desired Li_3AlH_6 phase. Comparisons with published data coincide with the results of current analysis and prove a single phase of the sample [18].

However, the pattern of the sample indicates impurities at an angle of 2Θ= 27.96°, which indicates a major phase with impurities. Based on gained experiences, these impurities are residual material that did not form into the desired phase. In course of study, this material was manipulated by the implementation of different dopants, such as titanium chloride, aluminum chloride and titanium oxide. The structural analysis of the doped samples clearly proved that the dopants titanium and aluminum are embedded into the matrix material structure. The XRD analysis could not prove the existence of the dopant precursor, which means that dopant and matrix material formed a modified phase. Published data showed a similar behavior, where the phase formation from a pure Li_3AlH_6 phase to a doped phase including $D0_{22}$-$TiAl_3$, and TiH_2 is formed, and stands in good agreement with current results [84, 85].

Furthermore, the hydrogen desorption characteristics of the material were tested. A TGA analysis provided information about the temperature of desorption and the amount of desorbed hydrogen. This analysis is a commonly used technique to prove the desorption characteristics of hydrides [13, 82]. In addition, the data will provide information about the influence of the different dopant materials on the desorption characteristics. The TGA results of the undoped material show a single step hydrogen desorption. Independently from the dopant agent, all materials showed an increase in weight in the temperature range of 25- 200℃. This effect is caused by reactions of the sample with ambient moisture and oxygen and can generally be expressed as followed.

$$Li_3AlH_6 + 6H_2O \rightarrow 3LiOH + Al(OH)_3 + 6H_2 \qquad 2.36$$

For the reaction with moisture

$$Li_3AlH_6 + 2O_2 \rightarrow 3LiOH + Al(OH)_3 \qquad 2.37$$

In general, both reactions can take place depending on the oxygen and hydrogen content in the ambient atmosphere. The formation of lithiumhydroxide results in an increase in weight of the sample and cannot be avoided. Therefore, the outcome has to be considered in further analysis and interpretations. Beginning at a temperature of 200℃, the material starts to decompose under hydrogen desorption to LiH.

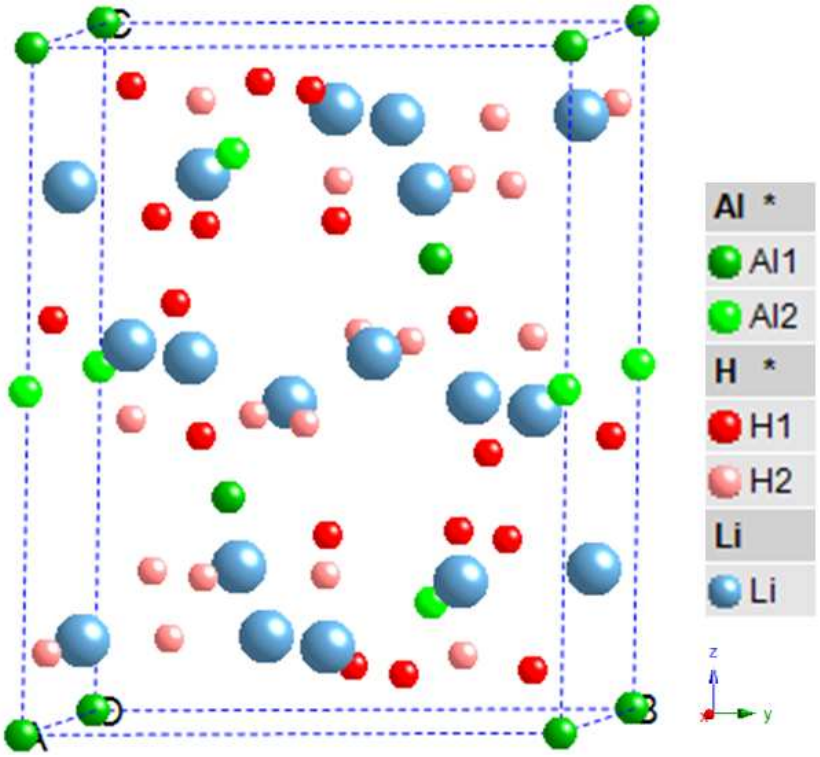

Figure 69 Crystal Structure of Li_3AlH_6

Figure 69 shows the crystal structure of Li_3AlH_6, which, similarly to Na_3AlH_6 , has a monoclinic crystal symmetry with an $R\bar{3}$ space group with lattice parameters “a”=4.208Å, “b”=7.801Å, and “c”=7.804Å. The atomic crystal structure cannot be determined because of the rhombohedral

pseudo symmetry of the material. The bond strength as well as the heat of the hydride formation are major factors that determine the desorption temperature. The Al- H bond length is 1.77Å with a covalent of strong ionicity. Furthermore, the entropy, ΔH= -102.8kJ/min, is another major desorption determining aspect [22, 26]. This value describes the heat, which needs to be induced to split the Al- H bonds to release gaseous hydrogen, and form the face- centered cubic LiH.

Regarding the doped materials, a clear trend is recognizable. Independently from the dopant, a shift to lower desorption temperatures is observable. Both the temperature shift and the amount of desorbed hydrogen are significantly dependent upon the dopant material. TiO_2 showed the weakest improvements in terms of lowering the desorption temperature, with values of 3.5wt % loss at a temperature range of 200℃- 235℃. The re sults reached with $TiCl_3$ and $AlCl_3$ have significantly improved in terms of desorption temperature when compared to the titanium oxide sample. The temperature could be lowered to 160℃ f or titanium chloride and 175℃ for aluminum chloride, whereas the amount of desorbed hydrogen decreased to 3.1wt % for $TiCl_3$ and 2.6wt % for $AlCl_3$. The reason for the improved desorption temperature lies in the catalyst itself. During the milling process of Li_3AlH_6 and $TiCl_3$, a new phase, the tetragonal $D0_{22}$-$TiAl_3$, is formed, which act as a catalyst for the hydrogen desorption [83]. In a similar way, the effect of $AlCl_3$ on the reaction dynamics can be explained and is the reason for the improved reaction. Since TiH_2 and AlH_3 are also byproducts of the catalytic reaction [83], the decrease in the total amount of desorbed hydrogen is reasonable. Both products have a significant higher desorption temperature than Li_3AlH_6, which results in a decrease of the desorbed hydrogen.

The DSC analysis of the materials underlines the results made by the TGA and provides additional information about the bond characteristics of the hydride. The DSC analysis shows a peak of endothermic character in a temperature range of 220℃. This result coincides with the results from the TGA analysis, which indicate the hydrogen desorption at 210- 240℃. It also coincides with published data, which achieved similar results [13, 82, 83]. The peaks of the DSC

analysis do not only prove the endothermic character of the desorption. The peaks also provide information about the strength of the metal- hydrogen bonds, which is directly correlated with the desorption temperature. Regarding desorption of hydrogen from Li_3AlH_6, the experiments showed a desorption at 200- 240℃ depending on the dopant. This temperature results from a strong covalent Al-H bond with strong ionicity. In a second step, LiH desorbs hydrogen and decomposes to elementary lithium. This reaction takes place at high temperatures and is beyond the temperature range of the analysis apparatus. Regarding the results of the doped samples, it can be seen that the peaks indicate endothermic desorption reactions at 215℃ for titanium oxide doped material, 188℃ for $TiCl_3$ doped material, and 175℃ for $AlCl_3$ doped material. All results agree with the TGA analysis of current results and published data [13, 82, 83]. Regarding the guidelines given by the DoE, this material cannot be used as a potential candidate for mobile applications mainly due to its weak desorption thermodynamics.

2.4.3.3. LiH

In a third series of experiments, lithium hydride is doped with different materials and tested for different characteristics. This particular material is chosen because of its exceptionally high gravimetric storage density of 12.7wt %. One hopes to improve the reaction kinetics in hope of establishing this material as one of interest for industrial application. For the preparation of the sample, components are weighed and mixed to the ratio presented in Table 7.

Table 7 Mixture of LiH and Dopants

	Matrix	Dopant

	Material			
Name of Material	LiH	$TiCl_3$	TiO_2	$AlCl_3$
Molecular weight [g/mol]	7.95	154.23	79.866	133.34
Sample weight [g]	1	-	-	-
mol% of dopant [%]	-	2	2	2
mole of Matrix Material [mol]	0.12579	0.00252	0.00252	0.00252
Amount of Material [g]	**1**	**0.388**	**0.2009**	**0.3354**

The mixtures are charged together with six steel balls in a vial and mixed for 30 minutes and prepared for the analysis.

XRD Analysis

For the XRD analysis, a discrete amount of material is put on the sample holder and covered with Kapton foil, which avoids a contamination of the sample during the analysis. An overview of the results is given in Figure 70.

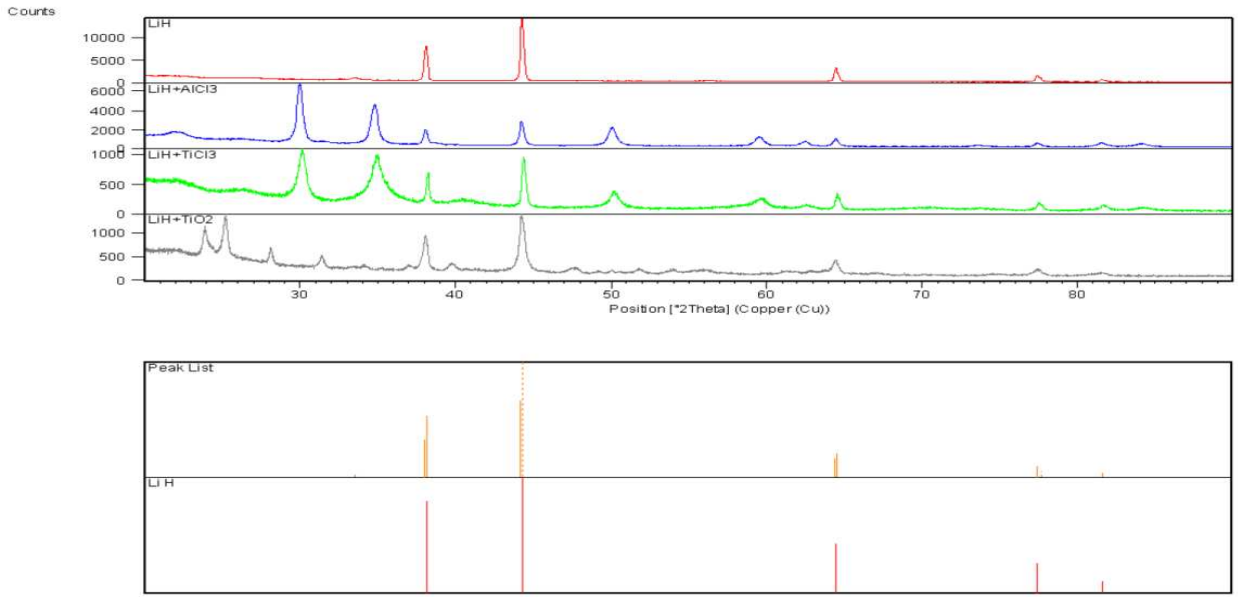

Figure 70 XRD analysis of doped LiH

The XRD analysis indicates the change of the material structure by adding a dopant into the system. Thereby, it can be assumed that the dopant diffuses into the matrix material. Further analyses will identify the effect of the dopants on the material characteristics.

TGA Analysis

The addition of dopants into the matrix material should decrease the desorption temperature from 670℃ to values that make it more attractive a s a commercial storage material. Samples are prepared and tested under standard conditions mentioned in the beginning of the chapter. The results of the analysis are presented in Figure 71.

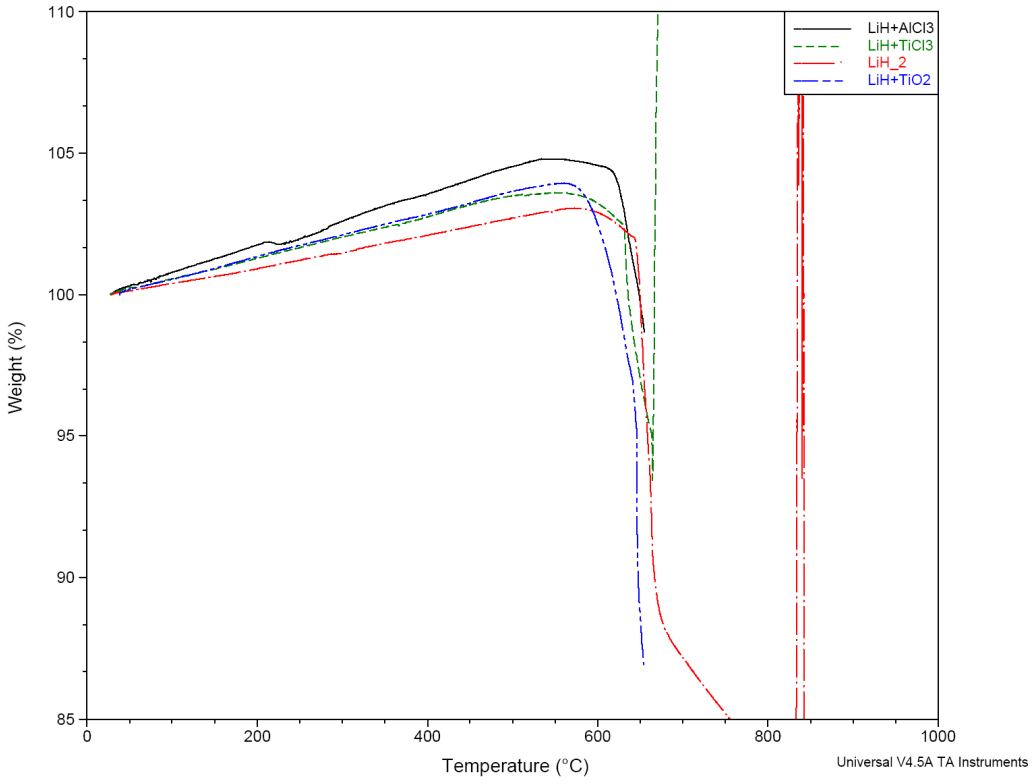

Figure 71 TGA analysis of LiH System

The TGA analysis basically provides two important sets of information. On the one hand, the temperature of desorption can be lowered by adding dopants into the material structure. Depending on the dopant material, the shift in desorption temperature ranges from 640℃ to

620°. On the other hand, the shift of the desorption temperature is much lower than the shift found in other materials. It can be assumed that the bonds between lithium and hydrogen are much stronger than the bonds in the $NaAlH_4$ structure, which is the reason the high desorption temperatures. Another possible explanation is based upon the fact that the influence of the dopant decreases with an increase in temperature. This would not only explain the low effect of the dopant on this material, but also the minor effect of the dopant on the sodium hydride decomposition, shown in Figure 77.

Since the hydrogen desorption in the doped samples occurs at temperatures of 640℃, no DSC analysis was performed because the hydrogen desorption takes place beyond the measuring range.

Analysis and Discussion

Due to its exceptionally high storage density of 12.7wt %, lithium hydride was of interest in the present study. Even though the decomposition temperature of 670℃ in its original state is too high for industrial application, one had hoped to lower this value to more moderate temperatures. Therefore, the material was doped with different dopants and analyzed based on its desorption characteristics. The analysis of this material is of particular interest because no publications of doped material are available, and therefore, new results are expected. Table 8 summarizes the results and compares them with published data.

Table 8 Overview of results of LiH

Material	Material Specifications				TGA				DSC					XRD
	molar weight	theoretical storage density [wt %]	chem. Reaction	reversible storage density [wt%]	experimental [wt%; ℃]		published [wt, ℃]		experimental [W/g, ℃]		theoretical [W/g]	published [W/g, ℃]		
					without catalyst	with catalyst	without catalyst	with catalyst	without catalyst	with catalyst		without catalyst	with catalyst	
LiH	7.95	12.7	$LiH \rightarrow Li + 0.5H_2$	-	11.5; 600-675	-	- ;720	-	beyond range	-	-		-	x
$LiH+TiO_2$	7.95	12.7	2LiH→no reaction	-	-	6.6; 560-640	-		-	beyond range	-	-	-	x
$LiH+TiCl_3$	7.95	12.7	LiH→no reaction	-	-	7.2; 630-660	-		-	beyond range	-	-	-	x
$LiH+AlCl_3$	7.95	12.7	LiH→no reaction	-	-	8.3; 560	-		-	beyond range	-	-	-	x

x= analysis performed

The structural analysis of the undoped material showed main peaks at angles of $2\Theta_1$= 38.25°, $2\Theta_2$= 44.31°, and $2\Theta_3$= 64.54°. The comparison with the JCPDF pattern identifies the material as lithium hydride and proves it high grade of purity. Unlike previously discussed samples, this sample does not show any peaks which indicate impurities. In order to analyze the change of the hydrogen desorption dynamics with the implementation of dopant materials, a sample of lithium hydride was doped with different dopant materials, such as TiO_2, $TiCl_3$ and $AlCl_3$.

The XRD analysis of the samples shows that besides the existing peaks, that indicates that the reaction between the hydride and the dopant was either not successful or that the materials react differently to other tested samples. Comparison with published data indicated that the position of the new peaks is significantly dependent on the dopant material.

The hydrogen desorption characteristics of the material are tested in a second set of analysis. The results of the TGA analysis provides information about the hydrogen desorption temperature and the total amount of desorbed hydrogen. The undoped sample of lithium hydride proved a total amount of desorbed hydrogen of 11.5wt % at 600- 675℃, which is compared to the theoretical value of 12.7wt % and within acceptable published data [20]. In a similar way, the doped materials were tested for their hydrogen desorption behavior. All materials showed a general improvement in terms of desorption temperature. The titanium oxide sample showed a total amount 6.6wt % of desorbed hydrogen at 560℃, the titanium chloride sample an amount of 7.2wt % at 630℃- 660℃, and the aluminum chloride sample at 8.3wt % weight loss at 560℃. The hydrogen desorption temperature of the materials is strongly correlated to the bond strength of the metal- hydrogen bond. The bond between lithium and hydrogen is from mixed, ionic and covalent character. As described in Chapter 2.2.3.1.1., LiH decomposes when enough energy is induced to Li^+ and H^- due to their partially ionic

character under hydrogen release [28, 29]. Besides the improved desorption temperature, a second effect caused by the dopant is recognizable at all samples. While the undoped sample showed a weight loss close to the theoretical value, all doped samples showed degraded values for the amount of desorbed hydrogen. It can be assumed that the formation of catalytic phases during the milling process improve the reaction dynamics, but also results in the formation of new hydrogen containing byproducts, which are more stable than the material itself. A model for this behavior as well as the structural change has to be tested and developed through further analysis.

However, both the XRD analysis and the TGA analysis indicate a manipulation of the matrix structure, which is linked with a shift of the hydrogen desorption temperature to lower values. It can be assumed that the dopant material forms new catalytic phases in the material during the milling process, which improves the desorption dynamics. Since the hydrogen desorption takes place in a temperature range above 600℃, even by including a catalyst into the structure, no effort was spent in a DSC analysis.

2.4.3.4. $LiNa_2AlH_6$

This material is of special interest to the present study, since no data about the impact of dopants on the reaction dynamics is available. Initial experiments and theoretical calculations have predicted a possible hydrogen desorption of approximately 5.5wt % and 6.9wt %, respectively, at temperatures around 290℃. The addition of dopants should result in a drop in desorption temperatures and in decrease in the amount of desorbed hydrogen. Matrix material and dopants are weighed and mixed as shown in Table 9.

Table 9 Mixture of $LiNa_2AlH_6$ and Dopants

	Matrix Material	**Dopant**		
Name of Material	$LiNa_2AlH_6$	$TiCl_3$	TiO_2	$AlCl_3$
Molecular weight [g/mol]	85.95	154.23	79.866	133.34
Sample weight [g]	0.2	-	-	-
mole% of dopant [%]	-	2	2	2
mole of Matrix Material [mol]	0.00233	0.00005	0.00005	0.00005
Amount of Material [g]	**0.2**	**0.0072**	**0.0037**	**0.0062**

The mixture of the dopant and matrix material is charged with six steel balls in a tungsten carbide vial and milled for 30 minutes in a planetary ball mill.

XRD Analysis

The XRD analysis is performed to get an overview of the impact of the dopant on the materials structure. Furthermore, the XRD analysis allows the determination of whether or not a desired phase formation took place during the milling process. Therefore, the material was prepared for the analysis in a glove box and moved to the apparatus where the analysis is performed. The analysis is performed under standard condition, as mentioned previously. The results of the sample with the different dopants are presented in Figure 72.

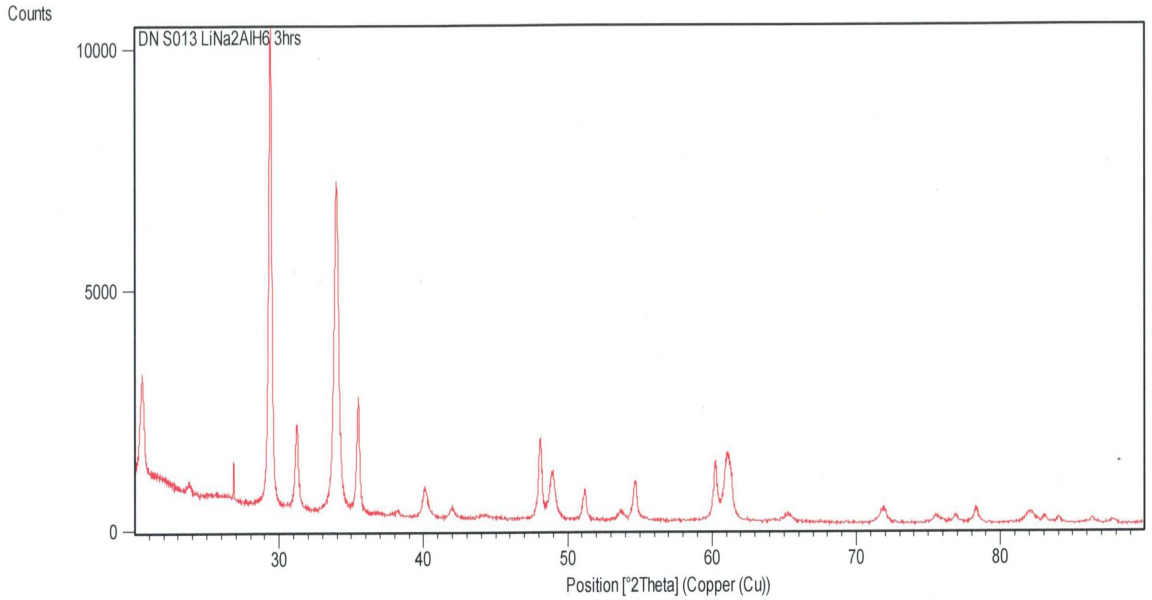

Figure 72 XRD analysis of doped $LiNa_2AlH_6$

The XRD analysis gives a clear overview of the structural impact of the dopant on the matrix structure. In all samples, the $LiNa_2AlH_6$ phase can be identified, even though impurities of precursor material are present. This indicates an unfinished synthesis of the material. Based on the data, gained by the XRD analysis, the transition to the desired material was finished to approximately 70%. Furthermore, the pattern of the doped samples shows additional peaks at discrete angles, which indicate the presence of the dopant atom in the sample structure.

TGA Analysis

Besides the XRD analysis, which provides an image of structural composition of the sample, the TGA analysis provides information about the desorption kinetics of the material. This analysis is important because it predicts the influence of the dopant on the materials. Therefore, the material is prepared in the glove box for the analysis and moved to the apparatus, where it is tested for its hydrogen desorption characteristics. Figure 73 presents the experimental data of the TGA analysis.

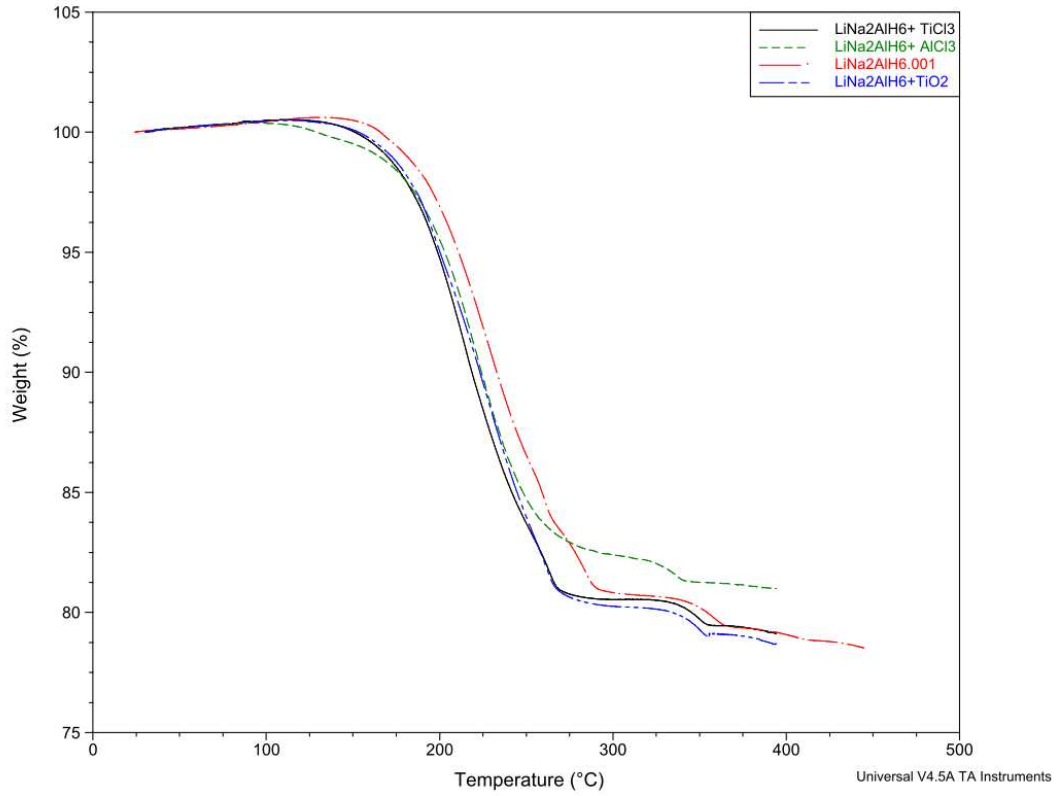

Figure 73 TGA analysis of doped $LiNa_2AlH_6$

Basically the TGA pattern shows a significant drop, beginning at 175℃ and going until 260℃, independently of the sample. This drop is linked with a weight loss of approximately 20wt %, which is too much to be a result of hydrogen desorption alone. Previous analysis has already indicated that $NaAlH_4$, which is present in this sample, decomposes at temperatures around 150℃, and that sodium hydride begins to evaporate within this temperature interval as well. It is assumed that these effects are the cause of the dramatic weight loss. A second step is visible at a temperature of 350℃ and indicates the hydrogen desorption from sodium hydride, which is a byproduct of the $LiNa_2AlH_6$ decomposition. The actual $LiNa_2AlH_6$ decomposition is not clearly visible. It is assumed that the decomposition takes place at a temperature range around 250℃, since a shoulder in all curves is recognizable. The addition of the dopant causes a shift in the desorption temperature independently of the dopant. This shift is caused by the

dopant being less strong than in other samples. It can be assumed that different phases compared to $NaAlH_4$ or Li_3AlH_6 are formed, which do not have the same impact on the formation of catalytic phases.

DSC Analysis

The DSC analysis of the samples provides information about the bond characteristics of each sample and verifies the assumption about the strong weight loss of 20wt % in the sample. Therefore, the material is prepared for the DSC analysis and moved to the apparatus, where it is tested under standard conditions. The results of the DSC analysis are shown in Figure 74.

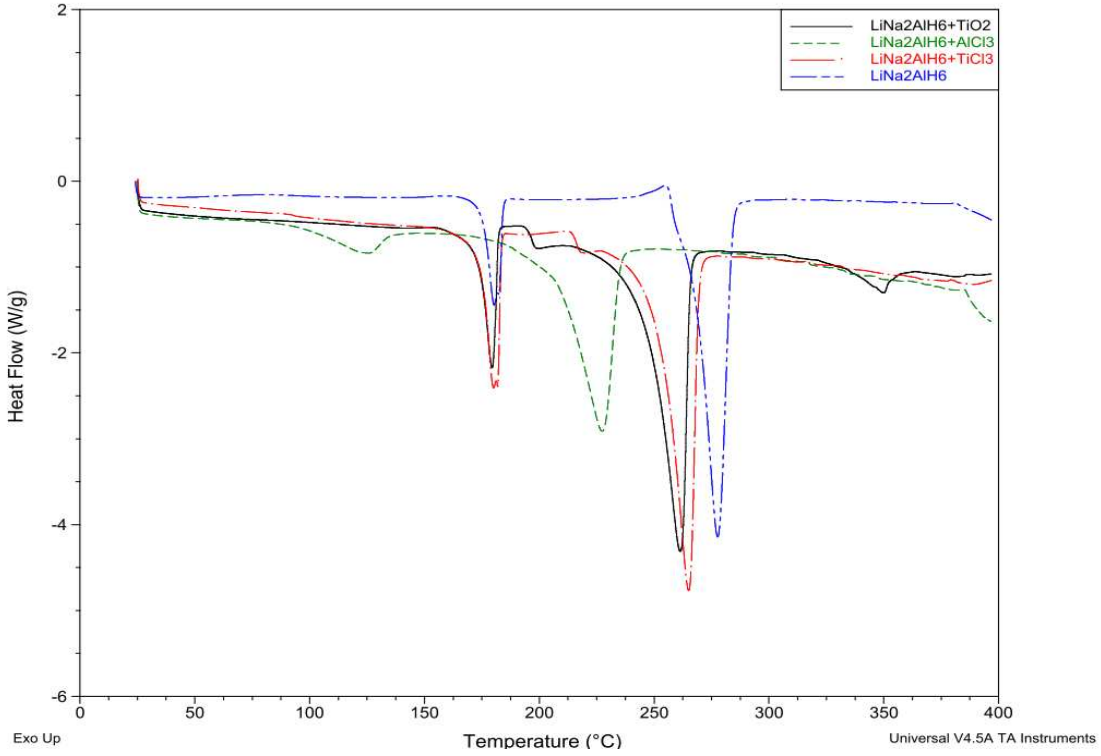

Figure 74 DSC analysis of doped $LiNa_2AlH_6$

The DSC pattern of the materials coincides with the results and assumptions of the TGA pattern. The initial weight loss of 20wt %, which was assumed to be the decomposition of $NaAlH_4$ is proven by this analysis. The first peak, occurring at approximately 175℃,

indicates a transformation and agrees with data for that specific material. The second peak in each material occurs, depending on the dopant at 225- 275℃, and indicates the decomposition of $LiNa_2AlH_6$. This result matches the assumption of the TGA analysis, where a shoulder in the curve indicates the hydrogen desorption. The decomposition of NaH at a temperature of 350℃ can be proven by with an endothermic peak.

Analysis and Discussion

This material is of interest for current research because of the lack of publications dealing with this material. Currently, no information about the effect of doping materials on hydrogen desorption dynamics are available. Therefore the undoped material as well as samples, doped with different doping agents are tested on their desorption characteristics.

Table 10 shows the results of the analyses.

Table 10 Overview of the results of $LiNa_2AlH_6$

Material	**Material Specifications**			
	molar weight [g/mol]	theoretical storage density [wt %]	chem. Reaction	reversible storage density [wt%]
$LiNa_2AlH_6$	85.948	6.9	(1. $LiNa_2AlH6 \rightarrow LiH+2NaH+Al+1.5H_2$) (2a. $2NaH \rightarrow 2Na+H_2$) (2b $LiH \rightarrow Li+0.5H_2$)	1. 3.4 2a. 2.3 2b. 1.1
$LiNa_2AlH_6+TiO_2$	85.948	6.9	$2LiNa_2AlH_6+TiO_2 \rightarrow 4Na_2O+2Li_2O+2Al+6H_2$	6.9
$LiNa_2AlH_6+TiCl_3$	85.948	6.9	$2LiNa_2AlH_6+TiCl_3 \rightarrow 4NaCl+2LiCl+2Al+Ti+6H_2$	6.9
$LiNa_2AlH_6+AlC_{l3}$	85.948	6.9	$2LiNa_2AlH_6+AlC_{l3} \rightarrow 4NaCl+2LiCl+3Al+6H_2$	6.9

Continuation of the overview of the results of $LiNa_2AlH_6$

Material	TGA				DSC					XRD
	experimental [wt%; ℃]		published [wt, ℃]		experim ental [W/g, ℃]		theoretical [W/g]	published [W/g, ℃]		
	without catalyst	with catalyst	without catalyst	with catalyst	without catalyst	with catalyst		without catalyst	with catalyst	
$LiNa_2AlH_6$	5.5; 276	-	- ;220	-	-4.1; 276	-	-	52.3J/mole;254	-	x
$LiNa_2AlH_6+TiO_2$	-	5.5; 230-265	-	Data n.a.	-	-4.3;255	-	-	Data n.a.	x
$LiNa_2AlH_6+TiCl_3$	-	5.5; 230-265	-	Data n.a.	-	-4.7;265	-	-	Data n.a.	x
$LiNa_2AlH_6+AlCl_3$	-	6.5; 215-235	-	Data n.a.	-	-2.9;225	-	-	Data n.a.	x

n.a.= not available

x= analysis performed

The mechanochemical synthesis of $LiAlH_4$ and NaH leads to the final product, $LiNa_2AlH_6$, which is of high interest for further analysis, since no experimental data on the influence of dopants on this material is available. The product material is analyzed for its structural composition with an XRD apparatus and leads to the main peaks at angles of $2\Theta_1$= 20.51° and $2\Theta_2$= 33.97°, which indicates the desired $LiNa_2AlH_6$. The result of the current analysis agrees with the JCPDF data as well as published data [87, 88], and indicates a $LiNa_2AlH_6$ as a major phase in the sample material. However, current analysis showed, that the desired phase was not from high purity, since peaks at angles of $2\Theta_1$= 29.41° and $2\Theta_2$= 33.97° indicate a major phase with impurities.

In the course of study, the original material was doped in order to improve the reaction dynamics. Similar to the first material, TiO_2, $TiCl_3$, and $AlCl_3$ were chosen as dopant precursors and implemented into the matrix material structure. The XRD analysis of the doped material proved the implementation of the material into the structure since no indication of precursor dopant material in the pattern is recognizable.

Furthermore, the desorption behavior of both the doped and undoped material is analyzed. The TGA analysis is a commonly used technique to identify the hydrogen desorption temperature of a material, but is also used to determine the total amount of desorbed hydrogen [87, 88]. The results of the TGA analysis indicate a two-step desorption, which agrees with theoretical calculations [87, 88], where $LiNa_2AlH_6$ decomposes in the first step and sodium hydride at higher temperatures, in a second step.

The first step reaction takes place in a temperature range of 275℃ and is linked with a weight loss of 5.5wt % .The second step, which describes the decomposition of sodium hydride into its elements, takes place at a temperature range of 325℃- 350℃, and is linked with a weight loss of approximately 1wt %. The results of both decomposition steps agree with results from theoretical assumptions and previous analysis [87, 88].

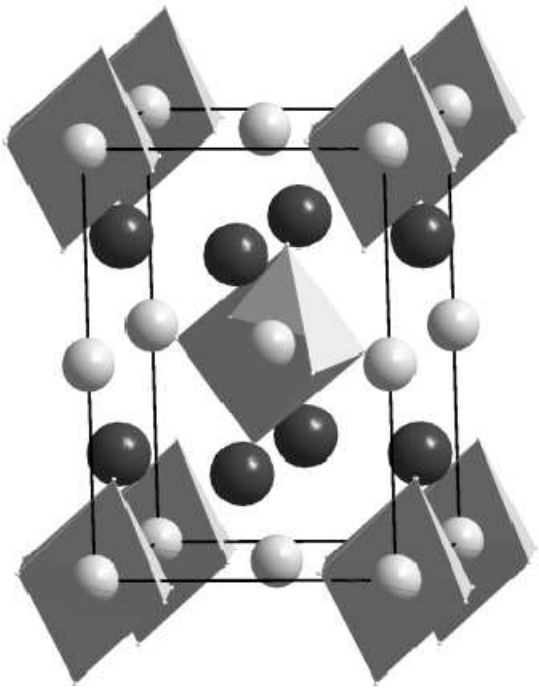

Figure 75 Crystal structure of $LiNa_2AlH_6$

Figure 75 presents the cubic crystal structure of $LiNa_2AlH6$, where the octahedrons the AlH6 group, light grey the lithium and dark grey the sodium atom are presented. The structure has the space group $P2_1/c$ and the lattice parameter "a"= 7.405Å, where the bond length can be assumed to be similar to other hexa aluminohydrides as approximately 1.7Å [88, 89]. Further analysis need to verify this assumption. Another desorption affecting parameter is, ΔH, which describes the heat that needs to be induced to the system to break the Al- H bonds. The value for ΔH= -84.5kJ/mol is also related to the height of the peak from the DSC analysis. At a temperature of 290℃, enough energy is induced to split the bonds by forming the face- centered cubic hydrides, LiH and NaH, under hydrogen release. In a second reaction process, both singularly hydrides decompose to Na^+ and Li^+ and H^- due to their partially ionic character at temperatures of 350℃ (NaH) and 650℃ (LiH), where only the decompo sition of NaH is in the analysis range. Detailed desorption characteristics are given for both, LiH and NaH in Chapters 2.2.3.1.1. and 2.2.3.1.2.

Regarding the doped material, a general trend of an improvement in the decomposition temperature can be seen. Independently of the dopant material, all samples show improved desorption temperatures when compared with the undoped sample. The TiO_2 sample showed a weight loss of 5.5wt % in a range of 230- 265℃, the $TiCl_3$ showed a weight loss of 5.5wt % at a range of 230- 265℃, and the $AlCl_3$ doped sample indicated a weight loss of 6.5wt % at a range of 215- 235℃. Even though the temperature of desorption of the material could be lowered with the implementation of the catalyst material, the effect was much weaker compared to the Li_3AlH_6 sample. In general, the implementation of the dopant material has a catalytic effect similar to the first material. In the example of $TiCl_3$, new phases are formed during the milling process such as $D0_{22}$-$TiAl_3$ which are responsible for the catalytic effect [87, 88]. In the case of $AlCl_3$, similar assumptions about the formation of new catalyst phases can be made, which explain the catalytic effect of the material. However, the catalytic effect of all samples was much weaker than that of the Li_3AlH_6 sample. A possible explanation for this behavior might be the formation of different catalytic phases, which do not have the same impact on the material as the catalytic phases in Li_3AlH_6 or $NaAlH_4$. Further analysis need to verify this assumption.

The DSC analysis, performed with the undoped and doped materials, gave further information about the bond characteristics and the desorption thermodynamics. Based on the results of the DSC analysis, it can be predicted whether the hydrogen desorption is of endothermic or exothermic character. Furthermore, it is possible to prove the results of the temperature of desorption through the TGA analysis, since the heat flow peaks appear at discrete temperatures. Referring to the undoped sample, the DSC signal verifies an endothermic phase transition at a temperature range of 276℃, which coincides with the results of the TGA analysis. Also the fact that the transition is of endothermic character agrees with theoretical calculations and published data [87, 88].

The DSC analysis provides information about the bond strength. The Al- H bonds of the material are of covalent character but show strong ionicity, which also indicates ionic character. These bonds are called polar covalent and have characteristics of both, covalent and ionic bonds. These bonds need to be split in order to release hydrogen. The amount of energy required to split the bonds correlates with ΔH, the enthalpy, and with the height of the peak. Since the value for the DSC peak correlates with the bond strength, important information can be assumed based on this result.

Regarding the doped materials, a general trend of a temperature shift to lower temperatures is verified. The TiO_2 sample shows a peak at 255℃, the $TiCl_3$ doped sample at 265℃, and the $AlCl_3$ sample at 225℃. These results agree with the results of the TGA analysis as well as with theoretical calculations.

Regarding the guidelines given by the DoE, it becomes clear that the material does not fulfill the guidelines. Even though, the amount of desorbed hydrogen is favorable for mobile application, desorption temperatures of 200- 250℃ are too high for industrial application.

2.4.3.5. Na_3AlH_6

Na_3AlH_6 showed in its undoped state moderate hydrogen desorption kinetics. Based on the theoretical value of 5.9wt %, experiments show hydrogen desorption of 5.5wt % at a temperature range of 250- 300℃. The fact that the desorption takes place at such high temperatures makes this material unfavorable in its original form. Therefore, the implementation of dopants can be used as a way to the desorption conditions. Based on the data in Table 11, samples of different dopant precursors were prepared and tested based on their reaction characteristics.

Table 11 Mixture of Na_3AlH_6 and Dopants

	Matrix Material	**Dopant**		
Name of Material	Na_3AlH_6	$TiCl_3$	TiO_2	$AlCl_3$
Molecular weight [g/mol]	102.00	154.23	79.866	133.34
Sample weight [g]	1	-	-	-
mol% of dopant [%]	-	2	2	2
mole of Matrix Material [mol]	0.00980	0.00020	0.00020	0.00020
Amount of Material [g]	**1**	**0,0302**	**0,0157**	**0,0261**

The mixtures were charged with six steel balls in a tungsten carbide vial and milled for 3 hours. The product is analyzed for its structural composition and its desorption behavior [66, 80, 81, 90].

XRD Analysis

The XRD analysis is done to provide information about the impact of the dopant on the material structure. The analysis is done under standard conditions, as mentioned in the beginning of the chapter. The XRD pattern in Figure 76 presents the results of samples with different dopants and the undoped sample.

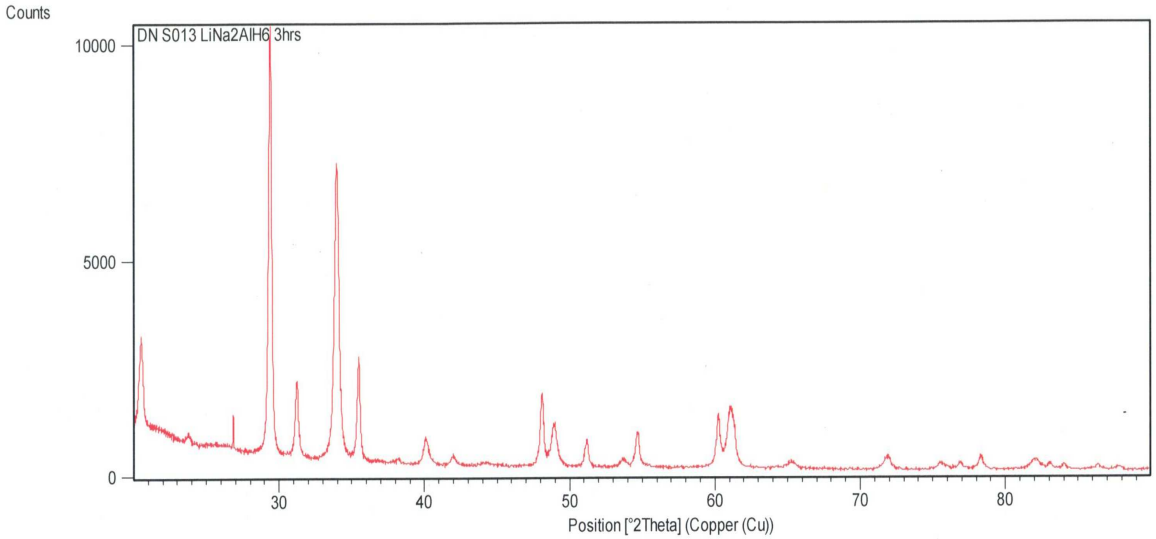

Figure 76 XRD analysis of doped Na_3AlH_6

The pattern of the doped samples indicates peaks from precursor material as well as peaks related to the desired phase. Similar to $LiNa_2AlH_6$, the transition to the Na_3AlH_6 phase is not yet finished. The results from the XRD analysis indicate a mixed phase of 70% of Na_3AlH_6 and 30% of precursor materials.

TGA Analysis

In addition to the structural analysis, the TGA analysis will provide new information about the desorption kinetics of the materials. Therefore, the weight loss of the material as a function of temperature is measured. Based on this information, detailed conclusions about reaction dynamics can be made. The material is prepared for the analysis in a glove box and moved to the location of analysis. An overview of the results is given in Figure 77.

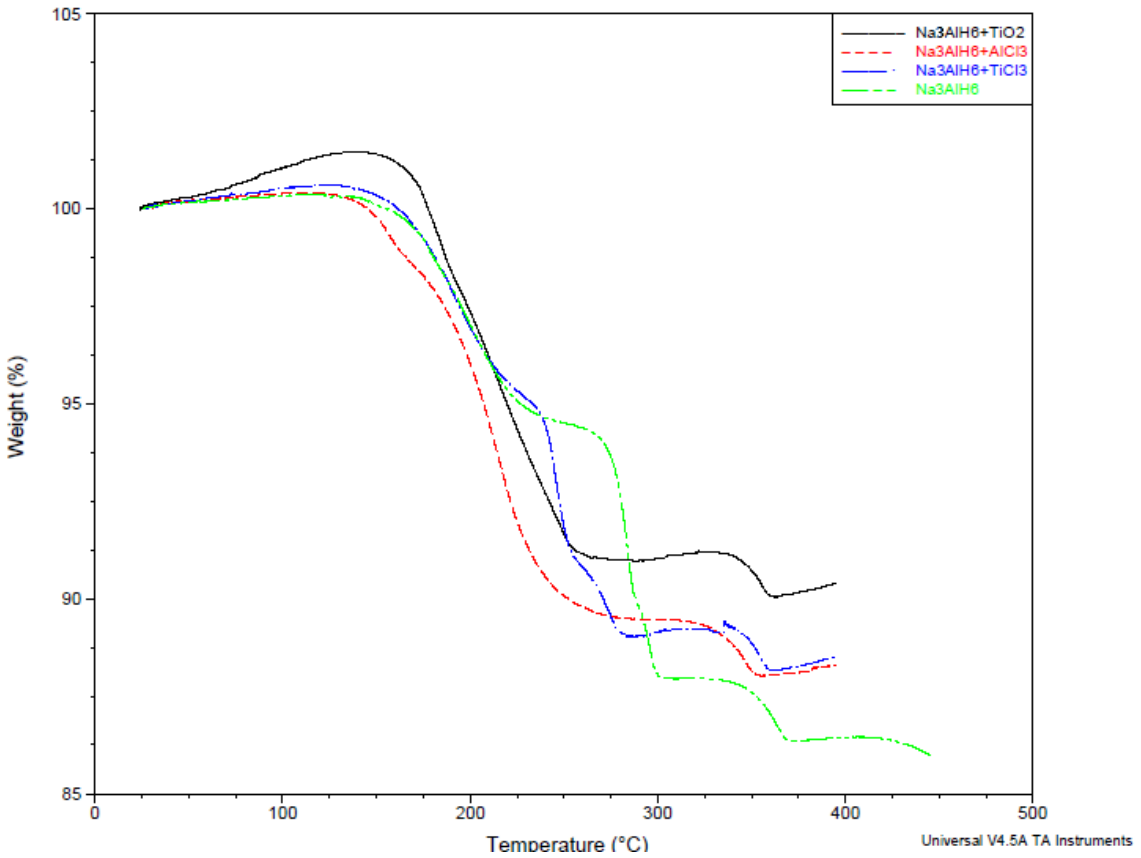

Figure 77 TGA analysis of doped Na_3AlH_6

The comparison of each curve indicates a general behavior, that all tested materials showed multi-step hydrogen desorption. The first shift is identified at a temperature of 160-180℃, depending on the material. This shift can be related to a decomposition of the $NaAlH_4$ phase. This material remained in the sample and indicated an incomplete synthesis. In the second step, the Na_3AlH_6 phase decomposes in a temperature range between 200- 275℃, depending on the material. In the last step, sodium hydride decomposes into its elements at a temperature of 350℃. Evidently, the last step is not influenced by the addition of a dopant. Further analysis will provide more in depth information about the bond characteristics of the material.

DSC Analysis

Additional data from the DSC analysis will enhance the knowledge of the materials behavior and characteristics. The preparation and analysis of the samples are done under standard conditions and resulted in following outcome.

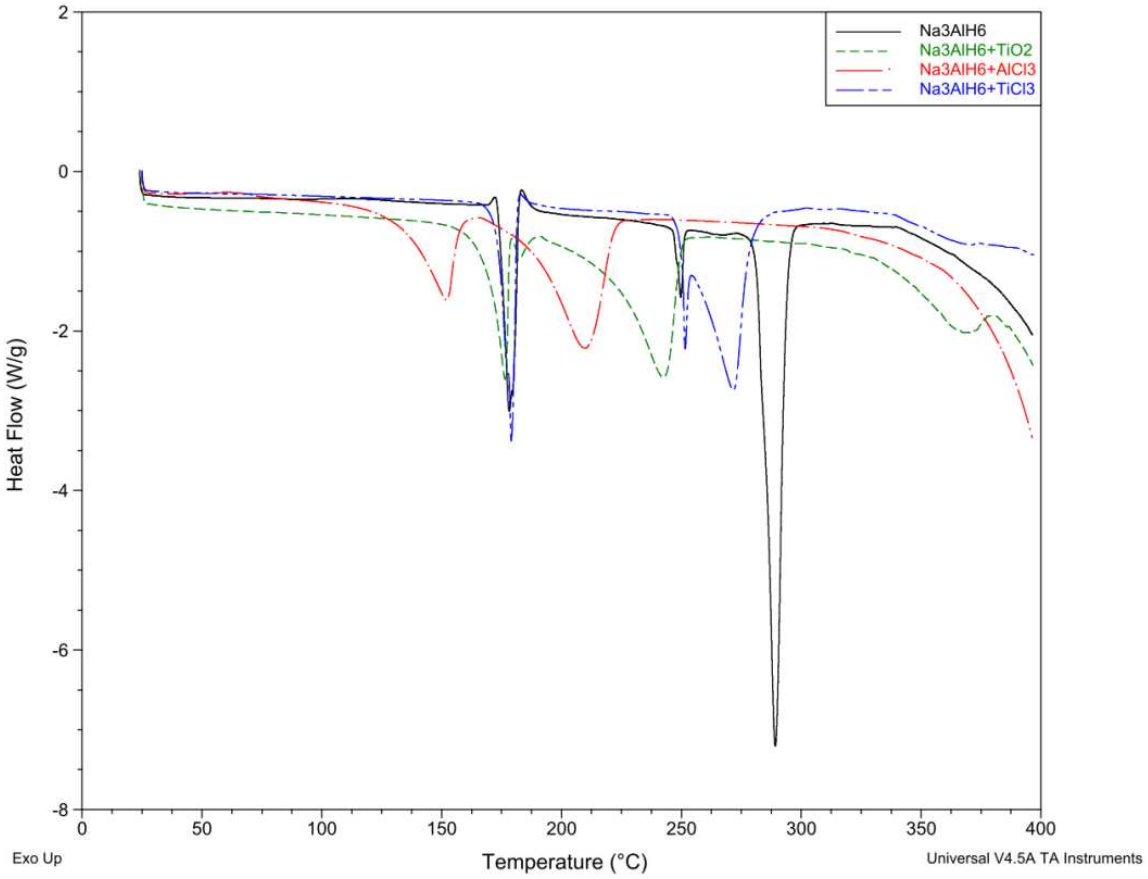

Figure 78 DSC analysis of doped Na_3AlH_6

The results of the DSC analysis coincide and outline the results of the TGA analysis. The first step of the TGA analysis, which is allocated to the $NaAlH_4$ decomposition, is proven with the DSC results. The second peak which took place in a temperature range of 200- 280℃ can be related to the decomposition of Na_3AlH_6 and coincides with both the results of the TGA analysis and the DSC analysis of the $NaAlH_4$ material.

The result of the decomposition of sodium hydride into its elements mentioned in the interpretation of the TGA, is visible in the DSC curve as well. Starting at a temperature of 350℃, all curves show a significant decrease, which can be related to the hydride decomposition.

Analysis and Discussion

Na_3AlH_6 was another material, synthesized and tested for its hydrogen desorption characteristics. Similar to all other materials, only little information about the desorption dynamics of doped samples are available. In the present study, both the undoped material as well as the doped material are tested on its characteristics and compared to each other. Table 12 depicts the results of each analyses, the impact of doping agents on the temperature of desorption and the amount of desorbed hydrogen.

Table 12 Overview of the results of Na_3AlH_6

Material	**Material Specifications**			
	molar weight [g/mol]	theoretical storage density [wt %]	chemical Reaction	reversible storage density [wt%]
Na_3AlH_6	101.996	5.9	1. $Na_3AlH_6 \leftrightarrow 3NaH+Al+1.5H_2$ 2. $NaH \rightarrow Na+0.5H_2$	1. 2.95 (2. 2.95)
$Na_3AlH_6+TiCl_3$	101.996	5.9	1. $Na_3AlH_6+TiCl_3 \leftrightarrow 3NaCl+Al+Ti+3H_2$	5.6
$Na_3AlH_6+AlCl_3$	101.996	5.9	1. $Na_3AlH_6+AlCl_3 \leftrightarrow 3NaCl+2Al+3H_2$	5.6
$Na_3AlH_6+TiO_2$	101.996	5.9	1. $4Na_3AlH_6+3TiO_2 \leftrightarrow 6Na_2O+Al+3Ti+12H_2$	5.6

Continuation of overview of the results

Material	TGA				DSC					XRD
	experimental [wt%; ℃]		published [wt, ℃]		experim ental [W/g, ℃]		theoretical [W/g]	published [W/g, ℃]		
	without catalyst	with catalyst	without catalyst	with catalyst	without catalyst	with catalyst		without catalyst	with catalyst	
Na_3AlH_6	5.5; 250-300	-	5.0; 270	-	-7.1;275	-	-	3600J/mole;268	-	x
$Na_3AlH_6+TiO_2$	-	5; 210-250	-		-	-2.5;240	-	-		x
$Na_3AlH_6+TiCl_3$	-	5.5: 240-270	-	1.5; 240-270	-	-2.7;260	-	-	-2.0;490	x
$Na_3AlH_6+AlCl_3$	-	5.9; 160-210	-		-	-2.2;210	-	-		x

x= analysis performed

Na_3AlH_6 was synthesized by its precursors, NaH and Na_3AlH_6. The final product is tested for its structural composition with an XRD apparatus. Main peaks at angles of $2\Theta_1$= 32.63° and $2\Theta_2$= 32.27°, $2\Theta_3$= 33.07°, identify the sample as Na_3AlH_6. Impurities are recognizable at $2\Theta_1$= 29.61° and $2\Theta_2$= 35.61°, and are related to precursor material. The result of the undoped material coincides well with the reference pattern from the JCPDF file and also with published data [80].

In the course of study, the sample was doped with different materials, such as TiO_2, $TiCl_3$, and $AlCl_3$. The results of the XRD pattern show no phases of the precursor dopant, which results in the conclusion that the material formed new phases with the matrix material. This assumption agrees with published results [66] and theoretical understandings of the catalytic effect of these dopants. Regarding the results of the TGA of the undoped materials, it points out that the hydrogen desorption takes place in a temperature range of 250- 300℃, with a total amount of desorbed hydrogen of 5.5wt %, in a two-step reaction based on theoretical assumptions [81]. This value coincides with both previous published papers, and the theoretical storage density of that material [90].

All samples, especially the TiO_2 doped sample, show an increase in weight during the heating process of 0.5wt % (undoped, $TiCl_3$, and $TiAl_3$) to 1.5wt % (TiO_2). Interactions with ambient moisture and air can be assumed as responsible for this behavior. Reactions take place in the following form depending on their appearance in the atmosphere [25, 30, 32].

For the reaction with oxygen:

$$Na_3AlH_6 + 6H_2O \rightarrow 3NaOH + Al(OH)_3 + 6H_2 \qquad 2.38$$

For the reaction with moisture:

$$Na_3AlH_6 + 2O_2 \rightarrow 3NaOH + Al(OH)_3 \qquad 2.39$$

The resulting NaOH does not affect further hydrogen desorption processes, but needs to be considered in further analysis.

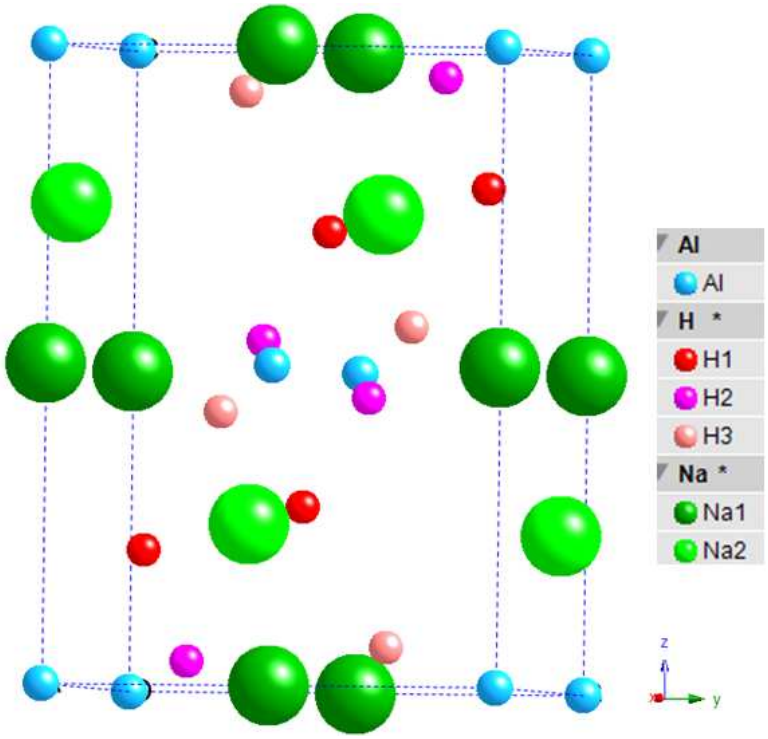

Figure 79 Crystal Structure of Na_3AlH_6

Figure 79 shows the crystal structure. At low temperatures, it has a monoclinic $P2_1/n$ symmetry, whereas at higher temperatures the symmetry changes to orthorhombic Immm. The lattice parameter of this structure are “a”= 5.322Å, “b”= 5.516Å, and “c”= 7.679Å, with a Al- H bond length of 1.77Å [22, 26]. The Al- H bonds are of covalent character, but due to their ionicity they also share ionic characteristics. Besides the bond structure of the Al- H bonds, the enthalpy, ΔH (-69.8kJ/mol) [80, 81], is an important aspect of the hydrogen desorption temperature. If the energy amount is high enough, the material starts to decompose to NaH under hydrogen release. At a temperature of 275℃, enough energy in the form of heat is induced into the system to split the bonds of the material, and Na_3AlH_6 starts to decompose.

The same analysis was performed with doped materials. The hydrogen desorption of the TiO_2 doped material took place in a range of 210-250℃, with a total weight loss of 5 wt%. The decomposition of the titanium chloride doped sample took place in a range of 240℃- 270℃, with a total weight loss of 5.5wt %. Finally, the aluminum chloride doped sample desorbed hydrogen in a range of 160℃- 210℃ , with a total weight loss of 5.9wt %.

Independent from the dopant precursor, a shift to lower temperatures is recognizable. The reason for this is the formation of the catalytic phases $D0_{22}$- $TiAl_3$, which is formed alike sodium chloride. Deeper information about the atomic crystal structure of the doped material are not available and no prediction about can be done. This catalytic phase is evidently responsible for the temperature shift to lower values [90]. Similar assumptions can be made about the precursor TiO_2 and $AlCl_3$, where the dopant itself has significant influence on the shift. Unlike Na_3AlH_6 hydride, the total amount of desorbed hydrogen does not decrease by doping the material. This fact leads to the assumption that the thermodynamics of the decomposition are more favorable when compared to the other material. This occurrence coincides with previously published data [66, 80, 81, 90].

The DSC analysis was performed in order to gain deeper information about bond characteristics and hydrogen desorption kinetics. Therefore, the undoped and doped samples were tested and compared with each other. Regarding the undoped sample, an endothermic peak at 275℃ is recognizable, which id entifies the hydrogen desorption and coincides with the results of the TGA analysis, as well as with published data [66, 80, 81, 90]. Besides bond characteristics, entropy is a second major factor that influences the hydrogen desorption temperature. This value is equal to the amount of heat to bring the hydride to its ground state [31, 34, 91, 92]. Comparing the height of the peaks of the undoped and doped sample, peaks of the doped samples are lower than these of the undoped sample, with values of -7.1$\frac{W}{g}$ for the undoped sample and -2.5$\frac{W}{g}$ for

the doped samples. This result coincides with published data, where similar results have been proved [87]. This results verifies the assumption that the height of the peak is related to the desorption temperature and that the peak shifts to lower temperatures by adding dopants into the structure.

Regarding the doped samples, a general improvement is recognizable in terms of desorption temperatures. The values for the peaks from the DSC analysis match well with the steps occurring at the TGA analysis and can be allocated to each other. Additionally to the reaction characteristics of the desorption steps, the DSC analysis also gives information about the bond strength between the involved atoms. Doping of the material leads to the formation of new phases, such as $D0_{22}$-NaCl and TiH_2, which have favored bond characteristics referring to the hydrogen desorption kinetics. However the atomic crystal structure of these materials is not yet determined and no prediction about bond character is possible. The results from the current analysis also match with published data [66, 80, 81, 90]. Regarding the requirements and guidelines given by the DoE, the material must be excluded as potential candidate for mobile application due to its unfavorable desorption temperatures, but also due to its low amount of reversible hydrogen storage. The guidelines require a reversible storage density of 6%, whereas these material 3wt % reversible stores.

2.5. Summary

In the present study, several materials were synthesized and characterized on their hydrogen desorption dynamics. Singularly and binary hydrides consist of a metal host atom and one or two, respectively, hydrogen atoms. These materials are being used as precursor materials for complex structures. In the current study, LiH, NaH, and KH as singularly hydrides and CaH_2, MgH_2, and TiH_2 as binary hydrides were analyzed.

Therefore, LiH hydride was due to its favorable theoretical storage density of 12.7wt % from special interest. The material was being doped with Ti and Al based dopant materials in order to lower its hydrogen desorption temperature. It was possible to create a significant shifts towards lower temperatures but the desorption temperature of the doped samples was with 560℃ still too high to fulf ill the guidelines.

Another approach consisted in the synthesis of a composite including two binary hydrides TiH_2 and CaH_2. Therefore, samples with different TiH_2: CaH_2 were prepared and tested for their hydrogen desorption kinetics. Besides the desorption kinetics, the impact of each compound was of major interest. Results of the samples did not indicate hydrogen desorption in a temperature interval until 400℃.

Another approach to create a new storage material was the synthesis, doping and analysis of lithium and sodium based alanates. Therefore four different materials, Li_3AlH_6, $NaAlH_4$, Na_3AlH_6, and $LiNa_2AlH_6$ were synthesized and doped. As dopant material, TiO_2, $TiCl_3$, and $AlCl_3$ were chosen where all samples were doped with 2mol % of each dopant. As predicted, all samples indicated a shift towards lower temperatures when the dopant was implemented into the structure. The temperature shift is strongly dependent on the dopant material, titanium or aluminum. However, it is not possible to give a general statement about the dopant material and its effects on the temperature shift each material showed individual results, but even between TiO_2 and TiCl3 significant differences could be proved which lead to the assumption that each material has its individual optimal dopant material where it shows optimized hydrogen desorption dynamics.

3. Hydrogen based Infrastructure

3.1. Introduction

Based on the facts mentioned in chapters 1 and 2, hydrogen has the potential to replace existing technologies as a generator of heat and electricity. Directly connected to hydrogen challenges are technical problems that are connected to its devices, namely, the weight of fuel cells and the electric converter. In order to ensure a successful transition to a hydrogen based technology, indirect factors such as a network of refueling stations and a working hydrogen supply chain are of high importance as well.

The overall goal of government and industry must be a step by step transition towards a fully integrated hydrogen economy based on zero emission energy sources. Therefore, a solid framework set based upon science, technological knowledge, and political communication has to be established.

Hence, time is of major concern, not only because of rising pollution and energy demand, but also because other technologies stand in direct competition with the hydrogen sector. An introduction into high scale application will depend upon many factors, such as grants, state of art and support from the political viewpoint. Estimations predict an introduction of the first high scale hydrogen application in approximately 30 years. As a consequence, a working hydrogen based infrastructure will not be observable before the year 2030, assuming that serious research began 10 years ago. Current research focuses on small and middle scale production systems based on existing technologies. Thereby, an increase in the grade of efficiency and cost reduction

are important [3, 11, 12]. These, along with other aspects, define the term “hydrogen infrastructure”, which will be discussed in the following.

3.2. Transition Strategies

The transition to hydrogen based technology is characterized by two extremes. On the one hand, hydrogen is perceived as the immediate answer to all questions relating to pollution, climate change, and expensive fossil fuels. On the other hand, safety concerns paired with a lack of technological knowledge are blocking its development.

Hydrogen as an energy carrier is not seen as the ideal solution to all policy objectives. Especially as a short term solution, hydrogen seems to be impractical due to its complex technological challenge. Therefore, the aim for politics, industry and academia is a solution which enables the fastest possible transition independently of the technological standpoint. A strong driving force for each country is the oil dependency on other countries. As a result, many European countries set themselves the goal of developing a sustainable energy infrastructure by 2050, when the limitations of fossil fuels will become recognizable. This infrastructure includes the reduction of energy demand, the establishment of renewable resources and the decrease of greenhouse gas emissions.

Since hydrogen is difficult to regard as a short term solution, alternative technologies have to be found to initiate the transition starting away from fossil fuels to renewable fuels. The transition will consist of many components, each with its own set of challenges and solutions. Participating countries have agreed to split the challenge into six individual parts, listed below

- Green raw materials
- Sustainable mobility
- Chain efficiency

- New gas
- Sustainable electricity
- Energy use in the constructed environment

Possible solutions to each part of the issue need to be developed and embedded into a functional system. Since the process of energy transition takes time, current pathways to this transition must be flexible and adaptable to variations in solutions within state of the art technologies. Currently involved institutions have identified the most promising pathways for each of the six themes.

At first, participating countries were confident about the success of their design ability to establish a transition. In the following years, criticisms about the existing design come to the surface. Basically, there was a debate that the energy transition is a niche process and will not have a significant impact on broader policy. Furthermore, details of energy supply and sustainability are still divided, which disables the possibility of a successful transition.

Another setback is the lack of communication between the leading organizations and positions. Politicians seem to not be deeply interested in the transition for various reasons. As a result, the necessary amount of effort is not being put forth. From an academic standpoint, universities do research, but instead of transferring and publishing these research results, most departments hide breakthroughs from each other, which results in blocked pathways. Lastly, industry has a great influence on research projects. Since industry provides the majority of the funding for research for all the projects, pathways and solutions are fit to their individual agenda.

Criticisms made in the recent past led to a general analysis of barriers and driving forces for a transition. Research groups came to the conclusion that both the, driving factors and the barriers play a significant role in a hydrogen based transition.

Environmental aspects

The effect of greenhouse gases on climate change can be allocated to two main aspects: increasing energy demand and the development of industry. As a result, environmental issues emerge as a leading driving factor for politics and industry. In the recent past, strict standards were set in order to improve local and national air quality. Unfortunately, the regeneration of the environment takes a lot of time so significant changes will not be recognizable within the next decade. Fuel cells and their peripherical devices will play an important role in that change. Once it became clear that the existing energy demand could not be satisfied by hydrogen alone, a combination of several alternative fuels emerged as a possible solution.

Security of energy supply

Concerns about future availability, geographical sensitivity and energy prices, have recently emerged. A dependency on the importation of fuels is a huge security risk for a country. Taking that into account, the development of alternative fuels is linked with a certain amount of independence in terms of energy supply and demand. Since fossil fuels are limited and have become rare in this century, prices will continue to increase and will have detrimental effects on the on the transportation sector. Therefore, hydrogen seems to be a favorable technology in order to avoid these stresses. Its properties enable a direct link between energy source and consumer. Furthermore, hydrogen allows for competition with each field of application and will put all energy sources on an equal level.

Innovation and Competiveness

Another driving force is politics and the industry itself. The competition within international markets leads to high investments in the development of new technologies.

Technical knowledge is not only a trademark, but also the basis for a successful development of new technologies. In order to guarantee a zero emission infrastructure, existing technologies have to be upgraded and new technologies have to be found. Even though a strong sense of international competition exists, it is vital that countries share their specific knowledge with each other.

Absence of Infrastructure

The main barrier to a transition is the fact that even after many years of research, no transition or infrastructure can be recognized. Existing infrastructures have only limited space for renewable energies, even though, the development of hydrogen is attractive for reasons, such as

- The utility of infrastructure increases with standardization
- The economics increase proportionally with the amount of users
- Learning effects, that provide more efficient services, are a result of experiences.

Costs

Costs are a prime factor to the success of a transition to an alternative energy based infrastructure. If it is possible to reduce the cost of fuels produced by alternative energies to the level of fossil fuels, chances for a transition increase substantially. Currently, the cost of fuel cells and all of their applications are significantly higher than cost of commonly used engines. Latest cost predictions show that fuel cells will become more affordable and cheaper than combustion engines with an increase in production volume. This fact allows for hope in the future, but it should be kept in mind that these predictions are based upon many assumptions that are not yet clarified.

Even though, hydrogen has a large potential to be a future energy carrier due to its physical and chemical properties, people realize the problems connected with this technology. Therefore, several countries and institutions have ceased efforts in hydrogen and are focusing on other promising technologies [3, 11].

3.3. Examples of a Hydrogen based Infrastructure Strategy

The development of a hydrogen technology and its devices is the basic requirement for a transition to a hydrogen based technology. In addition to these technological aspects, large- scale plans are an important aspect of guaranteeing a successful transition to this technology. As a result, roadmaps developed by different countries and research groups will help promote the establishment of hydrogen into the infrastructure. In the following, two examples of this will be provided; the Japanese strategy and the US strategy, in order to show the different approaches to a transition.

3.3.1. The Japanese Strategy

The Japanese economy has realized the significance of PEM fuel cells and their stationary and mobile applications. Since 1999, several projects have been founded to create models for a transition. The Japanese Ministry for Economy, Trade, and Industry (METI) has taken the responsibility of controlling and managing the different projects from a governmental standpoint. Together with industry and academia, long term projects have been developed and implemented as test programs into the existing infrastructure.

Along with local and environmental issues, severe international competition in fuel cell technology and renewable energy is a driving force encouraging politics and government

to force a transition. In 1996, a group was founded that developed plans and programs to implement and commercialize fuel cell engine cars. The group consists of members from automotive and electric industry, universities, media, and many other influential institutions. Their original objectives were the following:

- Determine the state of the art fuel cell technology
- Identify issues and barriers to promotion and commercialization
- Recommend strategies to overcome barriers

After 12 months of research and analysis, they found results that describe the baseline for a transition.

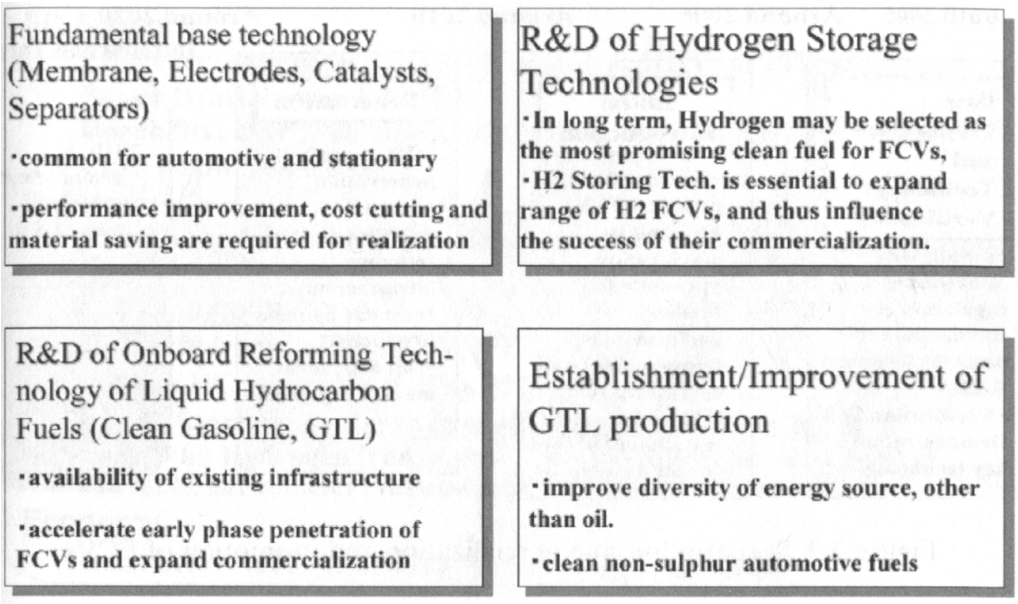

Figure 80 Basic Aspects to a Transition [3]

Referring to Figure 80, the results can be divided into four groups, depending on their content significance. Among the four mentioned points, the first two are considered to be critical and will determine the over success or failure of hydrogen technology as an alternative to a fossil fuel based infrastructure. In the course of research, the committee developed possible solutions to overcome these barriers and gave a timeline showing when these improvements should be introduced.

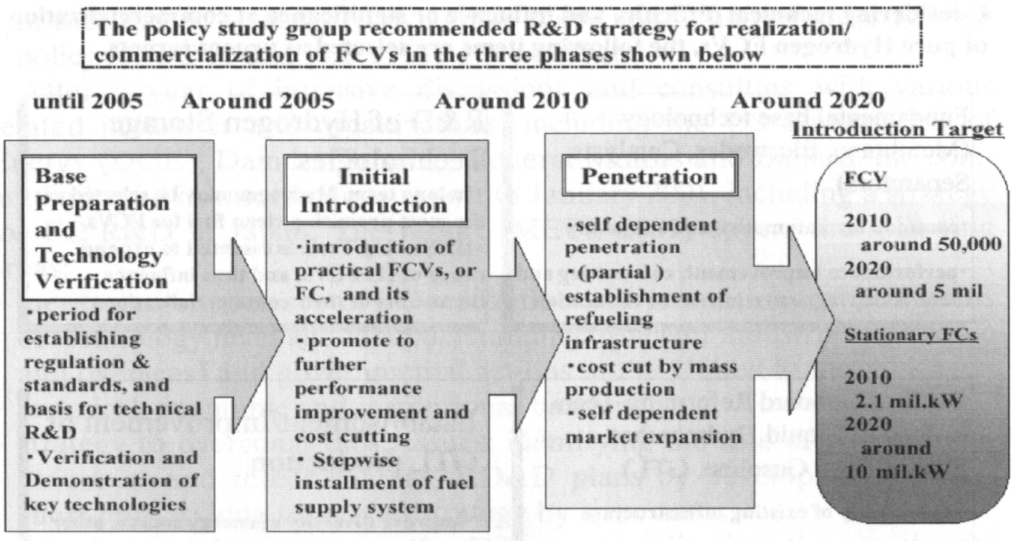

Figure 81 Pathway for possible Solutions[3]

In general, a transition can be divided into four stages, as shown in Figure 81: the establishment of test evaluation methods, standardization, education of human resources and fleet test& demonstration. Based on this initial analysis, a three year lasing pilot project was introduced in 2002. Due to its great success, the project was extended for three additional years. The project consisted of a regional network of hydrogen refueling stations and a fleet of fuel cell cars. The general objectives of the project were the following:

- evaluation of total energy efficiency
- collection of data for codes and standards
- issues for the real working condition

In 2005, after a three year testing phase, first data was collected, analyzed and published. Results showed a clear improvement in the economy at equivalent driving performances. Since the project was extended and just finished recently, data concerning durability and reliability still have to be interpreted and are not yet published.

3.3.2. The US Strategy

The significant value of hydrogen as an energy carrier has been recognized by the US government during the last decade. In 2003, President Bush announced $1.2 billion for research in renewable energies, which is the largest amount of money ever spent on alternative fuel project. This announcement has marked a clear turning point away from fossil fuels towards renewable energies. The limitations of fossil fuels and the dependence upon other states is a big security risk for every country. Recently, the US Fuel Cell Initiative has made significant progress in technological development.

Unlike the Japanese Initiative, which mainly focuses on hydrogen technology, the US initiative approach includes all forms of renewable sources as potential alternatives. The DoE as a governmental institution controls and regulates all national programs and provides funding for each project. The goal is to establish renewable energy sources until 2020, when fuel cell vehicles and industrial applications hope to be fully implemented. Therefore, the implementation of wind, water, nuclear, and photovoltaic energy enable a wide range of possible solutions. The US Fuel Cell Initiative splits the hydrogen plan into different parts, similar to the Chinese initiative. Hydrogen production is seen to be a key technology but also a barrier. Therefore, the development of sustainable production methods is important to the course of all projects. Current production methods involve fossil fuels, such as gas and coal, which produce greenhouse gases as a byproduct. The primary aim of this process is to replace fossil fuels. This is a long term process that requires technological developments and a highly developed infrastructure. Meanwhile, emission lowering process methods have to be developed in order to avoid a deceleration of the transition.

By 2015, the price of hydrogen as a fuel needs to be lowered, as shown in Figure 82 to a competitive level of $2.50/gge (**g**allon **g**asoline **e**quivalent).

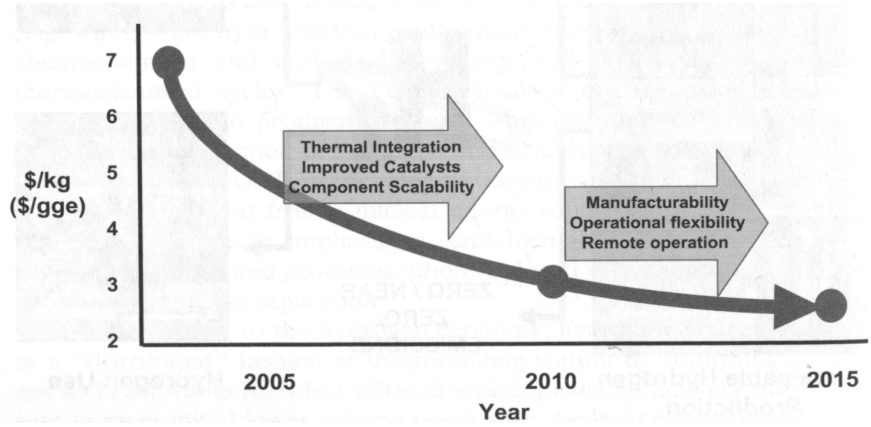

Figure 82 Prize developing for hydrogen fuel[3]

The price would stand in direct concurrence with fossil fuels and allow a transition to new technologies. Ensuring a safe hydrogen delivery from its point of production to its point of use is another important aspect of the hydrogen infrastructure. Nowadays, the transportation of hydrogen is connected with high energy losses caused by its physical properties. Current research is focusing on the optimization of compression and storage methods, while current pipelines and delivery facilities are being improved by introducing new materials and devices.

In order to guarantee a reliable hydrogen delivery, cost for compression and storage needs to be lowered to $0.80/gge, and costs of transportation to $0.90/gge. In addition to delivery, hydrogen storage is the second key technology and its development will determine the failure or success of the transition to a hydrogen based infrastructure. Due to the high value of this field of research, the national hydrogen storage project is divided into different parts, which focus on different storage methods. In order to establish hydrogen as an alternative to fossil fuels, a vehicular driving range of at least 300 miles at similar driving performances must be provided. Furthermore, a dense network of refueling stations must be developed.

	2010	2015
System gravimetric capacity (specific energy)	2.0 kWh/kg 7.2 MJ/kg 6 wt %	3.0 kWh/kg 10.8 MJ/kg 9 wt %
System volumetric capacity (energy density)	1.5 Wh/L 5.4 MJ/L 0.045 kg/L	2.7 Wh/L 9.7 MJ/L 0.081 kg/L
System cost	\$4/kWh \$133/kg H_2	\$2/kWh \$67/kg H_2

Figure 83 Technological Requirements to the Storage System [12]

In addition to this framework, technological issues, mentioned in Figure 83, have to be considered. High expectations are placed on metal hydrides and chemical hydrides, where new materials have to be found that fulfill the guidelines made by the DoE.

The trend within the last years of research had been a shift away from improving existing technologies and a movement towards the exploration of new technologies. Safety issues, codes and standards are other important aspects to ensure a successful transition to renewable energies. The government as a neutral institution catalyzes and coordinates different national projects to develop codes and standards. Therefore, data based on current studies are the main source for the development of codes and standards. The aim is to provide standards for residential and transportation application that act harmoniously with international programs. At the same time, safety issues have to be taken seriously. As a result, permanent practices and training for customers needs to be implemented into the existing infrastructure.

Lastly, the education of society is as important as the improvement of codes and standards itself. Since the customer has great influence over the success of the transition, demonstrations are required to make the technology public. Based on the concept that a customer will only buy a product if they are familiar with it, all forms of feedback are important to improve the future product.

3.4. Summary

The development of a fitting storage material is a major criterion for the transition to a hydrogen based infrastructure. Even though, the success of the transition will mainly be dependent on aspects such as hydrogen production and hydrogen storage, other aspects cannot be neglected. The hydrogen infrastructure can be down selected into six parts, namely, green raw materials, sustainable mobility, chain efficiency, new gas, sustainable electricity and energy use in the constructed environment. Each of these aspects has its own challenges, which have to be solved individually. Therefore the cooperation between government academia, and industry on a national but also international basis needs to be close to guarantee a successful transition. The transition to that infrastructure is covered with forcing factors such as environmental aspects, international competition and security of energy supply but also barriers such as the absence of an infrastructure and insufficient communication. Based on these aspects, countries all over the world established governmental institutions to induce a transition to an alternative fuel based infrastructure. Models differ significantly from each other. For example, the Japanese Model of the transition is focused on hydrogen as a fuel. Every aspect is aligned to hydrogen and its application. In contrast to that, the US strategy to an alternative fuel based transition does not focus on one particular energy source, but uses the advantages of all technologies and creates an infrastructure, where all applications find their place in the overall system depending on their individual excellence.

However the transition still is in the beginning phase and significant milestones have to be reached in order to guarantee the success of a transition. It is planned that a working infrastructure will be established in the year 2050 with major application based on alternative fuels.

4. Conclusion

The Department of Energy has set guidelines and requirements on the materials referring to gravimetric storage density, cost and other criteria. The challenge for researches and engineers is to find a material that fulfills all these requirements in order to replace existing hydrogen storage methods. In the present study, four systems of metal hydrides were synthesized and tested on their structural composition and their hydrogen desorption behavior. The synthesis of the materials was performed by a mechanochemical solid state reaction. Therefore, the precursors were charged with steel balls in a vial and milled for 3 hours. In this process, a chemical reaction between the precursors takes place and a new compound and composite, respectively, are formed. The structural analysis of the product is performed with an XRD technique, which provides a characteristic reflection pattern. Comparing these patterns with public data allows an undeniable identification of the sample. Desorption behavior and bond characteristics are tested with either thermogravimetric analysis methods or with differential scanning caliometric methods. Both methods enable a clear overview of the chemical properties of the material. Based on these results, materials are assessed by their practicability for industrial application.

Table 13 provides a summary about performed experiments and their results.

Table 13 Summary of Experiments

	Synthesis	Material Analysis			Doping			New Results			
		TGA	DSC	XRD	TiO_2	$TiCl_3$	$AlCl_3$	TiO_2 New result (theor. Stor. Density/Temp)	$TiCl_3$ New result (theor. Stor. Density/Temp)	$AlCl_3$ New result (theor. Stor. Density/Temp)	Synthesis
Singularly Hydrides											
LiH	-	x	x	x	x	x	x	6.6;560-640 (12.7;675)	7.2;630-660 (12.7;675)	8.3;560 (12.7;675)	-
NaH	-	x	x	x	-	-	-	-	-	-	-
KH	-	x	x	x	-	-	-	-	-	-	-
Binary Hydrides											
MgH_2	-	x	x	x	-	-	-	-	-	-	-
CaH_2	-	x	x	x	-	-	-	-	-	-	-
TiH_2	-	x	x	x	-	-	-	-	-	-	-
Composite											
$TiH_2 + CaH_2$ 75:25	X	x	x	x	-	-	-	-	-	-	**x**
$TiH_2 + CaH_2$ 50:50	X	x	x	x	-	-	-	-	-	-	**x**
$TiH_2 + CaH_2$ 25:75	X	x	x	x	-	-	-	-	-	-	**x**
$TiH_2 + CaH_2$ 95:5	X	x	x	x	-	-	-	-	-	-	**x**
Alanate											
Li_3AlH_6	X	x	x	x	x	x	x	3.5;200-235 (11.1;220)	-	-	-
$NaAlH_4$	X	x	x	x	x	x	x	2.5;160-200 (7.4;250)	-	-	-
Na_3AlH_6	X	x	x	x	x	x	x	5.0;210-250 (5.9;270)	-	-	-
$LiNa_2AlH_6$	X	x	x	x	x	x	x	5.5;230-265 (6.9;275)	5.5;230-265 (6.9;275)	6.5;215-235 (6.9;275)	-

Singularly Hydrides MH

In a first attempt, singularly and binary hydrides were tested for their hydrogen desorption dynamics. All singularly hydrides decompose in the general form of

$$MH \rightarrow M^{+} + H^{-} \qquad 3.1$$

where M stands for the metal atom and H for hydrogen. All singularly hydrides have a face- centered cubic crystal structures with individual lattice parameter and M- H bond lengths. All bonds show a mixed ionic and covalent character with the majority at the ionic side. As a result, the atoms are in an ionic state after they decompose into their elements. The materials showed unfavorable hydrogen desorption kinetics, where the desorption was too high to fulfill the DoE requirements. NaH has a value of 350˚C the lowest value, and LiH has 650˚C, the highest. However, LiH, due to its favorable mass ratio between lithium and hydrogen, is of special interest. Out of all singularly hydrides, this material has the highest theoretical storage density, with 12.7wt %. Therefore, the material was doped with TiO_2, $TiCl_3$, and $AlCl_3$ in order to improve its weak reaction kinetics. The TGA analysis could prove a shift of the temperature of desorption in a maximum of 40˚C for all doping agents, where TiO_2 showed the best results. Further analyses have to determine the phase change and the location of the catalyst atom within the crystal structure. Even though the analysis of the materials shows unfavorable desorption kinetics, these materials were still of interest as precursor materials for the synthesis of complex compounds as well as for the formation of composite materials.

Binary Hydrides MH_2

Similar to singularly hydrides, binary hydrides were tested as received for their hydrogen desorption dynamics. In general, binary hydrides decompose in the following form,

$$MH_2 \rightarrow M^{2+} + 2H^- \qquad 3.2$$

where M stands for the metal atom and H for hydrogen. All binary hydrides have either a tetrahedral face- centered cubic crystal structure or an orthorhombic face- centered cubic structure with individual lattice parameters and bond length. In the case of CaH_2 andMgH_2 the M- H bonds are of ionic character due to their earth alkali character. TiH_2 behaves differently to the two other binary hydrides. Other than these, its M- H bonds are from metallic character and the desorption takes place in a two-step process, where in the first step the crystal structure changes from cubic to rhombohedral, and in the second step, hydrogen desorbs. Even though no new results were found, the analyses were of major importance because these materials act as precursors for complex structures and composites, comparable to the singularly hydrides.

Composite TiH_2 + CaH_2

In another series, a composite consisting of TiH_2 + CaH_2 was synthesized and tested for its hydrogen desorption characteristics. Therefore, four different samples were synthesized, which differ in their hydride mass ratio, in order to determine the impact of each component on the desorption characteristics. Both analyses, TGA and DSC, were performed in a temperature range of 25- 400°C. This interval was chosen because desorption above these temperatures is not of interest for the present study. The results of all samples did not indicate hydrogen desorption in the desired interval. However, it

might be possible that the composite will show improved reaction dynamics, compared to its compounds TiH_2 and CaH_2.

Lithium- Sodium Alanate

Another attempt in the synthesis of materials was performed by an alanate system consisting of Li_3AlH_6, Na_3AlH_6, $NaAlH_4$, and $LiNa_2AlH_6$. Since alanates show, in the undoped state, good reaction kinetics, it is assumed that a dopant could lower the hydrogen desorption temperature to favorable temperatures.

A tested material was $NaAlH_4$, which is, in the undoped state, a well tested material. When heated, the material decomposes in two steps into its elements and showed 6.0wt % weight loss, which is close to the theoretical value of approximately 6.5 wt %. The material was doped with different doping agents and tested for its hydrogen desorption behavior. In general, all doped samples showed a shift to lower temperatures. For the current study, TiO_2 as dopant was of high interest because no data was available for this particular hydride: dopant combination. Similar to Li_3AlH_6, a change in the phase occurs during the implementation of the dopant. The new phase, $D0_{22}$-TiCl acts as a catalyst for the desorption, and causes the shifts in the DSC and TGA measurements. However, these samples showed a decrease in the total amount of desorbed hydrogen (2.5wt %) caused by a second TiH_2 phase that occurred during the dopant implementation. Even though the hydrogen desorption temperature could be lowered, the reversible storage density is still too low and excludes the material as potential storage material.

Li_3AlH_6 was chosen as a material to synthesize and to dope with different agents. The structural analysis of the synthesized material proved a sample of high purity with only minor impurities. The material itself has a monoclinic crystal symmetry with an $R\bar{3}$ space group. However, the analyses of the undoped material showed a two-step

decomposition, which coincides with theoretical assumptions. The material decomposed 4.5wt % hydrogen, which is less than the theoretical value of approximately 11wt %. The difference between experimental value and theoretical value is caused by the high heating rate during the analysis and the weak desorption rate of the material. Regarding the results of the doped materials, a general shift to lower desorption temperatures was recognizable. The reason for that is the phase change caused by the implementation of the catalyst. During the milling process, a $D0_{22}$-TiCl phase appears, which acts as a catalyst for the hydrogen desorption. All samples showed decreasing amounts of desorbed hydrogen. This behavior can be explained by the second phase, which is formed during the catalyst implementation. The more stable TiH_2 is formed and causes the decreasing amount of desorbed hydrogen. The implementation of TiO_2 was of high interest since no data about this material was available. It could be shown that TiO_2 improves the reaction dynamics even though, the desorption time is still too high for industrial applications.

Another attempt consisted in the synthesis and analysis of the desorption behavior of Na_3AlH_6. Similar to other materials, characteristics of Na_3AlH_6 is, in its undoped state, well known. However, the implementation of aluminum and titanium based dopants will change the hydrogen desorption kinetics of the material. The results of the XRD analysis indicated a major Na_3AlH_6 phase with impurities. The TGA analysis as well as the DSC analysis of the undoped material match each other, where the phase transition in the temperature range of 250-300˚C and 350-400˚C, depending on the desorption step, could be proved. The bonds in between Na- Al, as well as Al- H, mainly define the desorption temperature. These bonds are of ionic and covalent character, respectively, and release hydrogen by forming NaH when enough energy is induced into the system. The second reaction step is characterized by the decomposition of NaH, explained in the beginning of the chapter. Comparing the results with the doped material,

shifts towards lower temperatures for all samples could be shown. Of main interest was the TiO_2 doped sample, because no experimental data about the impact of this dopant on reaction kinetics has been published. The implementation of the dopant leads to a phase change in the material, which improves the reaction dynamics with a shift of the desorption temperature (~40˚C), but decreases the total amount of desorped hydrogen (1- 2wt %) depending on the dopant agent. Referring to the guidelines and requirements given by the DoE, the material, even if doped with titanium and aluminum, still cannot reach all requirements and requires further analysis with different dopant material to reach better results in terms of reaction dynamics.

$LiNa_2AlH_6$ was synthesized and tested under similar conditions as all other materials. This material is fairly unknown, where just few experimental data about the structure and no experimental data about the impact of dopant materials is available. Therefore, results will provide new information about reaction kinetics and desorption behavior. The XRD results showed a major $LiNa_2AlH_6$ phase with impurities from the precursor material. However, the TGA and DSC analyses of the undoped material, as well as the doped material, showed a general shift of the desorption temperature towards lower values connected with a weight loss as high as 6.5wt % for $AlCl_3$ doped material. Depending on the dopant material, shifts of 60˚C could be reached to values as low as 215˚C (with $AlCl_3$ as dopant). TGA and DSC analysis verified the decomposition in the form of

$$LiNa_2AlH_6 \rightarrow 2LiH + NaH \qquad 3.3$$

The material has a cubic $P2_1/c$ space group. Further analyses of this material must determine the phase change during the dopant implementation as well as the influence

of the amount of dopant material on the temperature of desorption in order to gain a deeper understanding of the desorption behavior of this material.

The present study provided new results, especially concerning the doping of materials. Alanates were synthesized in a mechanochemical synthesis and tested for their hydrogen desorption kinetics. Results for titanium and aluminum doped materials showed significant differences between each other. Additionally, the variation of different titanium dopant agents, $TiCl_3$ and $TiO_{2,}$ showed individual characteristics. Further analyses need to determine the reason for this behavior as well as the optimal combination for each material.

References

1. Züttel, A., *Hydrogen as a future Energy Carrier*. 2008, Weinheim, Wiley-Ch.

2. Leon, A., *Hydrogen Technology- Mobile and Portable Application*. 2009, Berlin: Springer.

3. Lynn K Mytelka, G.B., *Making Choices bout Hydrogen- transport issues for developing countries*. 2008, Ottawa: United Nations University.

4. Carl- Jochen Winter, J.N., *Hydrogen as an Energy Carrier*. 1988, Berlin: Springer Verlag.

5. Dickson, E.M., *The hydrogen Energy Economy- a realistic Appraisal of prospects and Impacts*. 1977, New York: Praeger Publishers.

6. Dunn, S., *Hydrogen Futures- Towards sustainable energy systems*. 2001, Danvers: World Watch Papers.

7. Hirscher, M., *Handbook of hydrogen storage: New Materials of future storage*. 2010, Weinheim: Wiley- VCH.

8. Senkov, O.N., *Metallic Materials with high Strutural efficiencey*. 2004, Dordrecht: Kluwer Academic Publisher.

9. Fukai, Y., *The Metal-Hydrogen System- Basic bulk properties*. 2005, Heidelberg: Springer.

10. Billings, R.E., *Hydrogen from coal- a cost estimation guidebook*. 1983, Tulsa: PennWell Publishing Company.

11. Council, N.R., *The Hydrogen Economy- Opportunities,Costs,Barriers, R&D Needs*. 2004, Washington D.C: The National Acadenies Press.

12. Gupta, R.B., *Hydrogen Fuel- Production, Transport and Storage*. 2009, Boca Raton: Taylor& Francis Group.

13. Balema, V.P., V.K. Pecharsky, and K.W. Dennis, *Solid state phase transformations in LiAlH4 during high-energy ball-milling.* Journal of Alloys and Compounds, 2000. **313**(1-2): p. 69-74.

14. Balema, V.K.P., K.W. Dennis, Journal of Alloys and Compounds, 2000. **69**: p. 313.

15. Balogh, M.P., et al., *Phase changes and hydrogen release during decomposition of sodium alanates.* Journal of Alloys and Compounds, 2003. **350**(1-2): p. 136-144.

16. Graetz, J., et al., *X-ray absorption study of Ti-activated sodium aluminum hydride.* Applied Physics Letters, 2004. **85**(3): p. 500-502.

17. Berube, V., G. Chen, and M.S. Dresselhaus, *Impact of nanostructuring on the enthalpy of formation of metal hydrides.* International Journal of Hydrogen Energy, 2008. **33**(15): p. 4122-4131.

18. Wang, J., A.D. Ebner, and J.A. Ritter. *New synthesis route for complex hydride hydrogen storage materials*. 2007. Houston, TX, United states: American Institute of Chemical Engineers.

19. Andreasen, A., *Effect of Ti-doping on the dehydrogenation kinetic parameters of lithium aluminum hydride.* Journal of Alloys and Compounds, 2006. **419**(1-2): p. 40-44.

20. Andreasen, A., T. Vegge, and A.S. Pedersen, *Dehydrogenation kinetics of as-received and ball-milled LiAlH4.* Journal of Solid State Chemistry, 2005. **178**(12): p. 3672-3678.

21. Xueping, Z. and L. Shenglin, *Study on hydrogen storage properties of LiAlH4.* Journal of Alloys and Compounds, 2009. **481**(1-2): p. 761-763.

22. Løvvik, O.M. and O. Swang, *Crystal structures and electronic structures of alkali aluminohexahydrides from density functional calculations.* Journal of Alloys and Compounds, 2005. **404-406**: p. 757-761.

23. Easton, D.S., J.H. Schneibel, and S.A. Speakman, *Factors affecting hydrogen release from lithium alanate (LiAlH4).* Journal of Alloys and Compounds, 2005. **398**(1-2): p. 245-248.

24. Shim, J.-H., G.-J. Lee, and Y.W. Cho, *Mechanochemical synthesis of ultrafine TiAl3 powder and its catalytic effect on dehydrogenation of Li3AlH6.* Journal of Alloys and Compounds, 2006. **417**(1-2): p. 69-71.

25. Chung, S.-C. and H. Morioka, *Thermochemistry and crystal structures of lithium, sodium and potassium alanates as determined by ab initio simulations.* Journal of Alloys and Compounds, 2004. **372**(1-2): p. 92-96.

26. LÃ¸vvik, O.M. and O. Swang, *Structure and stability of possible new alanates.* EPL (Europhysics Letters), 2004. **67**(4): p. 607.

27. Berube, V., M.S. Dresselhaus, and G. Chen, *Temperature dependence of the enthalpy of formation of metal hydrides characterized by an excess volume.* International Journal of Hydrogen Energy, 2008. **33**(20): p. 5617-5628.

28. Kawakami, M., et al. *Optimum hydrogen desorption properties in LiH-LiOH composites*. 2009. 1-14-32 Ichibancho, Aoba-ku, Sendai, 980-8544, Japan: Japan Institute of Metals (JIM).

29. Ren, R., et al., *Stability of Lithium Hydride in Argon and Air.* The Journal of Physical Chemistry B, 2006. **110**(21): p. 10567-10575.

30. Shpil'rain, E.E., *Thermophysical properties of Lithium hydride,deuteride,tridide and their solutions*. 1983: American Society of Physics.

31. Novakovic, N., et al., *First principle calculations of alkali hydride electronic structures.* Journal of Physics Condensed Matter, 2007. **19**(40).

32. Vajeeston, P., et al., *Theoretical modeling of hydrogen storage materials: Prediction of structure, chemical bond character, and high-pressure behavior.* Journal of Alloys and Compounds, 2005. **404-406**(SPEC. ISS.): p. 377-383.

33. Xu, Q., et al., *Reaction of hydrogen with sodium oxide: A reversible hydrogenation/dehydrogenation system.* Journal of Power Sources, 2006. **155**(2): p. 167-171.

34. Gunn, S.R. and L.G. Green, *The Heats of Formation at 25Â° of the Crystalline Hydrides and Deuterides and Aqueous Hydroxides of Lithium, Sodium and Potassium1.* Journal of the American Chemical Society, 1958. **80**(18): p. 4782-4786.

35. Bortz, M., K. Yvon, and P. Fischer, *Synthesis and structure determination of complex zinc hydrides Part 2. Tripotassiumtetrahydridozincate(II) hydride, K3[ZnH4]H.* Journal of Alloys and Compounds, 1994. **216**(1): p. 43-45.

36. Bortz, M., K. Yvon, and P. Fischer, *Synthesis and structure determination of complex zinc hydrides Part 1: Dipotassiumtetrahydridozincate(II): K2[ZnH4].* Journal of Alloys and Compounds, 1994. **216**(1): p. 39-42.

37. Wang, P., X.-D. Kang, and H.-M. Cheng, *KH+Ti co-doped NaAlH4 for high-capacity hydrogen storage.* Journal of Applied Physics, 2005. **98**(7): p. 1-5.

38. http://www.presschem.com/potassium-hydride.asp. [cited.

39. Fuster, V., G. Urretavizcaya, and F.J. Castro, *Characterization of MgH2 formation by low-energy ball-milling of Mg and Mg + C (graphite) mixtures under H2 atmosphere.* Journal of Alloys and Compounds, 2009. **481**(1-2): p. 673-680.

40. Ikeda, K., Y. Nakamori, and S. Orimo, *Formation ability of the perovskite-type structure in LixNa1 - xMgH3 (x = 0, 0.5 and 1.0).* Acta Materialia, 2005. **53**(12): p. 3453-3457.

41. Gill, P.M.W. and L. Radom, *A rationalization of unusually late transition structures for dication fragmentations.* Chemical Physics Letters, 1987. **136**(3-4): p. 294-298.

42. Tessier, J.P., et al., *Hydrogen production and crystal structure of ball-milled MgH2-Ca and MgH2-CaH2 mixtures.* Journal of Alloys and Compounds, 2004. **376**(1-2): p. 180-185.

43. Zaluska, A., L. Zaluski, and J.O. Ström-Olsen, *Nanocrystalline magnesium for hydrogen storage.* Journal of Alloys and Compounds, 1999. **288**(1-2): p. 217-225.

44. Chen, Y.-L., C.-H. Huang, and W.-P. Hu, *Theoretical Study on the Small Clusters of LiH, NaH, BeH2, and MgH2.* The Journal of Physical Chemistry A, 2005. **109**(42): p. 9627-9636.

45. Czujko, T., et al., *Synthesis and hydrogen desorption properties of nanocomposite magnesium hydride with sodium borohydride (MgH2 + NaBH4).* Journal of Alloys and Compounds, 2007. **427**(1-2): p. 291-299.

46. Larsson, P., *Role of catalysts in dehydrogenation of MgH2 nanoclusters.* Applied Physical Sciences, 2008. **105**(24).

47. Pauw, B.R., et al., *Cubic MgH2 stabilized by alloying with transition metals: A density functional theory study.* Acta Materialia, 2008. **56**(13): p. 2948-2954.

48. Li, Y., *High-pressure phase transformations in CaH2.* Journal of Physics: Condensed Matter, 2008. **20**(045211).

49. El Gridani, A. and M. El Mouhtadi, *Electronic and structural properties of CaH2: an ab initio Hartree-Fock study.* Chemical Physics, 2000. **252**(1-2): p. 1-8.

50. Talaty, E.R., *FSGO calculations of geometries and electronic structures of "argon-core" third-row hydrides* Theoret. Chim. Acta, 2005. **41**(2): p. 133-139.

51. Verbraeken, M.C., E. Suard, and J.T.S. Irvine, *Structural and electrical properties of calcium and strontium hydrides.* Journal of Materials Chemistry, 2009. **19**(18): p. 2766-2770.

52. Weaver, J.H., M. Gupta, and D.T. Peterson, *Electronic structure and bonding in CaH2: Experiment and theory.* Solid State Communications, 1984. **51**(10): p. 805-808.

53. Bulanov, A.D., *Synthesis of High-Purity Calcium Hydride* Russian Journal of Applied Chemistry, 2004. **77**(6): p. 875-877.

54. Luo, W. and K.J. Gross, *A kinetics model of hydrogen absorption and desorption in Ti-doped NaAlH4.* Journal of Alloys and Compounds, 2004. **385**(1-2): p. 224-231.

55. Prozorov, T., et al., *Sonochemical doping of Ti-catalyzed sodium aluminum hydride.* Journal of Alloys and Compounds, 2006. **419**(1-2): p. 162-171.

56. Vermeulen, P., et al., *Crystal structures of MgyTi100-y thin film alloys in the as-deposited and hydrogenated state.* International Journal of Hydrogen Energy, 2008. **33**(20): p. 5646-5650.

57. Kennedy, A.R., *The effect of TiH2 heat treatment on gas release and foaming in Al-TiH2 preforms.* Scripta Materialia, 2002. **47**(11): p. 763-767.

58. Kennedy, A.R. and V.H. Lopez, *The decomposition behavior of as-received and oxidized TiH2 foaming-agent powder.* Materials Science and Engineering A, 2003. **357**(1-2): p. 258-263.

59. Gupta, M., *Electronically driven tetragonal distortion in TiH2.* Solid State Communications, 1979. **29**(1): p. 47-51.

60. Yang, R., et al., *Transition metal alloying effects on chemical bonding in TiH2.* Acta Materialia, 2002. **50**(1): p. 109-120.

61. Andreasen, A., *Predicting formation enthalpies of metal hydrides*. 2004, Riso National aboratory: Poskilde.

62. Leon, A., et al., *Investigation of the nature of a Ti-Al cluster formed upon cycling under hydrogen in Na alanate doped with a Ti-based precursor.* Journal of Physical Chemistry C, 2008. **112**(32): p. 12545-12549.

63. Sartori, S., et al., *Studies of mixed hydrides based on Mg and Ca by reactive ball milling.* Journal of Alloys and Compounds, 2009. **476**(1-2): p. 639-643.

64. Bai, K., P.S.E. Yeo, and P. Wu, *Reversible Catalytic Reactions and the Stability of Ti Surface Defects in NaAlH4.* Chemistry of Materials, 2008. **20**(24): p. 7539-7544.

65. Chen, Y. and J.S. Williams, *Formation of metal hydrides by mechanical alloying.* Journal of Alloys and Compounds, 1995. **217**(2): p. 181-184.

66. Kang, X.-D., P. Wang, and H.-M. Cheng, *Advantage of TiF3 over TiCl3 as a dopant precursor to improve the thermodynamic property of Na3AlH6.* Scripta Materialia, 2007. **56**(5): p. 361-364.

67. Leon, A., et al., *Al K edge XANES measurements in NaAlH4 doped with TiCl 3 by ball milling.* Journal of Physical Chemistry C, 2007. **111**(9): p. 3795-3798.

68. Leon, A., J. Rothe, and M. Fichtner, *Variation and influence of the local structure around Ti in NaAlH 4 doped with a Ti-based precursor.* Journal of Physical Chemistry C, 2007. **111**(44): p. 16664-16669.

69. Ma, B., L.C. Collins, and F.H. Schaefer, *Periodic trends for transition metal dihydrides MH2, dihydride dihydrogen complexes MH2&middotH2, and tetrahydrides MH4 (M = Ti, V, and Cr).* Journal of the American Chemical Society, 1996. **118**(4): p. 870-879.

70. Leon, A., et al., *Evolution of the local structure around Ti atoms in NaAlH4 doped with TiCl3 or Ti13&middot6THF by ball milling using X-ray absorption and X-ray photoelectron spectroscopy.* Journal of Physical Chemistry B, 2006. **110**(3): p. 1192-1200.

71. Leon, A., et al., *Chemical state and local structure around titanium atoms in NaAlH 4 doped with TiCl3 using X-ray absorption spectroscopy.* Journal of Physical Chemistry B, 2004. **108**(42): p. 16372-16376.

72. Leon, A., et al., *Chemical state of Ti atoms in NaAlH4 doped with a Ti-based precursor by ball milling.* Journal of Metastable and Nanocrystalline Materials, 2005. **24-25**: p. 319-322.

73. Jensen, C.M., et al. *Characterization and mechanistic studies of the active titanium species in the reversible dehydrogenation of Ti-doped sodium aluminum hydride*. 2004. San Antonio, TX, United states: Electrochemical Society Inc.

74. Bogdanovic, B., et al., *Investigation of hydrogen discharging and recharging processes of Ti-doped NaAlH4 by X-ray diffraction analysis (XRD) and solid-state NMR spectroscopy.* Journal of Alloys and Compounds, 2003. **350**(1-2): p. 246-255.

75. Canton, P., et al., *Synchrotron X-ray studies of Ti-doped NaAlH4.* Journal of Physical Chemistry B, 2006. **110**(7): p. 3051-3054.

76. Fichtner, M., *Complex aluminium hydrides for hydrogen storage.* Annales de Chimie: Science des Materiaux, 2005. **30**(5): p. 483-494.

77. Jensen, C.M., et al., *Advanced titanium doping of sodium aluminum hydride:: segue to a practical hydrogen storage material?* International Journal of Hydrogen Energy, 1999. **24**(5): p. 461-465.

78. Kircher, O. and M. Fichtner, *Hydrogen exchange kinetics in NaAlH4 catalyzed in different decomposition states.* Journal of Applied Physics, 2004. **95**(12): p. 7748-7753.

79. Krishnan, R., D. Agrawal, and T. Dobbins, *Microwave irradiation effects on reversible hydrogen desorption in sodium aluminum hydrides (NaAlH4).* Journal of Alloys and Compounds, 2009. **470**(1-2): p. 250-255.

80. Fang, F., et al., *Formation of Na3AlH6 from a NaH/Al mixture and Ti-containing catalyst.* Acta Materialia, 2009. **57**(6): p. 1959-1965.

81. Wang, J., et al., *Diffusion of hydrogen vacancy in Na3AlH6.* Applied Physics Letters, 2009. **95**(11): p. 111910-111910-3.

82. Balema, V.P., et al., *Titanium catalyzed solid-state transformations in LiAlH4 during high-energy ball-milling.* Journal of Alloys and Compounds, 2001. **329**(1-2): p. 108-114.

83. Chen, J., et al., *Reversible Hydrogen Storage via Titanium-Catalyzed LiAlH4 and Li3AlH6.* The Journal of Physical Chemistry B, 2001. **105**(45): p. 11214-11220.

84. Hashimoto, S., *Lithium aluminum hydride and Sodium aluminum hydride (LiAlH4 & NaAlH4.* Yuki Gosei Kagaku Kyokaishi/Journal of Synthetic Organic Chemistry, 1994. **52**(7): p. 616-616.

85. Resan, M., et al., *Effects of various catalysts on hydrogen release and uptake characteristics of LiAlH4.* International Journal of Hydrogen Energy, 2005. **30**(13-14): p. 1413-1416.

86. Resan, M., et al., *Effect of TixAly catalysts on hydrogen storage properties of LiAlH4 and NaAlH4.* International Journal of Hydrogen Energy, 2005. **30**(13-14): p. 1417-1421.

87. Jeloaica, L., et al., *Thermodynamic Properties of Trialkali (Li, Na, K) Hexa-alanates: A Combined DFT and Experimental Study.* The Journal of Physical Chemistry C, 2008. **112**(47): p. 18598-18607.

88. Xiong, Z.T., et al., *Large amount of hydrogen desorption and stepwise phase transition in the chemical reaction of NaNH2 and LiAlH4.* Catalysis Today, 2007. **120**(3-4): p. 287-291.

89. Liu, Y., et al., *Reversible hydrogenation/dehydrogenation performances of the Na2LiAlH6-Mg(NH2)2 system.* International Journal of Hydrogen Energy. **In Press, Corrected Proof**.

90. Weidenthaler, C., et al., *Evidence for the existence of [beta]-Na3AlH6: Monitoring the phase transformation from [alpha]-Na3AlH6 by in situ methods.* Journal of Alloys and Compounds, 2005. **398**(1-2): p. 228-234.

91. Ozolins, V. and et al., *First-principles computational discovery of materials for hydrogen storage.* Journal of Physics: Conference Series, 2009. **180**(1): p. 012076.

92. Wolverton, C. and et al., *Discovery of novel hydrogen storage materials: an atomic scale computational approach.* Journal of Physics: Condensed Matter, 2008. **20**(6): p. 064228.